

Probing Structure and Dynamics of Soft Colloidal Glasses using Rheology and Light Scattering

Submitted in partial fulfillment of therequirements

for degree of

Doctor of Philosophy

By

Samruddhi Kamble

(Roll No. 07402703)

Supervisors

Prof. Rajdip Bandopadhyaya

Dr. Suresh Bhat

Dr. Ashish Lele



Department of Chemical Engineering

INDIAN INSTITUTE OF TECHNOLOGY BOMBAY

(2014)

Thesis Approval

The thesis entitled

Probing Structure and Dynamics of Soft Colloidal Glasses by Rheology and Light Scattering



by

Samruddhi Kamble




is approved for the degree of

Doctor of Philosophy

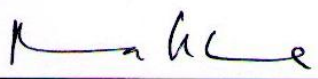
Examiners

1. PROF. ANUGRAH SINGH 
2. PROF. ROCHISH THAKAR 
3. _____

Supervisors

1. PROF. RAJDIP BANDOPADHYAYA 
2. DR. SURESH BHAT 
3. DR. ASHISH LELE 
4. _____

Chairman

PROF. PRASENJIT GHOSH 

Date: 16-04-2014

Place: IIT, BOMBAY

Declaration

I declare that this written submission represents my ideas in my own words and where others ideas or words have been included, I have adequately cited and referenced the original sources. I also declare that I have adhered to all principles of academic honesty and integrity and have not misrepresented or fabricated or falsified any idea/data/fact/source in my submission. I understand that any violation of the above will be cause for disciplinary action by the Institute and can also evoke penal action from the sources which have thus not been properly cited or from whom proper permission has not been taken when needed.

(Signature)

Samruddhi Bharat Kamble
Roll No. 7402703

Date: _____

Indian Institute of Technology Bombay

Certificate of Course Work

This is to certify that Miss. SAMRUDDHI KAMBLE was admitted to the candidacy of the Ph.D. degree on 24th July 2007, after successfully completing all the courses required for the Ph.D. program. The details of the course work are given below:

Sr.No.	Course Code	Name of the Course	Credits
1.	MM 653	Characterization of Materials	6
2.	CH 831	Advanced Laboratory Techniques	8
3.	CL 710	Aerosol Technology	6
4.	BM 631	Introduction to Bio-nanotechnology	4
5.	CL 610	Experimental Methods	6
6.	CL 656	Colloids and Interfacial Engineering	6
7.	HS 699	Communication and Presentation Skills	4
8	CLS 801, 802	Seminar	4+4

Dy. Registrar (Academic)

I.I.T. Bombay

Date: _____

Dedicated to my beloved parents..

Table of Contents

Abstract	i
List of Figures and Tables	v
1. Introduction	1
1.1 Colloids:	1
1.1.1 Colloidal interactions:	2
1.1.1.1 Van der Waals attraction	2
1.1.1.2 Electrostatic Repulsion	3
1.1.1.3 Steric Repulsion.....	3
1.1.1.4 Depletion Interactions	4
1.1.1.5 Hydrophobic interactions	4
1.1.2 Colloidal suspensions	5
1.1.3 Colloidal glass transition:.....	5
1.1.3.1 Cage model	7
1.1.3.2 Phase behavior of hard spheres with short range attraction	7
1.1.3.3 Gels, Glass and Jamming.....	8
1.1.3.4 Manifestation of kinetic arrest	10
1.1.3.5 Ageing	12
1.2 Soft Colloidal Glasses (SCGs):.....	13
1.2.1 Model soft colloids:.....	13
1.2.1.1 Stars	13
1.2.1.2 Microgels	14
1.3 Yielding in colloidal glasses:.....	15
1.4 Objectives:	18
1.5 Organization of the thesis:.....	18
2. Material Synthesis and Experimental Methods	20
2.1 Introduction	20
2.2 PNIPAm microgels:.....	21
2.2.1 Structure of the microgels.....	22
2.2.2 Mechanism for volume phase transition	24
2.2.3 Factors affecting the VPTT	25
2.3 Synthesis of PNIPAm microgels:	26
2.3.1 Materials	26
2.3.2 Synthesis of small PNIPAm microgels.....	27
2.3.3 Synthesis of larger size PNIPAm microgels	28

2.4 Experimental Methods:	29
2.4.1 Static Light Scattering (SLS)	29
2.4.2 Dynamic Light Scattering (DLS)	34
2.4.3 Diffusing Wave Spectroscopy (DWS)	36
2.4.4 Rheology:	41
2.4.4.1 Small Amplitude Oscillatory Shear (SAOS)	41
2.4.4.2 Large Amplitude Oscillatory Shear (LAOS).....	42
2.4.4.3 Strain Rate Frequency Superposition (SRFS)	42
2.4.4.4 Stress relaxation	43

3. Dynamics of Soft Colloidal Glasses investigated by Diffusive Wave Spectroscopy	44
3.1 Introduction	44
3.2 Experimental procedures:.....	46
3.2.1 Synthesis and characterization of microgels	46
3.2.2 Preparation of dense suspensions	48
3.2.3 DWS experimental protocol.....	50
3.3 Results and Discussions:.....	51
3.3.1 Glass transition.....	51
3.3.2 Mixed characteristic of a glass and gel.....	52
3.3.3 Glass-Glass transition	54
3.3.4 Cage modulus	55
3.4 Summary	57

4. Yielding in Soft Colloidal Glasses: Strain Rate Frequency Superposition (SRFS) under LAOS	59
4.1 Introduction	59
4.2 Materials and experimental protocol:.....	61
4.2.1 Sample preparation for soft solids	61
4.2.2 Experiments	62
4.2.3 Data analysis	62
4.3 Results and Discussions:.....	63
4.3.1 First harmonic moduli	63
4.3.2 Higher harmonics	64
4.3.3 Strain rate frequency superposition under LAOS	65
4.3.4 Relation between SRFS and strain sweep	68
4.3.5 Energy dissipation rate	68
4.4 Summary	70

5. Universal attributes of yielding in soft materials under Large Amplitude Oscillatory Shear (LAOS)	71
5.1 Introduction	71
5.2 Materials and experiments:.....	74
5.2.1 PNIPAm: Synthesis and characterization	74
5.2.2 Preparation of other complex fluids	77
5.2.3 Experimental protocol:.....	78
5.2.3.1 PNIPAm suspensions	78
5.2.3.2 Other soft materials	79
5.3 Results and Discussions:.....	80
5.3.1 Yielding in PNIPAm microgel suspension.....	80
5.3.2 Universal features of yielding	82
5.3.3 Effect of concentration on G'' peak	87
5.3.4 Double yielding in PNIPAm suspensions.....	88
5.4 Summary	93
6. Conclusions and Future Work	95
6.1 Conclusions:	95
6.1.1 DWS studies.....	96
6.1.2 Non-linear-rheology	98
6.2 Recommendation for future work:.....	100
6.2.1 Dynamics of homogeneously cross-linked microgels at $\varphi_{eff} > \varphi_{RCP}$...	100
6.2.2 Dynamics of polymer grafted hard sphere suspensions at $\varphi_{eff} > \varphi_{RCP}$	100
6.2.3 Application of microgels in biomaterials.....	101
References	104
List of Publications	120
List of presentation in Conferences	121
Acknowledgements	122

Abstract

Dense colloidal suspensions play a significant role in a wide range of commercially important products like gels, foams, emulsions, pastes etc., which are part of our daily life. These materials are sheared during various processing applications where they are required to yield. Yielding in these materials is complex because of their multicomponent nature and various interparticle interactions. The imposed flow induces changes in the microstructure, which in turn affects the mechanical properties of the final product. Thus it is important to investigate the structure-property relations in these complex fluids over a hierarchy of length and time scales, both under quiescent conditions, as well as under shear.

Colloidal suspensions undergo kinetic arrest at a critical volume fraction of ~ 0.58 , called the glass transition volume fraction (φ_g). There is a divergence of the mechanical properties at the φ_g and the suspension is called a colloidal glass. The kinetic arrest occurs due to caging of the particles by their nearest neighbours, also known as the “cage effect”. This results in two relaxation times; a fast mode of relaxation, t_β , related to the diffusive motion of the particle within the cage and a slow relaxation time, t_α , related to the cooperative motion of many particles for structural relaxation, where occasionally a caged-particle can escape its cage. While hard sphere colloidal suspensions are excellent model systems to investigate the behaviour of complex fluids, there is a growing interest in investigation of model soft colloids such as colloidal star polymers and microgels. Being soft and deformable, the soft colloids have an ability to be packed at an effective volume fraction, $\varphi_{\text{eff}} > 1$, unlike hard sphere suspensions where the maximum possible value is, $\varphi \sim 0.7$. Thus, the use of soft spheres allows investigation of the dynamics above the glass transition volume fraction (φ_g). The colloidal glass formed by the soft deformable particles is called a soft colloidal glass (SCG). Similar to the hard sphere colloidal glasses, the mechanical properties of SCGs also diverge as $\varphi_{\text{eff}} \rightarrow \varphi_g$, however functional dependence for SCGs is weaker, for eg. $G_p \propto \varphi_{\text{eff}}^m$, where G_p is the plateau modulus and $m = 2 - 15$ for soft particles. Although multiarm star polymers have been used as a model system to investigate SCGs, microgels are easier to synthesize and characterize.

In this work, we investigate dense aqueous suspensions ($\varphi_{\text{eff}} > \varphi_g$) of Poly(N,-isopropylacrylamide) (PNIPAm) microgels as a model for studying the structure and dynamics in SCGs, under quiescent conditions as well as under oscillatory shear. PNIPAm is a thermoresponsive polymer that undergoes a large decrease in volume with increasing temperature beyond its *Volume Phase Transition Temperature* ($VPTT$) of ~ 32 °C. The ability of PNIPAm microgel to change size with temperature, allows one to change φ without changing the number density. Typically, the PNIPAm microgel swells by a factor of two at temperatures below its $VPTT$ as compared to its size at temperatures above $VPTT$. Similar to the stars colloids, the PNIPAm microgel also has a core-shell like morphology with a highly crosslinked core and a lightly crosslinked brushlike surface. The interparticle potential can be changed from soft repulsive to attractive below and above $VPTT$, respectively. In this work, PNIPAm microgels were synthesised by free radical polymerisation, which gave highly monodisperse microgels. The microgels were further characterized for their particle size by standard light scattering techniques, static and dynamic light scattering. All the experiments were performed at temperatures below $VPTT$ to ensure that the interparticle interactions are always repulsive. The experimental timescales were much larger than the diffusion timescales of the microgels.

The microstructure of dense microgel suspensions under quiescent conditions was characterized by diffusing wave spectroscopy (DWS). In particular, the quiescent experiments on the DWS set up were performed on microgels of the order of micron-size having high crosslinker density (6.7% by weight of monomer). A traditional light scattering technique fails for such highly turbid samples, due to the problem of multiple scattering, resulting in a weak scattered radiation. Thus for this work, DWS, a state of the art technique to analyze turbid samples was used. As mentioned earlier, PNIPAm microgels are known to be highly monodisperse and thus tend to crystallize at volume fraction of ~ 0.54 . Here, crystallization of the dispersion was suppressed by using a bi-disperse microgel suspension. The temporal autocorrelation function $G_2(\tau)$, was measured as a function of φ_{eff} , by changing the temperature. Concentrated suspensions ($\varphi_{\text{eff}} > \varphi_{\text{RCP}}$, where φ_{RCP} is φ at random close packing), showed a non-zero plateau in the decay of $G_2(\tau)$, indicating a kinetically arrested state. Increasing φ_{eff} by decreasing temperature caused a continuous evolution of the plateau to higher values. It is unusual to see this gel-like response for a dense system of repulsive particles. At still lower temperatures ($\varphi_{\text{eff}} \gg \varphi_{\text{RCP}}$), the $G_2(\tau)$ showed an

extra plateau occurring at intermediate lag times. These experimental observations have hitherto neither been reported nor analysed in great detail. We attribute this complex dynamics to the heterogeneous morphology of the microgel with a dense-core and a brush-like soft-shell. The long-time plateau results from a core-core repulsive interaction, while the extra plateau at intermediate times occurs due to brush-core repulsive interaction, caused by the interpenetration of the brushes at high φ_{eff} . The size and modulus of the cage was calculated from the mean squared displacement, which was obtained by the Laplace inversion of the $G_2(\tau)$. The cage modulus obtained from suspensions of different ρ , collapsed onto a master curve when plotted against the φ_{eff} . The cage modulus showed a soft dependence on φ_{eff} , unlike hard sphere suspensions, which show a divergence at $\varphi_{\text{eff}} \sim \varphi_g$. Further increase φ_{eff} , showed a much weaker dependence, similar to that observed for other soft core-shell like systems at high concentration.

Further, we investigated the rheological behaviour of dense suspensions of PNIPAm microgels under oscillatory shear flow. Smaller size microgels (~ 130 nm) with a low crosslinking density (2% by weight of monomer) were used for these studies. These microgels are soft and compressible; hence they seldom crystallize at very high concentrations. In a strain sweep experiment, on application of increasing oscillatory strain amplitude at a constant frequency, the dense microgel suspension showed a characteristic response of a soft solid, with a peak in the loss modulus (G'') and a monotonic decrease in the elastic modulus (G') in the nonlinear region. The G'' peak intensity that represents the energy dissipated in a cage breaking process was further studied in detail to understand the relaxation process in a SCG under oscillatory shear.

Recently, Miyazaki *et al.* (2006) proposed an elegant qualitative argument for explaining the origin of the G'' peak, based on the reasoning, that, yielding involves a strain-induced decrease in the characteristic relaxation time t_α of the material. To validate this, we performed experiments related to the strain rate frequency superposition (SRFS) technique proposed by Wyss *et al.* (2007). In SRFS, the frequency sweep data generated from experiments done at various values of constant $\dot{\gamma}$, could be superimposed on to master curves, suggesting that t_α is governed by the imposed effective strain rate $\dot{\gamma} = \omega\gamma_0$. We studied contributions of the higher harmonics for PNIPAm microgel suspension and a few other soft

solids, such as xanthan gum solution and a commercial hair gel. We observed that the shift factors for the higher harmonic moduli were identical to that of the linear viscoelastic moduli. It was also proved experimentally by looking at surface plots, that the energy dissipated in the cage breaking process depends solely on the loss moduli of the first harmonic alone. With the knowledge of the contribution of higher harmonic moduli, we decided to restrict the analysis to the first harmonic moduli for further work on yielding in soft materials, under large amplitude oscillatory shear.

During yielding in a non-linear oscillatory shear flow, the characteristic peak in G'' was investigated in detail by experiments and modeling. Our experiments showed universal attributes of the yielding event in a variety of soft materials; PNIPAm microgel suspension, xanthan gum, commercial hair gel, gelatin, surfactant lamellar phase and polystyrene melt, irrespective of their microstructure and thermodynamic state. All materials studied here showed qualitatively identical linear viscoelastic frequency response, in which the G' increased weakly but monotonically with frequency, whereas G'' showed a non-monotonic behavior with a minimum at intermediate frequencies. The frequency at which G'' is minimum, marks the characteristic β -relaxation frequency $\omega_\beta = 1/t_\beta$ in the context of the mode coupling theory (MCT). To establish a relationship between the two, we performed the strain sweep test at frequencies below and above the ω_β . It was striking to observe that the maximum relative dissipation during yielding occurred, when the imposed frequency resonates with ω_β . We believe this to be a very useful observation as it represents an important link between the single particle dynamics and the collective dynamics (cage breaking or constraint release phenomena) in the system. In addition to the experiments, we use a phenomenological model given by Miyazaki *et al.* (2006) who modified a simple Maxwell-type model by incorporating the strain dependence in the relaxation time. This model is able to predict qualitatively all the features observed experimentally. At frequencies greater than ω_β , the yielding was even more complex with a double peak in G'' . Our data suggests that the secondary peak in G'' occurred because of shear melting of a strain-induced structure, formed at very high strains, which could be probed at higher frequencies. The qualitative shapes of the Lissajous curves (raw stress-strain curve) also support the existence of a strain-induced structure.

Abstract

In summary, we have focused our work on investigation of the microstructure and its relation to the rheological property of the soft glass, when subjected to flow as well as under quiescent conditions. We have recognized that although this system is a good model system, it also has complex dynamical signatures at very high packing fractions. This information would enrich the phase behavior of colloidal glasses and would be useful in elucidating various fundamental issues and commercial applications thereof.

List of Figures and Tables

Figure 1.1: Schematic showing steric repulsion by linear polymer chains grafted on a particle surface.....	3
Figure 1.2: Depletion interaction between two same sized spherical colloids.....	4
Figure 1.3: Phase diagram of hard sphere colloids	5
Figure 1.4: Schematic showing the ‘cage effect’ due to the topological constrains on a particle by nearest neighbors at increased concentration.....	7
Figure 1.5: Phase Diagram showing the re-entrant glass transition in colloid-polymer mixture at range of potential $R_{g(\text{polymer})}/R_{(\text{colloid})} = \xi = 0.08$	8
Figure 1.6: Transmission electron micrograph of a gel formed by Diffusion Limited Cluster Aggregation (DLCA) and Reaction Limited Cluster Aggregation (RLCA) of polystyrene particles.	9
Figure 1.7: Phase behavior for hard sphere colloids with short range attraction. (a) State diagram given by Sciortino <i>et al.</i> (2003), by theory and simulations for bidisperse hard spheres suspensions, (b) Simulation studies showing the four states DG, BRG, EF, NRG superimposed on the phase diagram shown in (a)	10
Figure 1.8: A composite jamming phase diagram for attractive colloids. Data from carbon black, PMMA and polystyrene was used to construct this phase diagram as it was difficult to explore full range of behaviors in a single colloidal system (Trappe <i>et al.</i> 2001).....	11
Figure 1.9: Various relaxation process (α and β) in hard sphere silica particles along with MCT predictions.....	12
Figure 1.10: Linear viscoelastic frequency response depicting the relaxation processes in a soft solid. (a) Hard sphere colloidal suspension of PMMA in dodecane at $\varphi = 0.6$ and (b) Star polybutadiene melt (Helgeson <i>et al.</i> 2007).....	16
Figure 1.11: Dynamic strain sweep test performed on an 8 wt.% PNIPAm microgel suspension at a constant angular frequency ($\omega = 1 \text{ rad/s}$, $T = 25 \text{ }^\circ\text{C}$) showing the linear viscoelastic regime (LVE) and the non-linear viscoelastic (NLVE) regime.	17
Figure 2.1: (a) Structure of Poly-N, isopropylacrylamide (PNIPAm) and (b) the cross-linker Methylene-bis acrylamide (BIS).....	22
Figure 2.2: Schematic of a PNIPAm microgel showing a radial density profile and also the volume change in response to change in temperature.....	23
Figure 2.3: Schematic representation of the mechanism of coil-globule transition in PNIPAm aqueous suspension.	24
Figure 2.4: Effect of hydrophilic copolymer, on the a.) V_{PTT} , b.) swelling capacity given by the swelling ratio $\alpha = R_h, T/R_h, T = 25 \text{ }^\circ\text{C}$	25
Figure 2.5: Effect of cross-linker content (methylene-bis-acrylamide) on the (a) V_{PTT} and (b) swelling capacity given by the swelling ratio $\alpha = R_h, T/R_h, T = 25 \text{ }^\circ\text{C}$	26

Figure 2.6: (a) Hydrodynamic size as a function of temperature for PNIPAm microgels with 2 % cross-linker content and (b) swelling capacity of these microgels given by the swelling ratio $\alpha = R_{h,T}/R_{h,T} = 25$ °C.	28
Figure 2.7: (a) Hydrodynamic size as a function of temperature for PNIPAm with 6.7 % cross-linker content and (b) swelling capacity of these microgels given by the swelling ratio $\alpha = R_{h,T}/R_{h,T} = 25$ °C.	29
Figure 2.8: Schematic of a light scattering experiment.	29
Figure 2.9: Particle form factor $P(q)$ as a function of scattering vector q for PNIPAm microgels $T = 30$ °C.	33
Figure 2.10: (a) Scattered intensity versus time in a dynamic light scattering experiment for PNIPAm microgel suspension and (b) Auto Correlation function $G_2(\tau)$, of a PNIPAm microgel suspension.....	34
Figure 2.11: Mean square displacement as a function of lag time for a concentrated suspension of PNIPAm microgel suspension $T = 25$ °C, $\rho = 2.3$ no/ μm^{-3}	38
Figure 2.12: Schematic for a diffusing wave spectroscopy set up.	40
Figure 3.1: (a) Hydrodynamic radius as a function of temperature for large size PNIPAm microgels and (b) Particle form factor $P(q)$ as a function of scattering vector q for bidisperse PNIPAm microgels ($T = 10$ °C) from a SLS measurement.....	46
Figure 3.2: Schematic of the heterogeneous morphology of a microgel (drawn to scale) exhibiting various length scales in the system at high volume fraction ($\phi_{\text{eff}} \sim 0.98$), at 15 °C for $\rho = 2.67$ μm^{-3}	47
Figure 3.3: (a) Autocorrelation functions $G_2\tau$ at different temperatures for PNIPAm microgel suspension at number density ρ of (a) $2.08 \pm 5\%$ μm^{-3} , (b). 2.18 μm^{-3} and (c) 2.67 μm^{-3} . Figure 3(c) shows zoomed-in view of the autocorrelation function for $\phi_{\text{eff}} > 0.8$	52
Figure 3.4: Mean square displacement as a function of lag time for PNIPAm microgel suspensions of concentrations (a) 2.08, (b) 2.3 and (c) 2.67 μm^{-3} at different temperatures.....	53
Figure 3.5: Modulus calculated by the MSD plateau value using equation 3.2 plotted as a function of angular frequency ($\omega = 2\pi/t$, here $t =$ lag time).....	56
Figure 3.6: Master curves for (a) Cage size as a function of volume fraction and (b) Modulus as a function of volume fraction for PNIPAm suspensions at different number density. The solid line is a fit for (a) Cage size $\propto \phi^{-8}$, (b) $G \propto \phi^{15}$	56
Figure 4.1: (a) Strain sweep at constant frequency $\omega = 1$ rad, $T = 25$ °C, for 14 wt. % PNIPAm microgel suspension and (b) Frequency sweep at constant strain $\gamma_0 = 0.01$. The dashed line is proportional to $\omega^{0.78}$	63
Figure 4.2: (a) A typical strain signal $\gamma(t)$ as a function of the time t from an oscillatory shear test with $\gamma_0 = 1.2$, $\omega = 1$ rad/s, (b) Plot of the resultant stress signal $\sigma(t)$ as a function of the time t with parameter values as in (a), (c) power spectrum $P\gamma$ of the strain signal and (d) power spectrum $P\sigma$ of the stress signal.	64

Figure 4.3: (a) Plot of the first harmonic moduli $G'1$ (solid circles) and $G''1$ (open circles) as a function of the angular frequency ω from constant strain-rate frequency sweep measurements at strain-rate amplitudes of $\gamma_0 = 4.2 \text{ s}^{-1}$ (blue), 2.1 s^{-1} (red), 1.2 s^{-1} (green), 0.9 s^{-1} (pink) using PNIPAm and (b) master curve obtained shifted the data to highest strain rate.....	66
Figure 4.4: Higher harmonic moduli for PNIPAm microgel suspension (14 wt %, $T = 25 \text{ }^\circ\text{C}$). (a) Master curve for third harmonic moduli, (b) master curve for fifth harmonic moduli and (c) shift factors for first third and fifth harmonic moduli.....	66
Figure 4.5: (a) SRFS curve showing the third harmonic moduli as a function frequency ω with constant strain-rate amplitude $\gamma_0 = 1.2 \text{ s}^{-1}$, using xanthan gum and (b) strain sweep showing the third harmonic moduli at $\omega = 5 \text{ rad/s}$	68
Figure 4.6: (a) Surface plot of the energy dissipation rate per unit volume as a function of the angular frequency ω , and the strain amplitude γ_0 , using xanthan gum. The color bar indicates the magnitude of energy dissipation rate $\dot{\epsilon}$ in units of Pa/s. (b) Curve of intersection of the surface $\gamma_0 = \gamma_0\omega = 2.1 \text{ s}^{-1}$ with the surface plot in (a).	69
Figure 5.1: Hydrodynamic radius of PEG-diacrylate crosslinked PNIPAm microgels as a function of temperature showing VPTT at $\sim 32 \text{ }^\circ\text{C}$	75
Figure 5.2: Relative viscosity as a function of concentration for PNIPAm microgel suspension.....	76
Figure 5.3: Schematic of experimental protocol used for measuring the rheology of PNIPAm microgel suspensions.....	78
Figure 5.4: Schematic of the experimental protocol for the step strain -stress relaxation experiments.....	79
Figure 5.5: (a) Frequency sweep data at low strain amplitude ($\gamma_{LVE} = 0.6 \%$) of a 6 wt. % ($\phi_{eff} \sim 1.5$, at $20 \text{ }^\circ\text{C}$) PNIPAm microgel suspension along with fit of the multi-mode Maxwell model and (b) strain sweep data for sample along with the Maxwell model fits.....	80
Figure 5.6: Strain sweep data at frequency where maximum in normalized G'' is observed (a-f).....	82
Figure 5.7: (a) Loss moduli G'' normalized with its values in the LVE regime as a function of the applied strain, probed at different frequencies $\omega = 0.1, 0.25, 0.5, 1.0$ and 2 rad/s (6 wt. % PNIPAm suspension $T = 20 \text{ }^\circ\text{C}$), (b) Maxwell model predictions of the strain dependence of G_{max}'' for various frequencies and (c) Maxwell model predictions of the strain dependence of normalized G'' for various frequencies.....	83
Figure 5.8: Comparison of experimentally determined normalized G_{max}'' (filled circles) as a function of frequency with predictions of the Maxwell model (dotted line) for the normalized G_{max}''	85
Figure 5.9: Prediction of the Maxwell model for the frequency dependence of G' and G'' at different strains $\gamma_0 = 1 \%$ LVE, 5, 20, 40, 60 and 90 %.....	86

Figure 5.10: (a) Storage modulus G' as a function of strain ($\omega=1\text{rad/s}$), (b) storage modulus G' and loss modulus G'' as function of frequency ($\gamma_{LVE} = 0.5\%$) and (c) normalized storage(G'/G'_{LVE})and loss (G''/G''_{LVE})modulus as a function of strain.	88
Figure 5.11: Effect of frequency on the height of the G' and 2 nd G'' peak (a) Normalised G' as function of strain for different frequencies $\omega = 5, 10, 20$ and 50 rad/s and (b) Normalized G'' as function of strain for different frequencies.....	89
Figure 5.12: (a) Linear Viscoelastic Spectrum for a 5 wt. % ($\phi_{\text{eff}} = 1.5$, at 10°C) PNIPAm microgels suspension.	90
Figure 5.13: Strain sweep performed on a 6 wt. % ($\phi_{\text{eff}} = 1.5$, 20°C) PNIPAm microgels suspension at $\omega = 20 \text{ rad/s}$	91
Figure 5.14: (a) Forward and (b) Reverse strain sweep test done on the same sample at a constant frequency of $\omega = 10 \text{ rad/s}$ for a 12 wt. % suspension of PNIPAm at 20°C , comparing the stress-strain curves of some important features in the forward and reverse strain sweep runs.	92
Figure 6.1: Cross-linked microgels of PNIPAm-co-Acrylic acid (10 wt.%aqueous suspension) forming thermoresponsive scaffold.....	102
Figure 6.2: Porous network formed by freeze drying of microgel suspension of PNIPAm	102
Figure 6.3: Self-assembly of PNIPAm microgels in a hexagonal meso-phase of a surfactant–water system at room temperature.....	103
Table 3.1 Various length scales in the heterogeneous morphology of PNIPAm microgel at high volume fractions.....	49
Table 4.1 Vertical $a_n(\gamma_0)$ and horizontal $b_n(\gamma_0)$ shift factors for the harmonic moduli G'_n and G''_n ($n=1,3,5$) for different strain-rate amplitudes γ_0 using PNIPAm, Xanthan gum, and hair gel.	67
Table 5.1: Hydrodynamic radius ' R_h ', calibration constant ' k ' and effective volume fraction ϕ_{eff} at different temperatures.	77
Table 5.2: Thirteen mode relaxation spectrum for a 6 wt.% PNIPAm microgel suspension at 20°C obtained from the Rheometer software by fitting the Maxwell model to the experimental Linear viscoelastic frequency response shown in Figure 5.5(a).....	81

Chapter 1

Introduction

This chapter provides a brief introduction to colloids and their interparticle interactions. It provides an adequate background literature on glass transition in hard sphere colloidal suspensions, and the motivation to study SCGs. This chapter also discusses other model systems used to investigate SCGs and the advantages in using aqueous suspension of thermoresponsive PNIPAm microgels, as a model system for SCG. Next, it describes the phenomenon of yielding in SCG under shear; the complex relaxation processes, which motivates further investigation of the complex dynamics in SCG. Lastly, it enlists the prime objectives and the structure of this thesis.

1.1 Colloids:

Colloids are microscopic particles dispersed in a liquid to form a colloidal suspension. Some of the common examples of colloids are mayonnaise, yoghurt, milk, shampoo, detergent, ink, paint and blood. Colloids exhibit random diffusive motion known as *Brownian motion* (Brown, 1985), and the energy for this motion is given by the thermal energy $k_B T$, where k_B is the Boltzmann constant and T is the temperature which sets the energy scale for all colloidal interactions. The particle diffusion coefficient ‘ D ’, is related to the size of the colloidal particle ‘ a ’ and the viscosity of the solvent η by the *Stokes–Einstein–Sutherland equation* (Einstein, 1905; Sutherland, 1905) equation 1.1.

$$D = \frac{k_B T}{6\pi\eta a} \quad 1.1$$

If the particle diffuses a distance equal to its radius, then the characteristic timescale for this diffusive motion is given by equation 1.2 and is known as the *Einstein–Smoluchowski equation* (Smoluchowski, 1906).

$$t = \frac{6\pi\eta a^3}{k_B T} \quad 1.2$$

This equation is valid in very dilute solution where the particle is considered to be isolated. It takes about 0.5 seconds for a 500 nm radius particle to move a distance equal to its radius in water at 20°C (Goodwin, 2004).

1.1.1 Colloidal interactions:

The interparticle forces between the colloids determine the stability of the colloidal suspension. The magnitude, range and the balance of the repulsive and attractive interparticle forces determine the overall stability, structure, and dynamics of the system. The repulsive interactions are mostly electrostatic, or steric, whereas the attractive forces mainly comprise of the Van der Waals, hydrophobic, and depletion interactions. These interactions will be discussed very briefly in the consecutive sections. The DLVO theory gives a quantitative description of the interactions in colloidal suspensions and was named after Derjaguin and Landau (1941) and independently by Verwey and Overbeek (1948). The model was developed by balancing the electrostatic repulsion and van der Waals attractive interactions by simply their linear addition.

$$V_T = V_{\text{VanderWaals}} + V_{\text{electrostatic}} \quad 1.3$$

The other interactions like the steric, excluded volume, hydrophobic and depletion interactions discussed above are not incorporated in the classical DLVO theory. Thus extended DLVO theories have been proposed which incorporate these non-DLVO interactions and has been reviewed by Grasso *et al.* (2002).

1.1.1.1 Van der Waals attraction

These are the forces that arise due to dipole-dipole, dipole-induced dipole and induced dipole-induced dipole interactions between the colloids. These are generally short-range interactions and are effective up to several hundreds of Å. Thus in dilute solutions the particles are far enough to feel the attractive potential. However as the concentration increases the attractive potential causes the colloidal particles to stick and coagulate. Thus, it is important to stabilize the colloidal particles by repulsive forces. Electrostatic repulsion occurring due to coulombic effects, steric stabilization, hydrophobic effects and entropic effects are frequently used for colloidal stability.

1.1.1.2 Electrostatic Repulsion

The electrostatic forces develop due to the surface charges on the colloids dispersed in a solvent. The surface charge is due to dissociation of any acidic or basic ionisable groups such as $-COOH$, $-SO_3H$, silanes, or adsorbed free ions, surfactants etc. The dissociated counter-ions float in the vicinity of the charged group forming an oppositely charged layer thus forming a double layer. It is the repulsion of the diffusive layer which keeps the particles away from each other and also leads to the concept of the excluded volume. The potential at the hypothetical boundary of the diffusive layer is called the *zeta potential*. The magnitude of the zeta potential gives an indication of the potential stability of the colloidal system. Dispersion of particles with zeta potential more positive than +30 mV or more negative than -30 mV are normally considered being stable. The Debye length (κ) that characterizes the range of the interaction is given by equation 1.4.

$$\kappa^{-1} = \sqrt{\frac{\epsilon_0 k_B T}{e^2 \left(\sum_i z_i^2 n_{i,\infty} \right)}} \quad 1.4$$

where, $n_{i,\infty}$ is the number density of ion i in the bulk solution, z is the valency of the ion, ϵ_0 is the electric constant and k_B is the Boltzmann constant. Typical values for the Debye length ranges from 0.3 – 300 nm (Larson, 1999; Crocker and Grier, 1994).

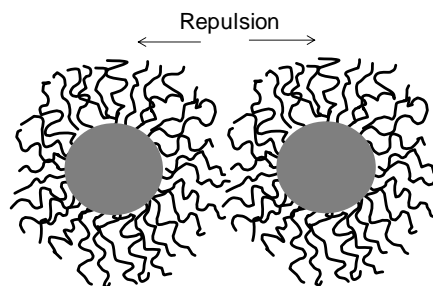


Figure 1.1: Schematic showing steric repulsion by linear polymer chains grafted on a particle surface.

1.1.1.3 Steric Repulsion

An alternate way to stabilize the colloidal suspension is through steric interactions that are brought about by grafting one end of a short polymer chain (~50 nm in length) or surfactant molecules on to the surface of the particles shown in Figure

1.1. The magnitude and range of the steric repulsion depends on the grafting density and the molecular weight (length) of the polymer. With enough graft density and molecular weight, the steric repulsion prevents the particles from coagulating. These parameters are chosen such that the range of the steric interaction is larger than the range of the Van der Waals attraction between the colloids (Hiemenz and Rajagopalan, 1997).

1.1.1.4 Depletion Interactions

Depletion interactions are brought about by addition of small particles or non-adsorbing polymers to a colloidal suspension. The size and concentration of the particles are chosen to be such that they are depleted (excluded) from the overlap region in between the colloidal particles. This creates an osmotic imbalance between the overlap region and the bulk solvent. This imbalance of forces around the colloidal particles pushes them towards each other as shown in Figure 1.2.

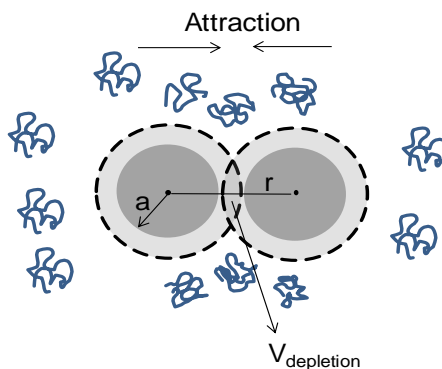


Figure 1.2: Depletion interaction between two same sized spherical colloids.

1.1.1.5 Hydrophobic interactions

Hydrophobic interactions in aqueous solutions come from the entropy of the three dimensional network of water molecules formed at room temperature due to hydrogen bonding. If non-polar groups are introduced they disrupt the 3D structure, as a result, the water molecules arrange themselves around the nonpolar surface so as to minimize the disrupted hydrogen bonds. In case the hydrocarbon chain consists some ionic or polar groups such as $-\text{COOH}$, $-\text{HC}=\text{O}$, $\text{NH}-\text{C}=\text{O}$, etc., they form hydrogen bonds with the surrounding water reducing the hydrophobic interactions. This interaction is important in the context of phase transition in PNIPAm microgels; the model system used in this work (See section 2.2.2).

1.1.2 Colloidal suspensions

In addition to its utility as materials of daily use, or commercial importance, colloidal suspensions are extensively used as model systems to study phase behavior of atomic or molecular systems. Phase transitions in colloidal suspensions can be studied in real time using optical techniques and are analogous to phase transitions in liquids (Krieger *et al.* 1969; Hiltner *et al.* 1971; Aastuen *et al.* 1986; Sirota *et al.* 1989). With recent technological advances, it is possible to directly investigate atoms by using atomic force microscopy or scanning tunneling microscopy. However, experiments with colloids are always simpler. The microscopic size scale of colloids allows them to be easily characterized by microscopy and various light scattering techniques (Prasad *et al.* 2007; Mejen and Underwood, 1993).

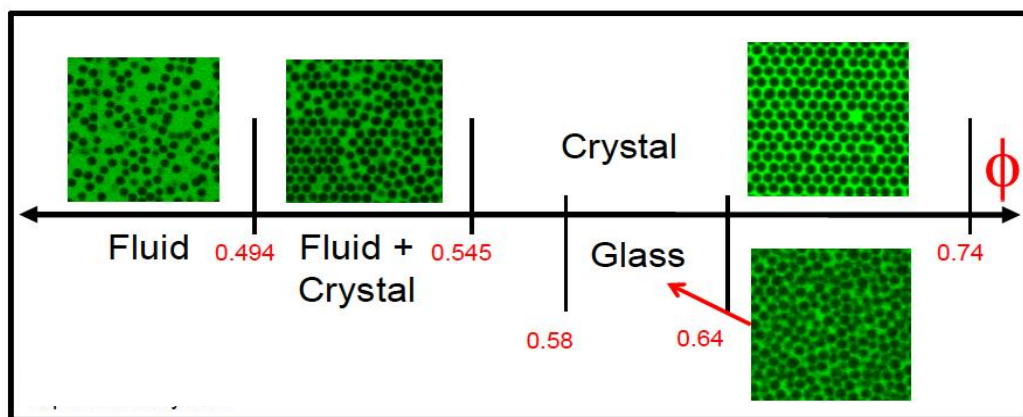


Figure 1.3: Phase diagram of hard sphere colloids (adopted from <http://www.weitzlab.seas.harvard.edu/research>).

There have been advances in synthetic routes to prepare monodisperse colloidal particles which is essential for a system to behave as a model system (Blaaderen and Vrij, 1992; Nyffenegger *et al.* 1993; Pelton and Chibante, 1986; Antl *et al.*, 1986; Bosma *et al.* 2002; Elsesser and Hollingsworth, 2010; Campbell and Bartlett, 2002). Thus colloids are frequently investigated as model systems to study phase transitions in molecular as well as colloidal glasses.

1.1.3 Colloidal glass transition:

A suspension of hard sphere colloids shows different phases depending on the concentration of particles. A more reliable measure of concentration is the particle volume fraction (ϕ). Hard spheres interact purely via excluded volume interactions.

Figure 1.3 shows a phase diagram for a hard sphere colloidal suspension indicating the different thermodynamic and kinetic states. At lower volume fractions ($\varphi < 0.49$) the particles can diffuse through the sample and thus the hard sphere suspension is an ergodic fluid. As the particle number density is increased, the system undergoes a fluid-crystal coexistence phase at $\varphi \sim 0.49 - 0.54$, followed by a FCC or a HCP crystalline phase above $\varphi > 0.54$. The maximum volume fraction a hard sphere colloid can attain is the hexagonal close packing with $\varphi_{\text{hcp}} \sim 0.74$. If a suspension of high volume fraction ($\varphi > 0.58$) is quenched, there is an abrupt increase in the viscosity and the suspension ceases to flow within the experimental timescales (Meeker *et al.* 1997). The amorphous solid formed in the process is called a colloidal glass, whose microstructure is similar to that of a fluid. This abrupt transition from a fluid to a disordered solid state is called the glass transition, and occurs at a critical volume fraction of ~ 0.58 , called the glass transition volume fraction (φ_g). The hard sphere suspension can get in to a glassy state at volume fractions greater than random close packing of $\varphi_{\text{RCP}} \sim 0.64$. The phase behavior for hard sphere colloids was first observed by Pusey and Megen (1986) and has been confirmed by various experimental and theoretical investigations. Above the glass transition the suspension becomes viscoelastic (Mason *et al.* 1995; Conrad *et al.* 2006) and is in a predominantly elastic state.

Observation of the glass transition requires $\sim 8\%$ of size polydispersity in the system. Highly monodisperse systems eventually crystallize on annealing (Auer and Frenkel, 2001; Zaccarelli *et al.* 2009). The boundaries of the phase diagram shift to higher values for a slightly polydisperse system (Bolhuis and Kofke, 1996; Fasolo and Sollich, 2003). On the other hand, for highly charged hard sphere colloids the phase boundaries shift to lower values (Hynninen and Dijkstra, 2003; Hartl, 2001). The dynamics of a colloidal suspension considerably slows down as it goes through glass transition. This kinetic arrest is mainly a result of decreased diffusion of a particle at larger distances due to crowding of neighboring particles. Thus the particle is considered to be trapped in a virtual cage formed by its nearest neighbors; well-known as the “cage effect” (Pusey and Megen, 1986) and will be discussed in the following section.

1.1.3.1 Cage model

The kinetic arrest in hard sphere colloidal glasses occurs due to topological constraints formed by the crowding of particles around each other to form a virtual cage-like structure. Figure 1.4 shows a schematic of a cage model occurring at increased concentration. The red particle in the figure is a caged particle and the surrounding grey particles form a virtual cage around the red particle. Similarly every particle is caged as well as is part of a cage for some other particle.

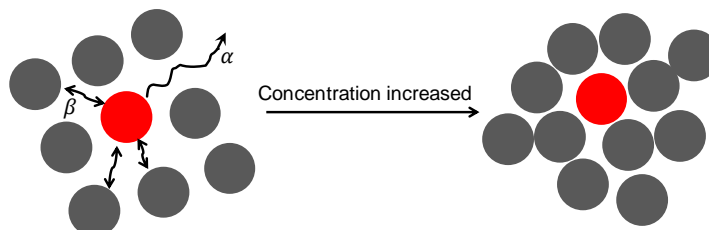


Figure 1.4: Schematic showing the 'cage effect' due to the topological constraints on a particle by nearest neighbors at increased concentration.

The cage model was first proposed by (Pusey and Megen, 1986) and has been frequently used to investigate dynamics of colloidal glasses (Cola *et al.* 2009; Weeks and Weitz, 2002; Brader, 2011; Zaccarelli and Poon, 2009). The elastic component in a soft solid is due to restricted diffusion of its particles over longer distances at higher packing fractions (Conrad *et al.* 2006). However, the particle has some freedom to diffuse within the cage formed by its nearest neighbours. This diffusive motion occurs at a characteristic frequency of the system called the β -relaxation frequency (ω_β). The β -relaxation is a faster mode of relaxation as compared to the slower relaxation called the structural relaxation or the α -relaxation frequency (ω_α), where occasionally a particle can eventually escape the cage by co-operative motion of surrounding particles. The relaxation times are simply the inverse of the characteristic frequencies ($t_\beta = 1/\omega_\beta$ and $t_\alpha = 1/\omega_\alpha$).

1.1.3.2 Phase behavior of hard spheres with short range attraction

Phase behavior of repulsive hard sphere colloids have been investigated considerably; however incorporating softness through attractive potential alters the phase behavior, and results in complex, but interesting phase transitions, especially near the glass transition. There are many reports on incorporating short range attractions in hard sphere suspensions, through depletion interaction (Ilett *et al.*

1995) or by addition of non-adsorbing linear polymers to hard sphere suspensions (Eckert and Bartsch, 2002; Yang *et al.* 2006). The depletion effect makes the repulsive hard spheres sticky giving rise to a new glass transition called the *reentrant glass* transition (Figure 1.5). The size and concentration of the added polymer sets the range and strength of the interaction. Inducing short range attractions near the glass line results in melting of the colloidal glass into fluid-crystal coexistence phase. On increasing the strength of attraction further, the system is again arrested in another nonergodic state. Thus there is a glass-to-glass transition through a fluid like phase. The two nonergodic phases can be termed as repulsive glass and attractive glass depending on the strength of the interparticle attraction.

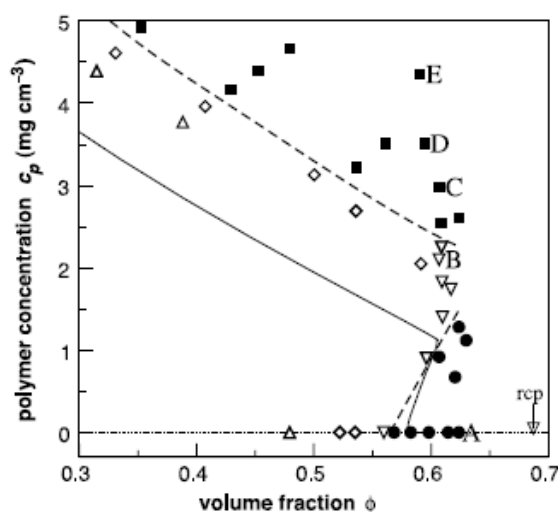


Figure 1.5: Phase Diagram showing the re-entrant glass transition in colloid-polymer mixture at range of potential $R_{g(\text{polymer})}/R_{(\text{colloid})} = \xi = 0.08$. Samples that reached thermal equilibrium (open symbols) are as follows: fluid (triangles), fluid-crystal coexistence (diamonds), and fully crystalline (inverted triangles). Samples that did not reach thermal equilibrium (solid symbols) are as follows: repulsion- driven glass (circles) and attraction- driven glasses (squares). Dashed curves are guides to the eye of the observed glass transition lines. Solid curves are MCT predictions of glass transition lines Pham *et al.* (2002) (Reprinted with permission from AAAS ©).

1.1.3.3 Gels, Glass and Jamming

Classification of materials as glasses, gels or jammed states is done on the basis of the range and strength of the interparticle potential. From the previous discussions, we have seen that hard sphere (repulsive) glasses are formed at high volume fraction, due to topological constraints of particles, which restricts their long distance diffusion. Also, when attraction is induced near the glass transition there is a glass-glass transition to form an attractive glass.

Gelation takes place at low particle concentrations, with strong interparticle attractions over a short range. This causes aggregation of particles to form clusters which percolates and subsequently undergoes kinetic arrest. Thus gels have a more open structure as compared to the colloidal glasses. There are two types of mechanism recognized for gelation, Diffusion Limited Cluster Aggregation (DLCA) and Reaction Limited Cluster Aggregation (RLCA). In DLCA the particles encounter each other by diffusion and stick irreversibly. These have a low fractal dimension with a loose and open structure as shown in Figure 1.6(Weitz and OLiveria, 1984).

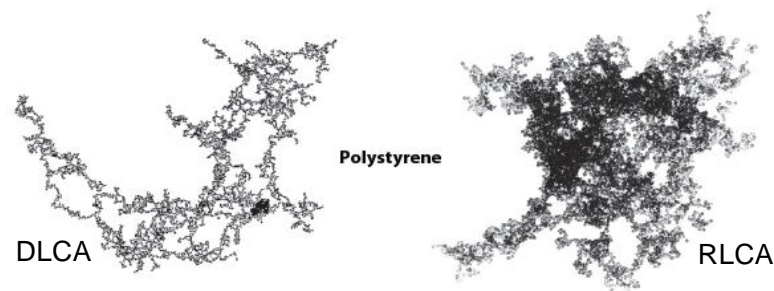


Figure 1.6: Transmission electron micrograph of a gel formed by Diffusion Limited Cluster Aggregation (DLCA) and Reaction Limited Cluster Aggregation (RLCA) of polystyrene particles. (Lu and Weitz, 2013). [Reprinted with permission from Annual Reviews in Condensed Matter Physics ©].

On the other hand, in RLCA the particles have to overcome an energy barrier in order to bond to each other. Thus they require more number of attempts to form bonds, as a result these structures are more compact and have high fractal dimensions, as shown in Figure 1.6(Weitz *et al.* 1985). The DLCA and RLCA mechanisms have been found to be a universal feature in gelation, as confirmed by light scattering experiments and simulation studies on a variety of colloidal particles (Zhou and Chu 1991; Lin *et al.* 1989; Burns *et al.* 1997).

Recently, Zaccarelli and Poon (2009), named the highly dense repulsive glass as non-bonded repulsive glass (NBRG) and the attractive glass as the bonded repulsive glass (BRG). They also recognized the gels formed by very high attractions from the ergodic fluid (EF) states as “Dense gels” (DG). Their phase diagram thus depicts the glass-glass as well as glass-gel transitions by interplay of the volume fraction and interparticle potential.

Figure 1.7(a) shows the phase diagram for hard sphere colloids with short range attractions (Sciortino *et al.* 2003), and Figure 1.7(b) shows a modified phase diagram

given by Zaccarelli and Poon (2009) marking the glass and gel lines for the phase transitions between EF, DG, BRG, and NBRG.

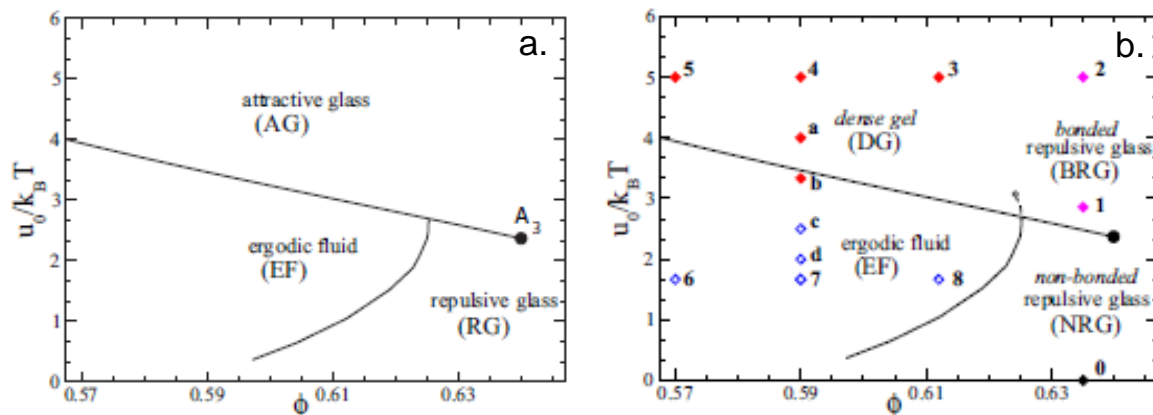


Figure 1.7: Phase behavior for hard sphere colloids with short range attraction. (a) State diagram given by Sciortino *et al.* (2003), by theory and simulations for bidisperse hard spheres suspensions, (b) Simulation studies showing the four states DG, BRG, EF, NRG superimposed on the phase diagram shown in (a) (Zaccarelli and Poon, 2009) [Reprinted with permission from Proceedings of National Academy of Sciences©].

Jammed states are formed by glassy states at very high volume fraction near the close packing i.e. deep in the glassy state. Liu and Nagel (1998) proposed a speculative three dimensional phase diagram for jamming and mentioned the importance of attractive potential in understanding the jamming transition. The three dimensional phase diagram was confirmed by experiments with attractive particles (Trappe *et al.* 2001) and is shown in Figure 1.8. The jamming transition was broadly studied by various parameters such as number density of particles, temperature which governs the interparticle potential, and the stress or load which forces the system to flow. This work provided a unique link between glass transition, gelation and aggregation. The three dimensional phase behavior was also confirmed by molecular dynamic simulations using DLVO forces between the particles (Kumar and Wu, 2004). Glasses as well as gels exhibit kinetic arrest in the sense of slow structural relaxation.

1.1.3.4 Manifestation of kinetic arrest

The simplest way to manifest a kinetic arrest is the visual observation of an inverted tube, containing the colloidal suspension. However the microscopic manifestation of dynamic arrest can be investigated by observing the $G_2(\tau)$ or MSD obtained either

from dynamic light scattering (DLS), video microscopy, or computer simulations. For a diffusive particle in a colloidal suspension the $G_2(\tau)$ will decay to zero.

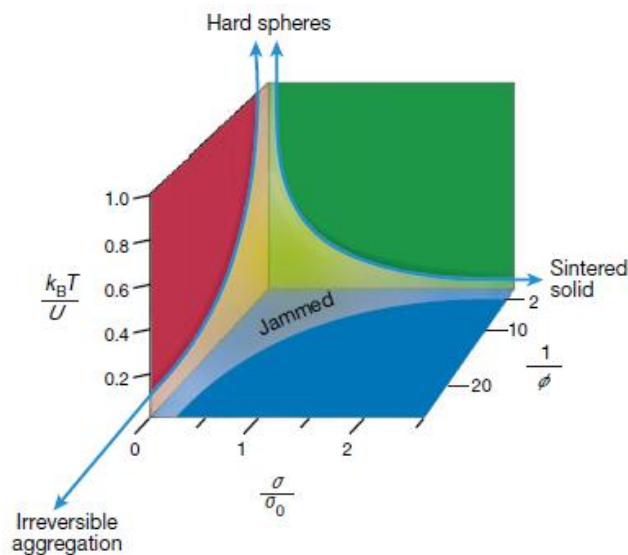


Figure 1.8: A composite jamming phase diagram for attractive colloids. Data from carbon black, PMMA and polystyrene was used to construct this phase diagram as it was difficult to explore full range of behaviors in a single colloidal system (Trappe *et al.* 2001)[Reprinted with permission from Nature publishing group ©].

With increase in the particle number density, the particle diffusion slows down and results in a delay in the decay time. As the concentration nears the glass transition, the $G_2(\tau)$ attains an intermediate plateau before decaying to zero (Figure 1.9). This feature illustrates the double relaxation times in a glassy state. The relaxation process responsible for the intermediate plateau is due to the β -relaxation (t_β), whereas the long time decay from the plateau represents the α -relaxation (t_α). With further increase in the ϕ , the α -relaxation cannot take place in the observed experimental time, and the system is arrested resulting in a plateau that does not decay to zero. These features can be seen in Figure 1.9.

Incorporating attractions in the system gives rise to qualitatively different $G_2(\tau)$ than that of a hard sphere glass. Recent computer simulations which have data extended over two decades in the lag time (up to 10^6 s), have exemplified the qualitative difference between a gel and glass (Zaccarelli and Poon, 2009; Chaudhuri *et al.* 2010).

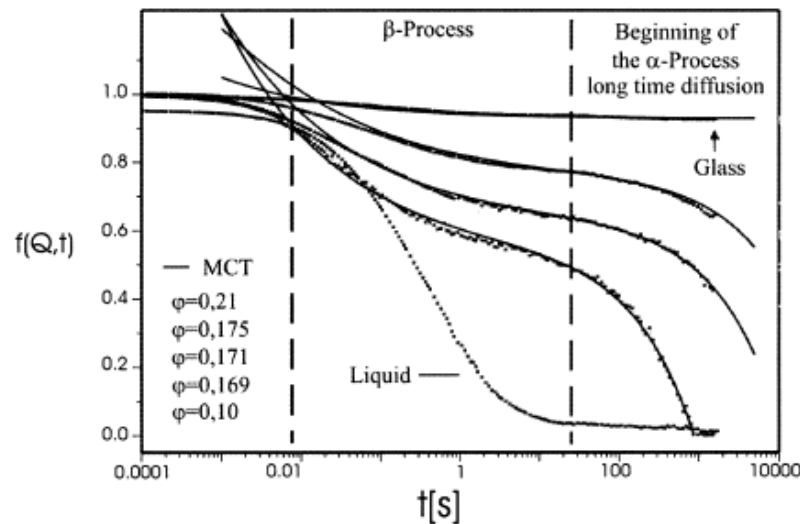


Figure 1.9: Autocorrelation function showing various relaxation process (α and β) in hard sphere silica particles along with Mode coupling theory (MCT) predictions. (Hartl 2001)[Reprinted with permission from Current Opinion in Colloid and Interface Science ©].

The $G_2(\tau)$ can be transformed to the temporal MSD, which gives physical insights about the microstructure such as cage size and the cage modulus. A mechanical rheological measurement of the storage modulus and loss modulus as a function of frequency, also gives supporting information about the structure and dynamics of the glassy state. For instance, the observation of a predominantly elastic response in an experimentally accessible range of frequencies, probed at low strains, indicates the formation of an arrested state. Correspondingly, the occurrence of a shallow minimum in the viscous moduli indicates the β -relaxation frequency (ω_β), characteristic to the system. However the α -relaxation (τ_α) is typically not observed in the range of frequencies accessible experimentally. One of the reasons for this is 'ageing', which will be discussed in the following section.

1.1.3.5 Ageing

Analogous to molecular glasses, colloidal glasses are also non-equilibrium states and are continuously evolving towards equilibrium (Martinez *et al.* 2008; Hodge, 1995; Kob and Barrat, 1997). Consequently, the material properties of a colloidal glass change with time; this is referred to as ageing. It is important to know the rate of ageing, since it is not desirable to let the material age while doing an experiment. Assigning an initial time for an ageing system is important and is done by giving a

controlled shear history and waiting time t_w . This is done by flowing the sample at very high shear rates, well above its yield stress, and then wait for the sample to evolve (age) until the material property, for example the time dependent moduli, attains a quasi-plateau value (i.e. evolving very slowly) (Helgeson, *et al.* 2007; Erwin *et al.* 2013). The ageing time is also studied by observing the temporal MSD as a function of waiting time (Courtland and Weeks, 2003). Laponite suspensions have been extensively investigated as a model to study ageing systems (Joshi and Reddy, 2008).

1.2 Soft Colloidal Glasses (SCGs):

As discussed in the preceding sections, the microstructure and flow behavior of hard sphere glasses have been investigated in great detail over a couple of decades. Recently, there has been growing interest in studying soft materials like surfactants, polymers, microgels and star colloids as model systems for SCGs because of their use in commercial products.

1.2.1 Model soft colloids:

1.2.1.1 Stars

Multiaarm star polymers are excellent model systems for studying SCGs. These materials show the colloid/polymer duality depending on the number and the length of the star arms. The number of arms is usually denoted as functionality f . When f and the length of the arms are sufficiently large, the star polymers have a dense core-brushlike shell morphology. This makes the star polymers to behave like colloids with a soft interaction potential. If $f \sim 1 - 4$, then the polymer dynamics dominate, whereas for $f \rightarrow \infty$ the behaviour is colloidal. Unlike hard spheres, the brushlike surface of star colloids can interpenetrate (Vlassopoulos, 2004), thereby making it possible to reach effective volume fractions $\varphi_{\text{eff}} > 1$, where $\varphi_{\text{eff}} = \rho \frac{4}{3} \pi R_h^3$, calculated based on the R_h measured from dilute solutions and the number density ρ . The interpenetration of the brushes results in complex dynamics in dense suspension of stars (Kapnistos *et al.* 1999). However, hyper-branched star polymers are difficult to synthesize (Roovers *et al.* 1993). Therefore microgels are often used as model system for SCGs.

1.2.1.2 Microgels

Microgels are chemically crosslinked microspheres, that can be swelled or deswelled, depending on the nature of the solvent they are suspended in. Most of them are stimuli responsive and thus their size, surface charge, swellability and interaction potential can be changed by external stimuli, such as temperature, pH, ionic strength (Shibayama *et al.* 1996), electric field (Pelton *et al.* 1989) etc. Amongst all other responsive microgels, PNIPAm is the most widely used because of its thermoresponsive nature; an experimentally amenable stimuli (Pelton and Chibante, 1986). Change in temperature modulates the size of the microgels; this unique property allows one to tune the ϕ by changing temperature, without changing the number density. The volume phase transition occurs at a critical temperature, ~ 32 °C. Being soft and deformable the microgels can be packed at $\phi_{\text{eff}} > 1$.

The content of the cross-linker decides the stiffness and the swelling capacity of the microgel. A highly cross-linked particle will be stiffer and will swell less than the one with a lower crosslink density. The interparticle potentials in these systems can also be tuned by changing the temperature (Wu *et al.* 2003; Huang and Hu, 2007). At $T < VPTT$, the particles are soft repulsive, as they are in equilibrium with the surrounding solvent. At $T > VPTT$, intra-molecular attractive (hydrophobic) interactions dominate and a single microgel particle shrinks by expelling water. For dense microgel suspension above the $VPTT$, the interparticle potential becomes attractive. If the concentration of particle is above the percolation limit, gelation will take place.

The morphology of microgels is similar to that of star colloids viz. they have a highly cross-linked core and loosely cross-linked brush-like surface. This happens due to the faster reaction rate of the cross-linker than the monomer during the synthesis process (Wu *et al.* 1994). The study of microgels at high volume fractions has unearthed a very rich phase behaviour and other complex but interesting dynamics.

Mattsson *et al.* (2009), investigated the concept of fragility in molecular glasses by using microgels of varying stiffness. Fragility in molecular glasses is related to the variation in the rate at which the relaxation time increases near the glass transition. Molecular glasses approach the glass transition in a variety of ways. For some glass formers the viscosity changes quite sharply approaching the glass transition, while for

some of them the transition is smooth. Thus, fragile glasses are the ones where the viscosity diverges abruptly; a small change in the temperature near the glass transition would melt the glass. On the other hand, those with smooth transitions in viscosity are called strong glasses (Angell *et al.* 2000). To have an analogous situation in model systems, Mattsson *et al.* (2009) used microgels of varying stiffness, which was controlled by the content of cross-linker; a highly cross-linked microgel is stiffer than the loosely cross-linked microgel. They demonstrated that softer microgels made stronger glasses. The suspensions with stiffer particles showed an abrupt transition similar to the fragile glasses whereas the microgel suspensions with softer microgels showed a smoother transition.

1.3 Yielding in colloidal glasses

Colloidal glasses under quiescent conditions show predominantly elastic response in a small amplitude oscillatory shear (SAOS) rheology experiment. Figure 1.10(a) shows a typical frequency response of a hard sphere colloidal glass where the storage modulus G' is dominant and has weak frequency dependence over the range of frequencies probed. In contrast the viscous modulus G'' shows non-monotonic frequency dependence with a shallow minimum at intermediate frequencies which marks the β -relaxation time ($t_\beta = 1/\omega_\beta$). The α -relaxation time (t_α) is shown by an extrapolation because for most practical purposes t_α remains elusive as the system ages, shifting the probability of observing the crossover to even lower frequencies. The linear viscoelastic (LVE) frequency response for star colloids shows an extra relaxation time called t_μ , which is related to the disengagement time of the interpenetrated arms of the stars, at high volume fractions as shown in Figure 1.10(b) (Kapnistos *et al.* 1999; Helgeson *et al.* 2007). The α and β -relaxation modes observed in the $G_2(\tau)$ in Figure 1.9, are closely related to the linear viscoelastic behaviour of SCGs.

Many complex fluids including colloidal glasses, when subjected to strong flows transform from a predominantly elastic state to a predominantly plastic state (liquid like). This transition is called yielding (Chambon *et al.* 1986). A colloidal glass yields by a shear induced cage breaking process. Recently, Wyss *et al.* (2007) and Miyazaki *et al.* (2006), showed that the t_α in soft solids is a function of the applied strain rate $\dot{\gamma}$ and has a power law dependence of $t_\alpha(\dot{\gamma}) \propto \dot{\gamma}_0^\nu$ with exponent $\nu \sim 1$. They measured

the viscoelastic frequency response at a constant strain rate ($\dot{\gamma} = \gamma_0 \omega$) and showed that the frequency responses for different strain rates could be shifted on to master curves confirming the universality of the equation $t_\alpha(\dot{\gamma}) \propto \dot{\gamma}_0^{-\nu}$ for soft solids. This technique was called the Strain Rate Frequency Superposition (SRFS). The strain rate decreased the structural relaxation time and thus made it observable in the experimentally accessible frequency scale.

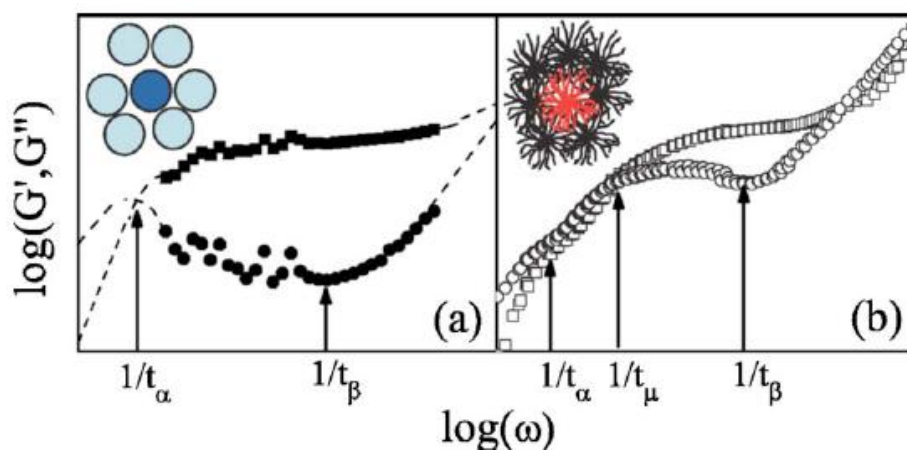


Figure 1.10: Linear viscoelastic frequency response depicting the relaxation processes in a soft solid. (a) Hard sphere colloidal suspension of PMMA in dodecane at $\phi = 0.6$ and (b) Star polybutadiene melt (Helgeson *et al.* 2007). (squares represent G' and circles G'') [Reprinted with permission from Society of Rheology].

In the SRFS experiment, to obtain data in the low frequency region requires imposition of large strains. In this non-linear regime the stress waveform is no longer sinusoidal and it can be expressed as a Fourier series of higher harmonics. Kalelkar *et al.* (2010) validated the SRFS for the higher harmonic moduli for a variety of soft solids. They observed that the SRFS curves for higher harmonic moduli can also be superimposed onto master curves using shift factors that are identical to those required for shifting the first harmonics of viscoelastic moduli. In general there is a growing interest in using large amplitude oscillatory shear (LAOS) as a rheological technique for finger printing of soft materials (Ewoldt *et al.* 2008).

The cage breaking also occurs on application of increasing oscillatory strains at a constant frequency. In a typical strain sweep experiment, the SCG yields at a critical strain value indicated by a crossover of G' and G'' as shown in Figure 1.11.

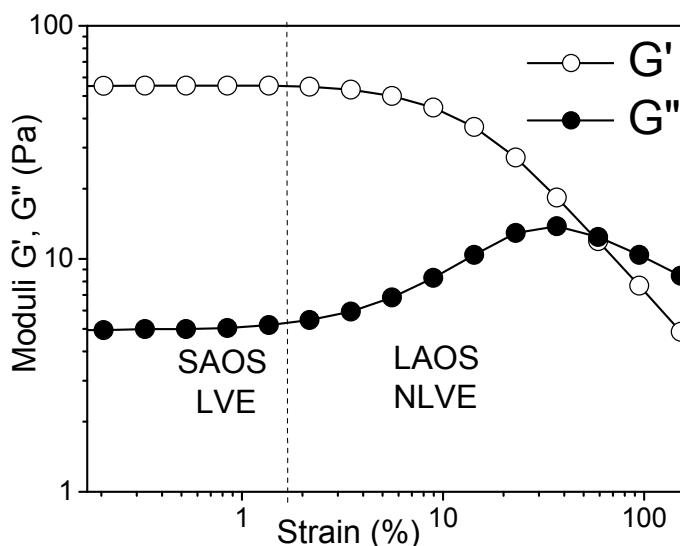


Figure 1.11: Dynamic strain sweep test performed on an 8 wt.% PNIPAm microgel suspension at a constant angular frequency ($\omega = 1 \text{ rad/s}$, $T = 25 \text{ }^\circ\text{C}$) showing the linear viscoelastic regime (LVE) and the non-linear viscoelastic (NLVE) regime.

The critical strain, marks the end of the LVE response after which the G' decreases monotonically with increasing strain, whereas the G'' shows a non-monotonic dependence, with a peak at the crossover of G' and G'' , marking the yield point. The peak in G'' is a characteristic feature of soft materials and is also called the Type-III LAOS behaviour (Hyun *et al.* 2002). It has been reported earlier for carbon composites of butyl rubber (Payne 1963), soft colloidal glasses (Brader *et al.* 2010), emulsions (Mason *et al.* 1995; Bower *et al.* 1999), gels (Altmann *et al.* 2004) and also modelled by the mode coupling theory (Brader *et al.* 2010; Kunimasa Miyazaki *et al.* 2006). In a strain sweep experiment, suspensions with weak attractions show a double yielding phenomenon (i.e. double peak in G''). These weak physical attractions in the system are termed as bonds and are not covalent bonds. The increasing deformation first breaks the bonds that results in the first peak in G'' followed by the cage breaking peak at higher strains (Kramb and Zukoski, 2010). Anisotropic particles have also shown a double yielding behavior where the anisotropy in the surface charge distribution is believed to induce attraction. However, a strongly repulsive or a strongly attractive colloidal system does not show a double yielding (Kramb and Zukoski, 2010). Dense suspensions of stars also show a double peak in G'' attributed to the disengagement of the interpenetrated star arms, followed by the cage breaking process. The probe frequency also plays an important role in observation of the secondary peak in G'' (Helgeson *et al.* 2007).

1.4 Objectives:

Listed below are the objectives of this work pertaining to investigation of the structure and dynamics of SCGs formed by dense microgel suspensions of PNIPAm.

1. **Synthesis and Characterization of PNIPAm microgels:** Synthesis of monodisperse microgels of PNIPAm. Determination of particle size by Light Scattering techniques. Preparation of bidisperse dense suspension of PNIPAm microgels to suppress crystallization.
2. **Structure and Dynamics of SCG under quiescent conditions:** Influence of the ϕ_{eff} (controlled either by changing the number density or temperature) on the dynamics of SCG, particularly at ϕ_{eff} close to or equal to one.
3. **Dynamics of SCG under Nonlinear strains:** Effect of nonlinear strains on the higher harmonic moduli by using a recently developed technique; SRFS under LAOS. The effect of imposed strain on the structural relaxation; particularly, frequency dependence of the loss modulus peak (G'').
4. **Universal attributes of yielding:** To extend the study for a variety of soft materials and to identify common mechanisms of relaxation in these materials and to complement the experiments with simple model predictions.

1.5 Organization of the thesis

This Thesis has been structured in to six chapters as follows.

Chapter 1 provides a brief introduction and background literature on colloids, colloidal interactions, glass transition, model for colloidal glasses, yielding in colloidal glasses etc. The discussion in this chapter sets the motivation and objective of this study.

Chapter 2 gives a detailed prescription of the synthesis of PNIPAm microgels along with some of their preliminary characterization depicting the thermoresponsive behavior. This chapter also provides a detailed description of the experimental techniques and the methods used in this work to investigate the structure and flow behavior of SCGs.

With a brief background of the model system as well as the experimental techniques; the **Chapter 3** presents the results on the structure and dynamics of dense

suspensions of PNIPAm microgels under quiescent conditions. The temporal autocorrelation functions $G_2(\tau)$ were observed at $\varphi_{\text{eff}} \geq \varphi_{\text{RCP}}$ by using DWS.

In **Chapter 4** and the consecutive chapter, the yielding behavior of SCG is studied by application of linear as well as non-linear strains. In this chapter we study the effect of nonlinear strains on the higher harmonic moduli by performing the SRFS under LAOS. This study was extended to a variety of soft solids such as xanthan gum solution and commercial hair gel in addition to PNIPAm microgels suspension.

In **Chapter 5** the characteristic yielding feature of the soft solids; the G'' peak was investigated in great detail. The role of the frequency on the amplitude of the G'' peak has been studied for a variety of soft materials that include a colloidal suspension, xanthan gum solution, commercial hair gel, aqueous gelatin solution, Lamellar mesophase of anion-ionic surfactant and polystyrene melt. A phenomenological model based on the Maxwell type model was proposed to predict the characteristic features of the yielding process in soft materials. The latter part of this chapter investigates a complex yielding phenomenon wherein a double yielding is observed at higher probe frequencies in the strain sweep tests.

Chapter 6 summarizes the salient conclusions from each chapter enriching the literature on soft materials and further ends with the recommendation for future investigations in this field.

Chapter 2

Material Synthesis and Experimental Methods

This chapter provides a detailed procedure used for the synthesis of PNIPAm microgels and also gives background information on the experimental protocols and methods that are pertinent to the results presented in Chapters 3, 4 and 5. The chapter begins with a brief background on the structure and phase transition of PNIPAm microgels. It is then followed by the synthesis procedure and description of the various characterisation techniques such as Static Light Scattering (SLS), Dynamics light scattering (DLS), Diffusing Wave Spectroscopy (DWS) as well as Linear and Non-Linear Rheology.

2.1 Introduction

PNIPAm microgels can be synthesized by various polymerization mechanisms, (see section 2.3). In this work we use the procedure given by Pelton and Chibante (1986), who were the first to synthesize PNIPAm microgels and to present their thermoresponsive nature. The microgels were synthesized by free radical polymerisation in the presence of a crosslinker and surfactant. The procedure is often referred to as precipitation polymerization because the reaction is performed above V_{PTT} . The synthesis conditions and the composition of the reactants allows for tuning the size, softness, swelling capacity, optical property and morphology of the microgel.

The size of the microgel can be controlled by the surfactant concentration, which stabilises the precursor particle during the synthesis and lowers the diameter of the primary particles with a concomitant increase in the number of particles. Wu *et al.* (1994) showed that for surfactant (sodium dodecyl sulfate (SDS)) concentration in the range of 0.2 – 4 mM, the relation between the hydrodynamic diameter of microgel and the SDS molarity is given by $D \propto [SDS]^{-0.71}$. The optical property of the microgel suspension depends on the size of the particle as well as the refractive index

difference between particles and the solvent. Suspensions of large size microgels ($\sim 1 \mu\text{m}$) would appear turbid, whereas those containing smaller size microgels ($< 200 \text{ nm}$) would be transparent. Compared to a lower cross-linked microgel, a highly cross-linked microgel will have greater refractive index contrast with the solvent. However if the cross-linking density is low and homogenous over the particle radius then even the larger sized microgel suspension would appear transparent (Acciaro *et al.* 2011). The crosslinker content also governs the softness and swelling capability (Zhang, *et al.* 2007). The crosslinking density and its distribution over the particle radius play an important role in the morphology of the microgel and interparticle pair potential at high concentrations. Thus the control over the reactants and the reaction temperature is essential to get the desired morphology of the microgel.

In this work, it was important to control the microstructure of the microgel since it plays an important role in the dynamics of dense suspensions. The size of the microgel was characterized by SLS and DLS. The yielding behavior of dense microgel suspension was studied by mechanical rheology. The turbid dense suspensions were characterized by DWS. Brief descriptions of these techniques and the protocols used for measurements in this work are described in section 2.4.

2.2 PNIPAm microgels:

A microgel is a cross-linked network of a high molecular weight polymer. Microgels made from hydrophilic polymers swell in water due to presence of polar groups on their polymeric backbone. The polar groups have non-covalent interactions with water and tuning these interactions causes reversible swelling and de-swelling of the microgels. Tuning can be achieved via external stimuli such as temperature (Pelton and Chibante, 1986), pH, ionic strength (Shibayama *et al.* 1996) and electric field (Pelton *et al.* 1989), making the microgels smart and responsive materials. Amongst the different stimuli, temperature and pH have been considerably investigated because they are relatively convenient to handle experimentally. Moreover, the thermosensitive approach can be advantageous for particular applications as it does not require the need for other solvents, co-polymerization agents, or any externally applied trigger (Garie and Leroux, 2004). Hence, temperature is the most widely used stimulus in smart polymer systems.

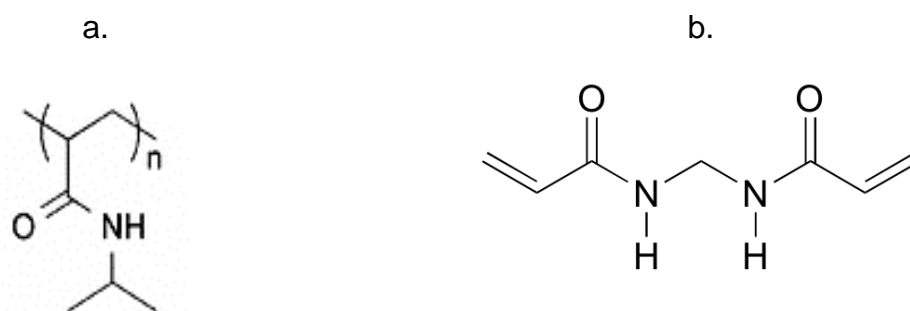


Figure 2.1: (a) Structure of Poly-N, isopropylacrylamide (PNIPAm) and (b) the cross-linker Methylene-bis acrylamide (BIS).

PNIPAm, first synthesized by Pelton and Chibante, (1986), is perhaps the most studied thermoresponsive polymer because of its potential applications in biomedical and membrane filtration technologies (Saunders *et al.* 2009; Nayak and Lyon, 2005; Jang *et al.* 2008; Fernández-Barbero *et al.* 2009). PNIPAm is a water soluble polymer that undergoes transition from a coil to globule state at a lower critical solution temperature (*LCST*) of 32 °C. Covalently crosslinked PNIPAm gels undergo corresponding volume phase transition at the *LCST*. PNIPAm microgels are synthesized by polymerizing the monomer NIPAm in the presence of a crosslinker, which is usually a difunctional comonomer. Most often methylene-bis-acrylamide (BIS), see Figure 2.1(b), is used as a cross-linker agent. In some cases poly-ethyleneglycol-diacrylate (PEGDA) a more hydrophilic cross linker is also used.

The as synthesized PNIPAm microgels are highly monodisperse and hence can be used as model systems to study colloidal dispersions including colloidal crystals. In general, microgels are resistant to aggregation because of the presence of charges on their surface from the initiator used during the synthesis. By adjusting the synthesis parameters the size of microgels and crosslinking density can be controlled which allows one to tune the microgel elasticity, swelling capacity and interaction potential.

2.2.1 Structure of the microgels

Microgels have core-shell morphology similar to that of a hyper branched star polymer colloid, which is yet another model system to study colloidal glasses. The ease of preparation and analogous particle morphology gives microgels an edge

over the star colloids to be used as model systems for colloidal glasses. The core-shell morphology of microgels is due to the intrinsic difference in the reaction rates of the monomer and the cross-linker. The cross-linker BIS has a faster rate of reaction as compared to the monomer NIPAm, and so the cross-linker gets consumed faster than the monomer during synthesis (Wu *et al.* 1994). Hence the crosslinking density at the center of the microgel is higher than that at the surface. This results in a gradient in the radial density profile in the form of a highly cross-linked core and a loosely cross-linked brushlike surface, see Figure 2.2. The loosely cross-linked brush at the particle surface provides steric stabilization and weakens the van der Waals attraction.

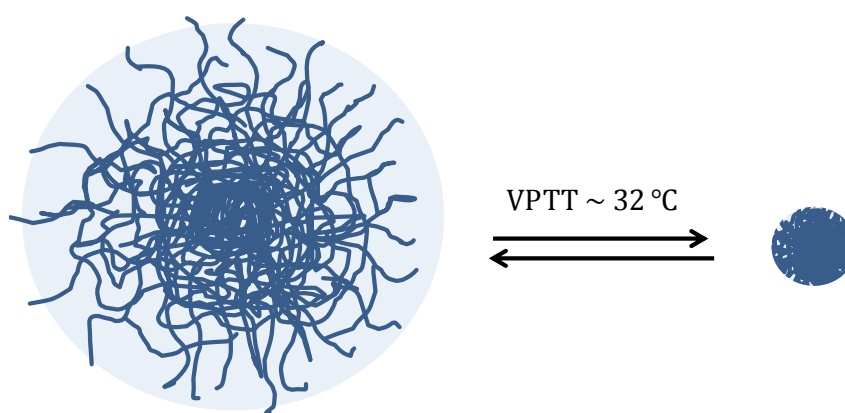


Figure 2.2: Schematic of a PNIPAm microgel showing a radial density profile and also the volume change in response to change in temperature.

However at higher temperatures ($T > V_{PTT}$) the brushes collapse and the particles behave similar to attractive colloids. The core-shell morphology of the microgels have been confirmed by small angle neutron scattering (SANS) and other light scattering studies, as well as by theoretical predictions (Scheffold *et al.* 2010; Eckert and Richtering, 2008; Stieger *et al.* 2004). The internal structure of the PNIPAm microgel can be made homogenous by carrying out the polymerisation in the presence of high surfactant concentration (Arleth *et al.* 2005). However, this results in small sized particles ($R_h < 50\text{ nm}$). Recently, it was shown that a continuous feed of appropriate amount of monomer and cross-linker during the course of reaction gave microgels, which have a homogenous distribution of the cross-linking density (Acciaro *et al.* 2011). The V_{PTT} can be tuned by incorporating appropriate comonomers and solvents. This can be explained better on the basis of

the mechanism of the phase transition in PNIPAm and is discussed in the following section.

2.2.2 Mechanism for volume phase transition

The monomer (NIPAm) contains a hydrophilic amide group and an isopropyl hydrophobic group as shown in Figure 2.1(a). Hydrogen bonding with the amide involves the carbonyl oxygen ($R-C=O \dots H-O-H$) and the protic hydrogen ($R'-NH \dots OH_2$). Each repeat unit of PNIPAm, when dispersed in water, has these hydrogen bonding interactions.

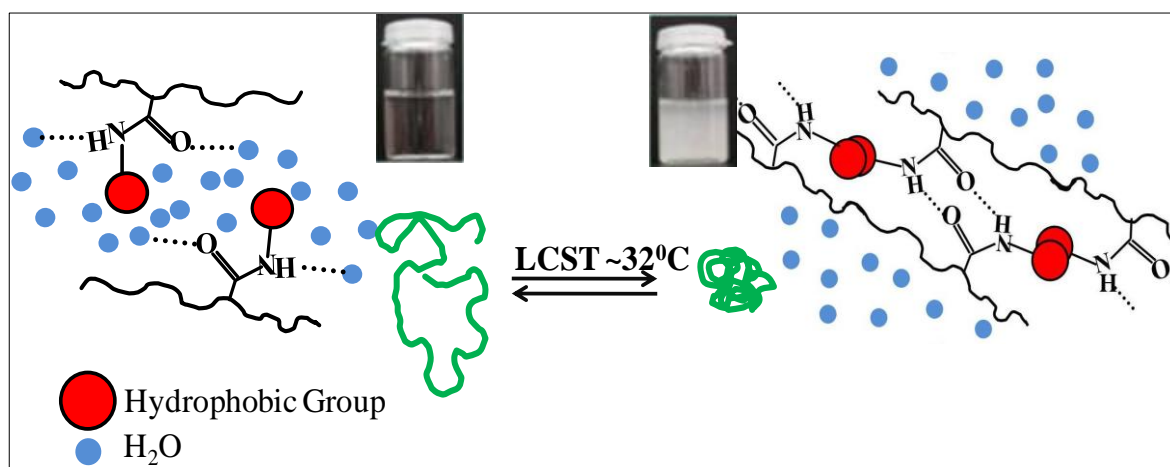


Figure 2.3: Schematic representation of the mechanism of coil-globule transition in PNIPAm aqueous suspension.

As the temperature is increased, the hydrogen bonding between the acrylamide and water molecules breaks due to increase in the thermal energy. These water molecules associated with the side-chain isopropyl groups are released as the temperature increases above the $\sim 32^\circ\text{C}$, as shown schematically in Figure 2.3. At $T < VPTT$, the hydrogen bonding between the acrylamide group and water keeps the hydrophobic isopropyl groups apart. However at $T > VPTT$ the hydrophobic interaction dominates and drives the coil to globule collapse. Thus water becomes a poor solvent above the $VPTT$ and hence the origin of the ‘smart’ behaviour arises from the entropic gain associated with the release of water molecules. The $VPTT$ corresponds to the region in the phase diagram at which the enthalpic contribution of hydrogen-bonded water to the polymer chain becomes less than the entropic gain of the system as a whole. The $VPTT$ thus largely depends on the hydrogen-bonding abilities of the constituent monomer units.

2.2.3 Factors affecting the VPTT

The mechanism of the collapse suggests that the *VPTT* can be tuned by changing the hydrophilic-hydrophobic character of the system. Incorporating a hydrophilic comonomer would shift the *VPTT* to higher values and vice versa for hydrophobic comonomer (Badiger *et al.* 1998; Varghese *et al.* 2000).

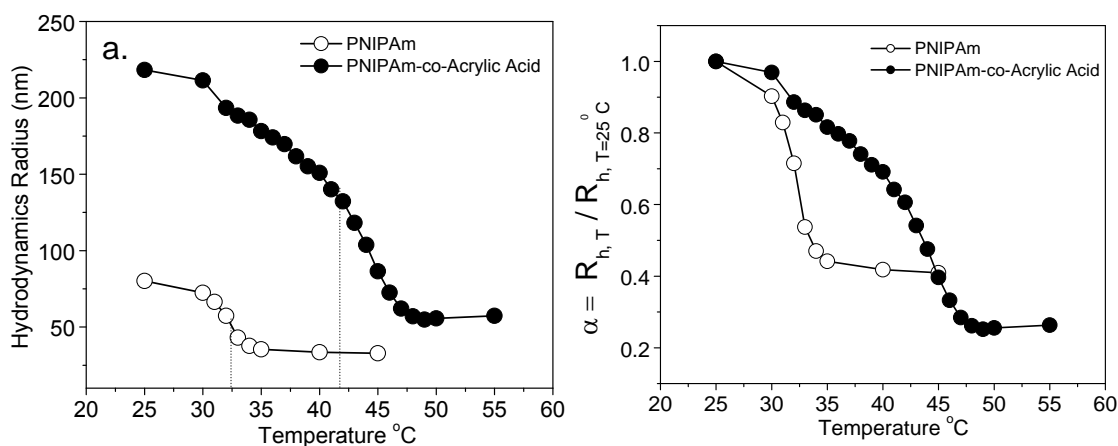


Figure 2.4: Effect of hydrophilic copolymer, on the a.) *VPTT*, b.) swelling capacity given by the swelling ratio $\alpha = R_{h,T} / R_{h,T=25^\circ\text{C}}$.

Figure 2.4(a) shows the phase transition for PNIPAm and PNIPAm-co-acrylic acid. Both the homo-polymer PNIPAm and the copolymer PNIPAm-co-acrylic acid have the same cross-linker density (~2% by weight of monomer); however the size of the copolymer is much larger than the homo-polymer. This is because of the larger number of hydrophilic groups in the copolymer are involved in hydrogen bonding. The *VPTT* shifts to higher temperatures, as higher energy is required to break the extra number and much stronger hydrogen bonds between water and the acidic groups -COOH on the acrylic acid comonomer. The presence of the extra -COOH groups also reduces the probability of hydrophobic interaction, thus shifting the *VPTT* to higher temperatures. The presence of the -COOH also increases the swelling capability of the microgels, as shown in Figure 2.4(b). The extent of swelling is usually measured by the swelling ratio $\alpha = R_{h,T} / R_{h,T=25^\circ\text{C}}$ where $R_{h,T}$ is the hydrodynamic radius at temperature T .

Similarly on copolymerisation of NIPAm with hydrophobic comonomers like the *t*-butyl-acrylate the *VPTT* can be reduced to as low as 24 °C (Zhang *et al.* 2007). In

some cases the $VPTT$ can be reduced to as low as 9 °C when the microgels are incorporated in self-assembled surfactant meso-phases of a non-ionic surfactant (Jijo *et al.* 2010). Thus a wide range of phase transition temperatures can be achieved by merely tuning the hydrophobic-hydrophilic balance. Other than these, there are many factors affecting the $VPTT$ such as the salt concentration (Wickramasinghe *et al.* 2010), effect of pressure (Kunugiet *al.* 1997) and added surfactant (Andersson and Maunu, 2006). However, the effect of molecular weight and polymer concentration does not affect the $VPTT$ (Fujishige *et al.* 1989).

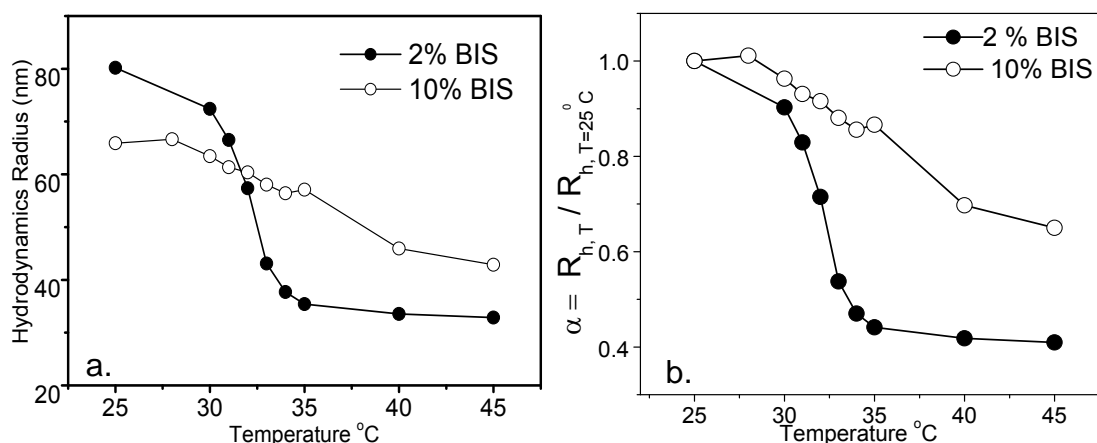


Figure 2.5: Effect of cross-linker content (methylene-bis-acrylamide) on the (a) $VPTT$ and (b) swelling capacity given by the swelling ratio $\alpha = R_{h,T} / R_{h,T=25^\circ C}$.

It is observed that a highly cross-linked microgel de-swells over a broad range of temperatures near the $VPTT$ in contrast to a sharp transition observed for microgels with low cross-linker density, see Figure 2.5(a). Increase in the crosslinking density reduces the swelling ability as shown in Figure 2.5(b).

2.3 Synthesis of PNIPAm microgels:

2.3.1 Materials

The monomer N-isopropylacrylamide (NIPAm; Acros Chemicals, recrystallized in a 3:1 mixture of toluene and hexane at 40 °C, initiator potassium persulfate (KPS; Sigma-Aldrich, recrystallized from deionised water), and cross-linker N,N-methylene-bisacrylamide (BIS; Sigma-Aldrich, recrystallized from methanol) were used for the polymerisation of NIPAm. Sodium dodecyl sulphate (SDS) as a stabilizer and Sodium

thiocyanate (SCN) salt (Sigma-Aldrich) required to screen the charges on the microgels were used as received.

Purification of Reactants:The monomer NIPAm was dissolved in a 3:1 mixture of Toluene and Hexane at 40 °C. The mixture was then recrystallized at 15 °C. The cross-linker BIS and the initiator KPS were recrystallized from HPLC grade methanol and deionised water respectively at 15 °C. The purified and dried crystals were then stored at 4 °C in a refrigerator.

2.3.2 Synthesis of small PNIPAm microgels

The polymerization reaction was carried out in a double-jacket cylindrical glass kettle reactor with baffles to ensure efficient stirring. The reaction mixture was stirred using an over-head stirrer (Heidolph Instruments) at 300 rpm. The temperature was maintained by water-circulating bath.

A 600 ml bottle of distilled, deionised water (Milli-Q Gradient A10, Millipore.) purged with nitrogen gas for 1 hour, was used for preparing the solutions. The purified reactants, monomer NIPAm (7.87 g), cross linker BIS (0.15 g) and stabilizer SDS (0.15 g) were mixed in 480 ml of N₂ purged water at 25 °C and stirred at 100 rpm for 30 mins under an inert atmosphere (continuous slow purging of Nitrogen). After complete mixing of these reactants, the temperature was increased to 70 °C and after about 5 mins waiting time for thermal equilibration, the initiator KPS (0.3 g of KPS in 20 ml N₂ purged Millipore water), was added to the reaction mixture. The reaction mixture changed from transparent to turbid in about 10 mins after addition of the initiator. Although the polymerisation completes within 10 – 15 mins, the reaction was allowed to proceed for 4 hours while stirring at 300 rpm to ensure complete conversion. After 4 hours, the temperature was then reduced to 25 °C and the product (microgels) stirred overnight at 100 rpm. The PNIPAm microgel dispersion was purified by dialysis against deionised water for about two weeks. This removes unreacted reactants and specially the surfactant from the polymer. Dialysis bags having a molecular weight cut-off of 10,000 g/mol was used for this purpose. The dialyzed sample was frozen using liquid nitrogen, and then freeze dried in a freeze drier (Heto Power Dry LL3000, Thermo- Electron Corp.) for 8 hours. The PNIPAm microgel in the form of powder was stored in a desiccator under vacuum. It is not necessary to freeze dry the microgels always; this method is used to avoid bacterial

growth which occurs in aqueous suspensions. Thus the freeze drying method should be followed only if the microgels have to be stored for a longer time.

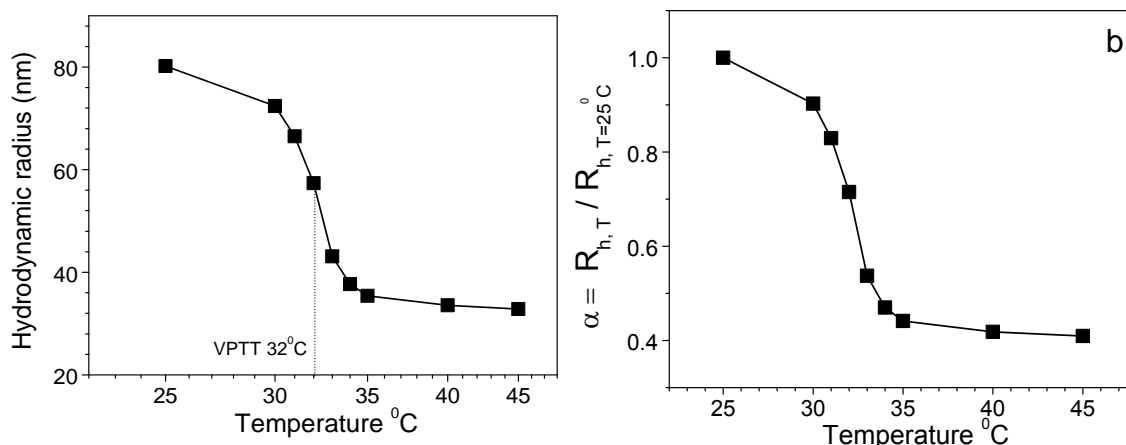


Figure 2.6:(a) Hydrodynamic size as a function of temperature for PNIPAm microgels with 2% cross-linker content showing the volume phase transition temperature ($VPTT$) = 32°C and (b) swelling capacity of these microgels given by the swelling ratio = $R_{h,T}/R_{h,T=25^\circ\text{C}}$.

This procedure gave microgels of hydrodynamic size ~ 80 nm in diameter at 25 °C. The volume phase transition for these microgels is shown in Figure 2.6(a) and confirms $VPTT$ at ~ 32 °C. The content of the cross-linker is 2% by weight of the monomer. This composition gives microgels which can swell ~ 2.5 times their size in the dry state as demonstrated in Figure 2.6(b), where the size of the microgels is normalised by the size of the microgel at $T = 25$ °C, i.e. in the fully swollen state.

2.3.3 Synthesis of larger size PNIPAm microgels

The synthesis of larger size PNIPAm microgels was done in the absence of the surfactant (Pelton *et al.* 1989). The cross-linker content was $\sim 6.7\%$ by weight of the monomer. This gives increased crosslinking density and thus increases the refractive index of the microgels and enhances the contrast when observed under an optical microscope. The synthesis protocol was similar to that mentioned in the previous section 2.3, except here the content of cross-linker was high and the polymerisation was done in the absence of the surfactant. Consequently, the purification of the microgels was easier. Two–three cycles of centrifugation and dispersion in water removes the unconverted reactants. However dialysis was also done for seven days to ensure complete removal of unreacted reactants. The suspension was not freeze

dried, instead, directly used to prepare concentrated stock solutions. This procedure gave large size microgels; $R_h \sim 412$ nm at 25 °C. The volume phase transition for these microgels shows a broad transition from a swollen state at 15 °C to a collapsed state at 40 °C as shown in Figure 2.7(a). The cross linker content of $\sim 6.7\%$ gives microgels that can swell ~ 1.5 times their size in the dry state, as demonstrated in Figure 2.7(b), where the size of the microgels is normalised by the size of the microgel at $T = 15$ °C, i.e. in the fully swollen state.

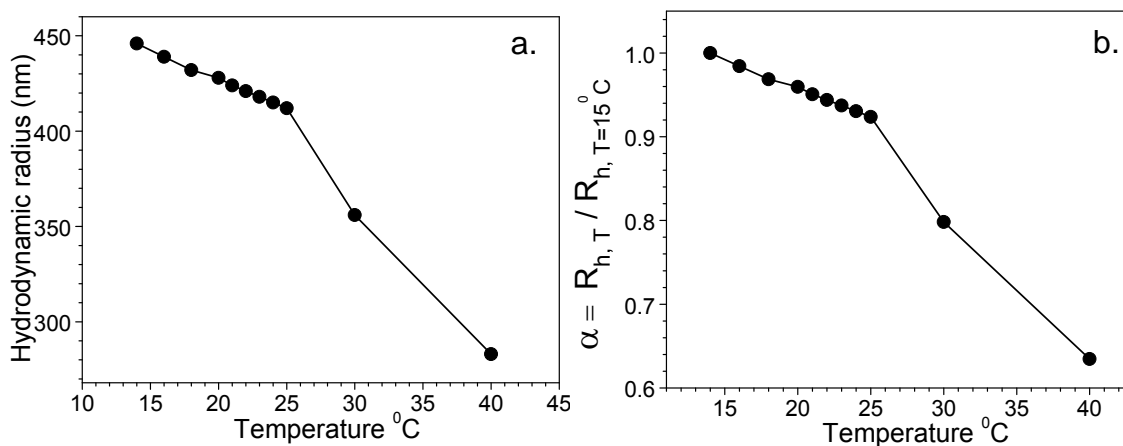


Figure 2.7: (a) Hydrodynamic size as a function of temperature for PNIPAm with 6.7% cross-linker content and (b) swelling capacity of these microgels given by the swelling ratio $\alpha = R_{h,T} / R_{h,T=25^\circ\text{C}}$.

2.4 Experimental Methods:

2.4.1 Static Light Scattering(SLS)

Light is scattered due to localised non uniformities in the medium through which it passes. These non-uniformities can be fluctuations of the dielectric constant or the refractive index 'n' in the medium occurring mostly by particles exhibiting Brownian motion (Brown, 1985). The schematic of a typical light scattering setup is shown in Figure 2.8.

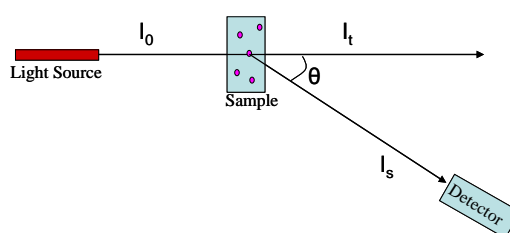


Figure 2.8: Schematic of a light scattering experiment.

A beam of light hits the particles in the sample and gets scattered in all directions. A detector measures the scattering intensity as a function of the scattering angle ' θ '. In a SLS experiment, the mean scattered intensity is measured as a function of the scattering vector q , which is experimentally available through a variation of the scattering angle θ .

The scattering vector ' q ' is defined as the difference between incident beam vector K_i and the scattered beam vector, K_f and depends on the refractive index ' n ' of the sample, angle between incident and scattered light θ and the wavelength of light λ as shown in equation 2.1

$$q = K_i - K_f = 4\pi n \frac{\sin \theta / 2}{\lambda} \quad 2.1$$

The scattering vector ' q ' is inversely proportional to the wavelength λ , thus smaller the λ of the incident radiation, larger the structures that can be investigated with a scattering experiment (Pecora, 1985).

The scattered intensity $I_s(q)$ is proportional to the scattering cross section $\sigma(q)$, which is a product of the particle form factor $P(q)$ and the static structure factor $S(q)$ (see equation 2.2). The former contains information about size and shape of the particles, while the latter gives information on the interactions between the particles.

$$\begin{aligned} I_s(q) &\propto \sigma(q) \\ I_s(q) &= Na^6 P(q) S(q) \end{aligned} \quad 2.2$$

where, N = the number of the particles and a = diameter of the particle. The total scattering cross section $\sigma(q)$ or the differential scattering cross section $d\sigma(q)/d\Omega$ is an important parameter, where Ω is the solid angle formed by the scattered intensity I_s to the incident intensity I_0 . This determines the dependence of the scattered intensity on the scattering vector q .

For a point scatterer,

$$\frac{d\sigma(q)}{d\Omega} = \frac{I_s(q) R^2}{I_0} = \frac{16\pi^2 \alpha^2}{\lambda^4} \quad 2.3$$

where R is the distance of the detector from the source of light, λ is the wavelength of the light used and α is the polarizability. It is important to note that the

differential cross-section and therefore, also the scattering intensity is proportional to λ^{-4} and to α^2 .

The static light scattering of dilute solutions is used to determine the average molecular weight M_w and radius of gyration R_g , whereas by measuring the scattering intensity for various concentrations, the second virial coefficient A_2 can be calculated. The Zimm equation is used to determine these important parameters of colloidal dispersion and/or polymer solutions and is shown in equation 2.4.

$$\frac{KC}{\Delta R(q, C)} = \frac{1}{M_w P(q)} + 2A_2 C = \frac{1}{M_w} \left(1 + \frac{q^2 R_g^2}{3} \right) + 2A_2 C \quad 2.4$$

where M_w = molar mass of the particle, $\Delta R(q)$ the excess Rayleigh ratio given by equation 2.5, K is the scattering wave vector given by equation 2.6 and $P(q)$ is the particle form factor which is described in the next section.

$$\Delta R(q) = \frac{I(q)_{\text{SOLN}} - I(q)_{\text{SOLVENT}}}{I(q)_{\text{REF}}} \quad 2.5$$

$$K = 4\pi^2 n^2 \frac{(dn/dC)^2}{N_A \lambda^4} \quad 2.6$$

where, n = refractive index of the solvent, C = particle concentration (mass/volume), dn/dC = refractive index increment, N_A = Avogadro's no. and λ = wavelength of the incident light.

Form factor $P(q)$:

The scattered intensity $I_s(q)$ from the particle is the superposition of the light scattered by all volume elements within a particle. Here interference effects due to the different optical path lengths from the volume elements to the detector results in the particle form factor $P(q)$, which is given by the scattering intensity $I_s(q)$ divided by the scattering intensity without interference effects in forward direction $I_s(q=0)$. Thus $P(q) = I_s(q)/I_s(q=0)$, decreases from unity at $q=0$ and shows an angular dependence, which is characteristic of the size and also the form of the particle.

When the particles are small compared to the wavelength λ of the light and for a small contrast between the particles and the solvent, the so-called 'Rayleigh scattering' takes place. The $P(q)$ can be calculated using the Rayleigh-Gans-Debye

(RGD) approximation (Bohren *et al.* 2004). The theory assumes that each of the small volume elements sees the same incident light wave.

$$P(q) = \left[\frac{1}{V} \int \exp(iqr') dv \right]^2 \quad 2.7$$

where $V = 4/3\pi R^3$ is the particle volume.

Evaluation of the integral after conversion to spherical co-ordinates gives

$$P(q) = \left[\frac{3}{(qR)^3} (\sin qR - qR \cos qR) \right]^2 \quad 2.8$$

Expanding the above expression in powers of q and using $R_{g,sphere} = \sqrt{3/5} R$ we get

$$P(q) = \exp \left[-(q^2 \langle R_g^2 \rangle) / 3 \right] \quad 2.9$$

This expression is known as the Guinier approximation which is used to determine the radius of gyration R_g which is a well-defined measure of size of any object as obtained from small q -scattering (i.e., $qR_g < 1$). Hence the plot of the corrected intensity or the excess Rayleigh ratio $\Delta R(q)$ versus q^2 or $\sin^2(\frac{\theta}{2})$ will yield a slope $R_g^2/3$. Thus by using the Guinier approximation R_g can be determined by a single concentration, rather than using equation which requires atleast three concentrations.

In case of microgels, which are soft particles and have heterogeneous internal structure, a modified form of RGD form factor is used and is given in equation 2.10 (Reufer *et al.* 2008). Microgels have a radial density gradient with a highly cross-linked core and a loosely cross-linked surface. Stieger and co-workers (2004) suggested the convolution of the density profile for a particle of radius R with a Gaussian of width σ , giving an effective radius of $R_{eff} \approx R + 2\sigma$. In the RGD approximation the scattering form factor is given by the following equation.

$$P(q) = [I(q)]^2; \quad 2.10$$

$$I(q) = 3 \exp \left[-(\sigma q)^2 / 2 \right] [\sin(qR) - qR \cos(qR)] / qR^3$$

Figure 2.9 shows the form factor for PNIPAm microgel suspensions at 30 °C, using the modified model used by Reufer *et al.* (2008). The root mean square radius $R \sim 331$ nm with $\sigma \sim 13$ nm giving the effective steric radius of $R_{eff} \sim 356$ nm.

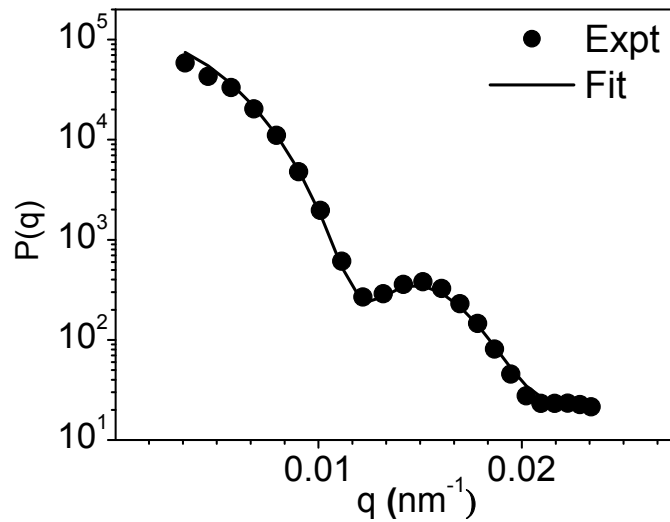


Figure 2.9: Particle form factor $P(q)$ as a function of scattering vector q for PNIPam microgels ($T = 30\text{ }^{\circ}\text{C}$).

Static Structure Factor:

The structure factor $S(q)$ describes the local structure based on the interactions between the individual particles in non-dilute suspensions. A superposition of the light scattered by all particles taking into account the interference reveals the static structure factor $S(q)$. Thus, static structure factor is a measure of the order in the system or the spatial correlation between particles. $S(q)$ is given by the following equation (Urban, 1999).

$$S(q) = \frac{1}{N} \sum_{i,j=1}^N \langle \exp i q (r_i - r_j) \rangle \quad 2.11$$

where the angular bracket denotes an ensemble average. For uncorrelated particles, e.g. in very dilute solutions, $S(q) = 1$ for all q . An expression for the local structure is the pair correlation function $g(r)$ which is related to the static structure and is given as follows

$$S(q) = 1 + \rho \int d^3 r e^{i q r} [g(r) - 1] \quad 2.12$$

In colloidal systems particles are in constant Brownian motion hence do not form perfectly regular lattices and have relatively weak interaction potentials compared to crystals formed by atoms. As a consequence, the static structure factor shows relatively broad peaks.

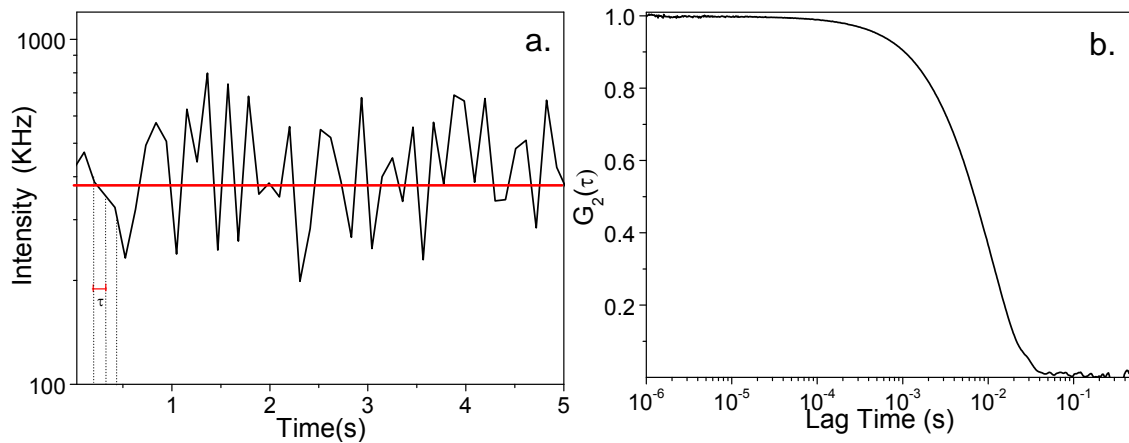


Figure 2.10: (a) Scattered intensity versus time in a dynamic light scattering experiment for PNIPAm microgel suspension and (b) Auto Correlation function $G_2(\tau)$, of a PNIPAm microgel suspension.

2.4.2 Dynamic Light Scattering (DLS)

Particles suspended in a liquid are constantly exhibiting Brownian motion (Brown, 1985). As a result, in a scattering experiment, the phase relations of the light scattered by different particles change randomly. The number of particles in the scattering volume also fluctuates. Both these effects lead to a fluctuation of the scattering intensity, see Figure 2.10(a), which contains information about the time scale of the movement of the Brownian particles, or more physically, their diffusion process in terms of a time correlation function (Berne and Pecora, 1976). The correlation function is given by a digital correlator which is a signal comparer. The intensity of a signal is compared with itself at a particular point in time t and a small time later $t + \tau$. If the intensity of signal at time t is compared to the intensity a very small time later ($t + \delta t$), there will be a strong correlation between the intensities of two signals. Thus the scattering intensity autocorrelation function $G_2(\tau)$ and the electric field autocorrelation function $G_1(\tau)$ are given by equation 2.13

$$G_2(\tau) = \frac{\langle I(t) \cdot I(t + \tau) \rangle}{\langle I(t) \rangle^2}; G_1(\tau) = \langle E(t) \cdot E(t + \tau) \rangle \quad 2.13$$

where $G_2(t) = \langle I \rangle^2 + |G_1(t)|^2$ is called the Siegerts relation (Berne and Pecora, 1976). However for a fluctuating signal, the correlation reduces with time. In the conventional DLS experiment the electric field autocorrelation function $G_1(\tau)$ is given by equation 2.14. The Figure 2.10(b) shows the correlogram, i.e. correlation

function, which decays with time. The auto correlation function is related to the translation diffusion coefficient by equation 2.14

$$G_1(\tau) = \exp(-q^2 D_t(\tau)) \quad 2.14$$

The size of a particle is calculated from the translational diffusion coefficient by using the Stokes- Einstein equation 2.15;

$$d_h = \frac{KT}{3\pi\eta D_t} \quad 2.15$$

where, d_h = hydrodynamic diameter, D_t = translational diffusion coefficient, k = Boltzmann's constant, T = absolute temperature and η = solvent viscosity.

Both SLS and DLS techniques discussed in the previous sections assume that the light is scattered by a single scattering event i.e., multiple scattering is negligible. However, in real situations this assumption is valid, only if the sample is very dilute (typically 10^{-5} to 10^{-2} wt %). The study of concentrated (turbid) suspensions is significant from the industrial as well as fundamental research view point. Additional averaging due to multiple scattering occurs both in static as well as in dynamic light scattering. The static experiment shows a shift of scattered intensity towards larger scattering angles. The dynamic experiment shows additional spectral components at higher frequencies. Both experiments show a decreased resolution (Schatzel, *et al.* 1990). Thus investigation or characterization of turbid systems cannot be achieved by conventional static or dynamic light scattering methods.

For this purpose, various techniques and methods like cross-correlation scheme (Pusey, 1999), the three dimensional dynamic light scattering (3DDLS) (Urban and Schurtenberger, 1998; Urban *et al.* 2000), use of thin flat cells (Medebach *et al.* 2007) etc. has been developed. Recently, the diffusing wave spectroscopy (DWS) has been used to analyse and characterize turbid media (Weitz and Pine, 1992). In addition to simple particle size measurements, it serves as a micro-rheological tool to determine viscoelastic properties without mechanically perturbing the sample (Mason and Weitz, 1995). In this report, the DWS technique is used to characterize the highly concentrated suspension of PNIPAm microgels and will be discussed in detail in the succeeding section.

2.4.3 Diffusing Wave Spectroscopy (DWS)

DWS is very similar to conventional DLS; both detect the intensity of speckle spot of the scattered light and a measurement of its temporal fluctuation. However, conventional DLS is restricted to single scattering limit. In this limit the characteristic decay time τ , obtained from $G_2(\tau)$ is related to the dynamics of the medium through a lengthscale set by the inverse of scattering wave vector, q^{-1} . The movement of the scatterers at lengthscales corresponding to q^{-1} leads to change in the path length of scattered light by one wavelength. This results in the phase change of the detected light by 2π and hence to change intensity of the scattered light to obtain meaningful information about the dynamics of the medium from this characteristic time-scale, knowledge of the length scale set by q^{-1} is required. A single speckle mode of scattered light is detected and the fluctuations are recorded over a time much longer than the relaxation time. However, the time averaging scheme is not applicable to rigid non-ergodic systems where the time average and spatial average correlations are not same.

In DWS the light undergoes a very large number of scattering events. In this limit, the direction of light is totally randomized. In this case the propagation of light and the effect of dynamics of the scattering medium can both be treated with statistical approximation. The total path length of the scattered light through the sample must change by one wavelength to cause a phase change and thus the fluctuation in intensity. Therefore each scatterer in the path needs to move only a fraction of the wavelength of the incident light. To calculate the temporal autocorrelation function in DWS entails two fundamental approximations. The first approximation is that the light should diffuse, such that the path of each scattered photon, which is scattered very large number of times, can be described as a random walk. The second approximation is that the individual scattering events are approximated by contribution of an average scattering event. This is because each photon is scattered a large number of times and the details of individual scattering events play a small role. Within the diffusion approximation, the diffusion coefficient (D) for propagation of light is given as, $D = v l^*/3$, where v is the speed of light in medium and l^* is the transport mean free path in the medium. It is the length that a photon must travel before its direction is completely randomized. This length is typically larger than the scattering mean free path l ; the length that a photon must

travel before it is scattered a single time i.e. $l^* > l$. This implies that the sample required for the DWS measurement should be sufficiently turbid. There is restriction on colored samples as there will be problems of absorption (Weitz and Pine, 1992). In the conventional DLS experiment the autocorrelation function is given by the following equation.

$$G_1(\tau) = \exp(-q^2 D(\tau)) = \exp(-q^2 \langle \Delta r^2(\tau) \rangle) / 6 \quad 2.16$$

where, $q = \left(\frac{4\pi n}{\lambda}\right) \sin\left(\frac{\theta}{2}\right)$ is the scattering vector, θ is the scattering angle, n is the refractive index of the medium, λ is the wavelength of incident light and $\langle \Delta r^2(\tau) \rangle$ is the mean square displacement. This is obtained from the measured intensity autocorrelation function using the Siegert relation as explained earlier. In case of DWS, the field autocorrelation function at a delay time τ is given by the following equation.

$$G_1(\tau) \propto \int_0^\infty P(s) \exp\left[-K_0^2 \langle \Delta r^2(t) \rangle \frac{s}{3l^*}\right] ds \quad 2.17$$

where $P(s)$ is the probability of light traveling a path of length s , and is determined by solving the diffusion equation for the propagation of light for the relevant geometry with the correct boundary conditions and $K_0 = 2\pi n/\lambda$ is the wave vector of the incident light. The transport mean free path of the light (l^*), is a characteristic of the sample itself and reflects the length the light must travel before its direction is randomized. The transport mean free path of each sample is obtained by measuring the ratio of the intensity of the light transmitted through the sample to that transmitted through a reference sample whose value of l^* is known, using identical optical geometries. When the signals are ergodic, the time averaged intensity correlation function $G_2(\tau)$ is measured and the field correlation function is obtained using the Siegert relation. However, for samples where the signal is no longer ergodic; the time averaged correlation functions do not represent true ensemble-averaged data. In these cases, we employ an averaging technique to obtain the true ensemble-averaged correlation function from the measured data i.e from the $G_2(\tau)$ since it is not easy to calculate the $G_1(\tau)$ using the Siegert relation. Thus DWS is always represented by $G_2(\tau)$ and DLS by $G_1(\tau)$. In effect, the MSD is calculated by using the measured mean free path and numerically inverting the field correlation function as shown in equation 2.17. The MSD of the particles

depends on the viscoelastic behavior of the surrounding non-ergodic media. If the material is purely viscous, the probeparticles will diffuse through it and the MSD will increase linearly with time $\langle \Delta r^2(t) \rangle \geq 6Dt$. By determining the diffusion coefficient D , one can calculate the viscosity of the material, $\eta = K_B T / 6\pi D a$; where 'a' is the radius of the beads. By contrast, the motion of the probe particles in an elastic medium will be constrained and the MSD will reach an average maximum plateau value $\langle \Delta r_{max}^2 \rangle$. Thus, for a viscoelastic material the MSD have slopes of one at short time scales indicating predominantly viscous behavior, while at longer time scales the slopes are closer to zero reflecting an elastic response as expected for solid samples Figure 2.11. The MSD reaches an average maximum plateau value $\langle \Delta r_{max}^2 \rangle$ seen at higher lag times due to the constraints from the elasticity of the system.

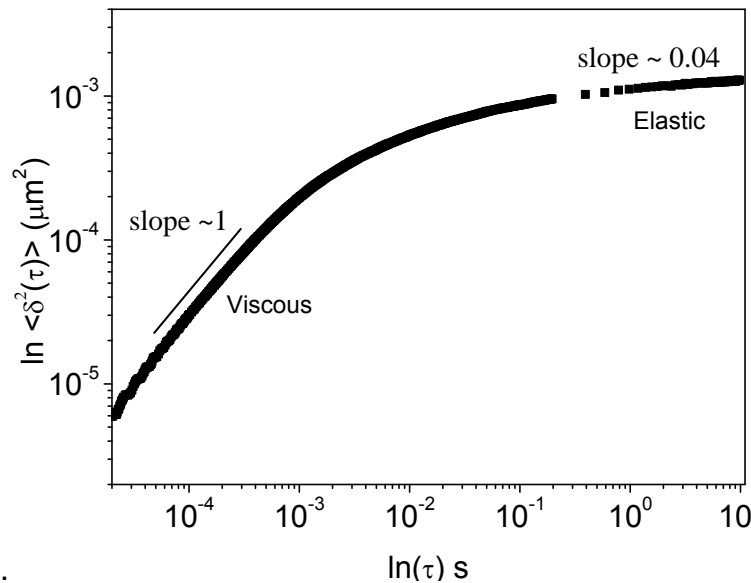


Figure 2.11: Mean square displacement as a function of lag time for a concentrated suspension of PNIPAM microgel suspension $T=25^\circ\text{C}$, $\rho=2.3 \text{ no}/\mu\text{m}^{-3}$.

By equating the thermal energy $K_B T$ with the elastic energy $\frac{\kappa \langle \Delta r_{max}^2 \rangle}{2}$, where κ is the effective spring constant that characterizes the elasticity of the surrounding medium, an expression for the spring constant $\kappa = \frac{K_B T}{\langle \Delta r_{max}^2 \rangle}$ can be obtained. The elastic modulus G' is related to the spring constant by a factor of length, which is the radius 'a' of the tracer particle. Using such an energy balance argument, a relation between the elastic modulus and the MSD is obtained as

$$G' = \frac{K_B T}{\langle \Delta r_{\max}^2 \rangle a} \quad 2.18$$

The time dependent MSD can be used to calculate the storage and loss modulus by using the Langevin Equation and Laplace transform as follows (Mason and Weitz, 2000). The Langevin Equation gives a force balance on the particles,

$$m \dot{v}(t) = f_R(t) - \int_0^t \zeta(t-\tau) v(\tau) d\tau \quad 2.19$$

where m is the particle mass, $v(t)$ is the particle velocity, $f_R(t)$ represents random forces acting on the particle which includes contribution from both direct forces between particles and the stochastic Brownian forces. The integral term represents the viscous damping of the fluid and incorporates a generalized time-dependent memory function $\zeta(t)$ given by the fluctuation dissipation theorem

$$\langle f_R(0) f_R(t) \rangle = K_B T \zeta(t) \quad 2.20$$

It is further assumed that the microscopic memory function is proportional to bulk viscosity of fluid hence $\tilde{\eta}(s) = \frac{\zeta(s)}{6\pi a}$ where 's' represents frequency in the Laplace domain. Thus in purely viscous limit, the modulus is given as follows,

$$G(s) = s\eta(s) = \frac{s}{6\pi a} \left[\frac{6K_B T}{s^2 \langle \Delta r^2(s) \rangle} - ms \right] \quad 2.21$$

The inertial second term in the bracket is usually negligible except at very high frequencies. The equation above represents a generalized frequency dependent form of Stokes Einstein relation. Thus by the DWS experiment we can get the correlation functions from which we calculate the mean squared displacement of the particles which is then used to determine the viscoelastic moduli of the nonergodic media. In the next section the experimental set up of the typical DWS is described.

Experimental Set up:

Figure 2.12 shows the schematic diagram of a typical multi-speckle DWS experimental set up by Zakharov *et al.* (2006). This particular set up works on the principle of a two-cell echo technique that is essential for better ensemble averaging. This technique is useful for slowly relaxing or nonergodic samples for which the traditional time average scheme is not applicable. For such samples, the ensemble average is usually obtained by rotating the sample cell and measuring the scattering

intensity of single speckle at different positions in the sample. Instead of rotating the sample cell, which would mechanically disturb the sample, a two cell technique was employed in which the laser was passed through an ergodic suspension before passing through the non ergodic sample cell (Romer *et al.* 2000). In the DWS set up by Zakharov *et al.* (2006) instead of the ergodic sample as the secondary cell, a rotating ground glass which acts a rotating diffuser is used. This allows for multiple speckle analysis of the scattered radiation in a short time, thus allowing for an efficient ensemble averaging without an additional time averaging scheme. This experimental scheme also provides large range of correlation times which is useful for slowly relaxing systems.

As shown in Figure 2.12(a) laser is passed through a circular ground glass before it passes through the sample cell. The ground glass creates speckle pattern with a Gaussian optical field. The transmitted beam from the ground glass is used to illuminate the sample with a spot size of diameter ~ 5 mm which illuminates a larger area of the sample for better statistics. The light scattered from the sample is then collected by a single mode optical fiber and analyzed by a photo multiplier tube (PMT) and a digital correlator.

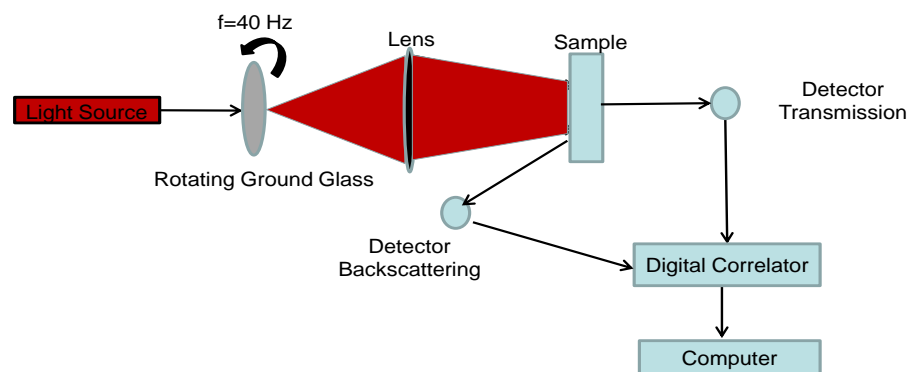


Figure 2.12: Schematic for a diffusing wave spectroscopy set up.

To implement the echo technique, scattering signal from a rigid sample with no internal motion was collected. For this purpose a 2 mm Teflon slab was used. The ground glass was rotated at a frequency $f_r = 50$ Hz. Any scattering signal detected by the Teflon block is from the motion of the rotating ground glass. The measured intensity correlation function is simply the product of the intensity correlation function of the sample and the rotating ground glass (equation 2.22)

$$[G_2(\tau) - 1]_{\text{measured}} = [G_2(\tau) - 1]_{\text{sample}} [G_2(\tau) - 1]_{\text{Teflon}} \quad 2.22$$

2.4.4 Rheology:

Rheology is the science of flow and deformation of matter. The study of the flow behavior of material is important while studying the structure property relations particularly for viscoelastic materials. On a laboratory scale, rheological measurements are done with the help of rheometers wherein a well-defined deformation, shear or extensional, can be imposed and the resulting stress response of the fluid is measured. This is called strain-controlled rheometry. Alternatively, a shear stress or an extensional stress is imposed on the fluid and the corresponding strain response is measured. This is called stress-controlled rheometry. The imposed flow could be a steady shear flow or a dynamic oscillatory flow. In this work we have particularly used the oscillatory strain measurements. Most often the linear viscoelastic fluids are characterized by imposing small amplitude oscillatory strain which gives important material properties i.e. storage/elastic modulus G' and the loss/viscous modulus G'' .

2.4.4.1 Small amplitude oscillatory shear SAOS

When a sinusoidal shear strain of the form $\gamma(t) = \gamma_0 \sin(\omega t)$ of small amplitude γ_0 and frequency ω is imposed on a viscoelastic fluid, the stress response is composed of in-phase and out-of-phase components and is given by

$$\sigma(t; \omega) = \gamma_0 [G'(\omega) \sin(\omega t) + G''(\omega) \cos(\omega t)] \quad 2.23$$

where G' is the in-phase component called as “storage” modulus and G'' is the out-of phase component known as the “loss” modulus and are functions of the angular frequency (Ferry, 1980). They represent respectively the stored and dissipated components of the energy input into the fluid by the imposed mechanical deformation. A particular experiment carried out in this work is called the strain-sweep experiment in which increasing amplitude of the sinusoidal strain is imposed on the sample, and the evolution of its response in terms of the G' and G'' is measured at a constant frequency. If $G' > G''$ then the fluid is predominantly elastic, and if the $G' < G''$ then the response is predominantly viscous. Change from a viscous to an elastic character is commonly used to track gelation or structural arrest due to topological

constraints, especially in concentrated colloidal suspensions. Another routinely carried test in the linear viscoelastic regime is the frequency sweep test. In this test the sample is subjected to increasing frequency of oscillatory shear at a constant small amplitude strain (γ_{LVE}). This test gives the spectrum of relaxation times in the system under quiescent conditions. A detailed description of both the strain sweep and frequency sweep experiments are given later in Chapter 4 and Chapter 5 respectively.

2.4.4.2 Large amplitude oscillatory shear (LAOS)

Linear viscoelastic response is limited to small strains or strain rates. The shear rates in the processing of materials on an industrial scale are usually large. Apart from their obvious utility in industrial processes, investigation of the large shear rheological behaviour are of fundamental interest in investigating structure-property relation which decide the final mechanical performance of the material. At large strains the stress generated in the material is related to the applied strain in a non-linear manner. Consequently, the resultant stress from a large-amplitude oscillatory shear (LAOS) contains higher harmonics which may be interpreted in terms of harmonic moduli G'_n and G''_n (subscript n refers to the n^{th} harmonic). These are functions of both the strain amplitude and the angular frequency,

$$\sigma(t; \omega, \gamma_0) = \gamma_0 \sum_{n=1,3,5,\dots} \left[G'_n(\omega, \gamma_0) \sin(n\omega t) + G''_n(\omega, \gamma_0) \cos(n\omega t) \right]$$

2.24

The non-linear response of a soft solid has characteristic yielding feature showing a peak in the G'' in a strain sweep experiment. We have investigated the yielding in soft colloidal glasses in particular the frequency dependence of the G'' peak, in Chapter 5.

2.4.4.3 Strain Rate Frequency Superposition (SRFS)

The SRFS technique was recently proposed by (Wyss *et al.* 2007), to probe the structural relaxation in soft materials by performing a frequency sweep at a constant strain rate. In this technique during a frequency sweep experiment the strain was also swept simultaneously to maintain a constant strain rate. The author showed that in such a constant strain-rate frequency sweep measurement, G'_1 and G''_1 could be

superimposed onto master curves. The utility of the SRFS procedure is that by increasing the strain rate amplitude, the crossover frequency can be shifted to a range where it may be directly probed. The strain rate decreases the structural relaxation time and thus makes it observable in the experimentally accessible frequency scale. The authors showed that the structural relaxation time τ_α of the material showed an inverse power-law on the strain-rate amplitude $\dot{\gamma}$, $\tau(\dot{\gamma}) \propto \dot{\gamma}_0^\nu$ where $\nu > 0$ is the exponent in the power law.

In Chapter 4 we investigate the SRFS response under LAOS for various soft solids. We explore whether the SRFS principle is applicable to the higher harmonic viscoelastic moduli also.

2.4.4.4 Stress relaxation

The SRFS technique helps to probe the shear induced structural relaxation in soft solids. In absence of the large shear deformation the long-time relaxation of soft materials can be probed by the stress relaxation measurement. In this test the material is subjected to a small constant step strain (γ_{LVE}) and the relaxation of the stress in the material is measured. The stress is related to the relaxation modulus by equation 2.25. The relaxation modulus $G(t)$ can be fit to a modified Maxwell model (Ferry, 1980) with a non-zero long-time value G_0 , characteristic of a glassy system

$$G(t) = G_0 + \sum_k G_k e^{-t/\lambda_k} \quad 2.25$$

$$G'(\omega) = G_0 + \sum_k \frac{G_k \lambda_k^2 \omega^2}{1 + (\lambda_k^2 \omega^2)}; G''(\omega) = \sum_k \frac{G_k \lambda_k \omega}{1 + (\lambda_k^2 \omega^2)} \quad 2.26$$

where G_k and λ_k are the modulus and relaxation time, respectively, for each individual mode. The Laplace transform of $G(t)$ gives the frequency dependent dynamic moduli given by equation 2.26.

Chapter 3

Dynamics of Soft Colloidal Glasses investigated by Diffusing Wave Spectroscopy

In this chapter we investigate dense microgel suspensions of PNIPAm close to and above the glass transition volume fraction φ_g , by using diffusing wave spectroscopy (DWS). The PNIPAm microgel changes its size as the temperature is changed. This thermoresponsive nature, allows precise tuning of volume fraction of the suspension by changing temperature. To suppress crystallization a bi-disperse microgel suspension was used. The decay of the temporal autocorrelation function $G_2(\tau)$, for different values of effective volume fraction φ_{eff} , were observed. The $G_2(\tau)$, showed complex dynamics at volume fractions close to one. We attribute this complex dynamics to the dense core/soft brushlike surface of the microgels, where the latter interpenetrates at $\varphi_{\text{eff}} \sim 1$.

3.1 Introduction

Although investigation of model hard sphere colloidal suspensions is of technological and fundamental interest, many complex fluids contain soft colloidal particles that interact via soft repulsive potential. Similar to the hard sphere colloidal glasses ($\varphi \sim \varphi_g$), the soft colloidal glasses (SCG) also show two characteristic relaxation times t_α and t_β . However, there can be further complexity in the interaction potential of soft colloids, like an added attractive or repulsive part to the repulsive interaction. Complex interactions give rise to rich dynamical phenomena in arrested states like glasses and gels. Zaccarelli and Poon (2009), have shown a logarithmic decay impending to a two-step decay in the self-diffusive autocorrelation function where there are attractive and repulsive interactions at longer and shorter length scales respectively. Chaudhuri *et al.* (2010) and Saw *et al.* (2011) have observed a double plateau where there is a competition between gelation and glass transition. For star polymer colloids, an extra plateau in the intermediate scattering function was

attributed to the formation of star clusters formed due to interpenetration of star arms at high volume fractions (Loppinet *et al.* 2001). Recently, it has been shown that a double plateau could also be observed due to two repulsive potentials at different length scales (Das *et al.* 2013; Sperl *et al.* 2010).

In this chapter, we investigate dense suspensions of bi-disperse PNIPAm microgels at $\varphi_{\text{eff}} \leq 1$. Similar to the stars, the loosely crosslinked brushlike surface of PNIPAm microgels can be expected to interpenetrate at high volume fractions (Stieger *et al.* 2004; Rahola, 2007). The interparticle potential of PNIPAm microgels measured in dilute suspensions, can be changed from soft repulsive to attractive, below and above the V_{PTT} , respectively (Wu *et al.* 2003; Huang and Hu, 2007; Stieger *et al.* 2004). All experiments were done at $T < V_{PTT}$, where the microgels are known to interact via soft repulsive potential. Although various studies have considered the heterogeneous structure of the microgels, the origin of the interparticle potential at high volume fraction and its relation to the structure of the suspension, is not yet fully understood. Thus, investigation of this complex system may help in providing essential information for theoretical studies on the determination of interparticle interactions.

The microgels used here are of the order of micron size and have a high crosslinking density (6.7 % by weight of monomer), thus their solutions are highly turbid. Traditional light scattering techniques cannot be used for such samples due to multiple scattering that results in weak scattered radiation. Thus in this work, DWS is used to interrogate the structure and dynamics of the dense PNIPAm microgel suspensions. We observe the decay of the temporal autocorrelation function $G_2(\tau)$ for various values of φ_{eff} , which is controlled by varying the temperature. We find that the core-shell morphology of the microgel results in additional relaxations in the system indicated by a two-step decay of $G_2(\tau)$. As mentioned earlier, except for the system interacting via repulsive potentials at different length scales (square shoulder potential) (Das *et al.* 2013; Sperl *et al.* 2010), such additional relaxations are usually observed for attractive glasses or gels at a higher density (Zaccarelli and Poon, 2009; Chaudhuri *et al.* 2010), where there is a combination of attractive and repulsive potentials at different length scales. For our system, the interactions between particles are ruled only by the excluded volume effect and we do not find the presence of any attractive interaction. Further, we not only observe a double decay, but the temporal autocorrelation function has mixed characteristics of gel and glass. The observation

of a constant evolution of the plateau is similar to that found in gels, however, the length scale obtained from the plateau value here is much smaller than the size of the microgel, which is a characteristic of a glassy system.

3.2 Experimental procedures:

3.2.1 Synthesis and characterization of microgels

The synthesis was done by precipitation polymerization in the absence of the surfactant (refer section 2.3.3 for a detailed procedure).

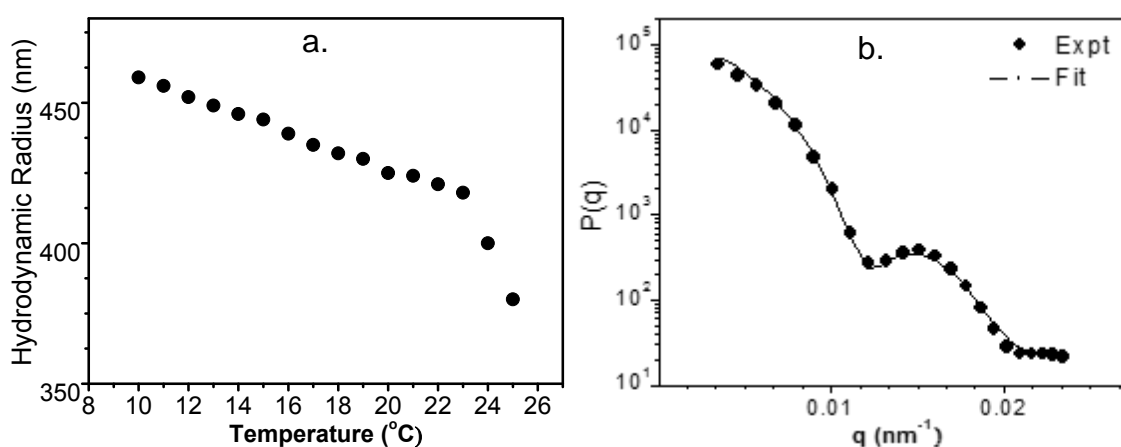


Figure 3.1: (a) Hydrodynamic radius as a function of temperature for large size PNIPAm microgels and (b) Particle form factor $P(q)$ as a function of scattering vector q for bidisperse PNIPAm microgels ($T = 10$ °C) from a SLS measurement.

Characterisation of microgels: We have used *SLS* and *DLS* experiments to measure the hydrodynamic radius R_h , geometric radius R and radius of gyration R_g , which represent the radial density gradients in the microgel, see Figure 3.2. For the sake of simplicity, we assume that R_g represents the size of the highly cross-linked impenetrable inner core region, R represents the size of a slightly lower cross-linked outer core region, and R_h represents the radius of the loosely cross-linked brush-like surface of the microgel. All measurements are done on dilute suspensions of microgels of two different sizes as well as on mixtures of these two sizes. In case of the latter, average values of the three radii are measured. The hydrodynamic radius R_h of the microgel is measured using the *3DDLS* set up (LS Instruments, Switzerland). The R_h , as a function of temperature is shown in Figure 3.1(a).

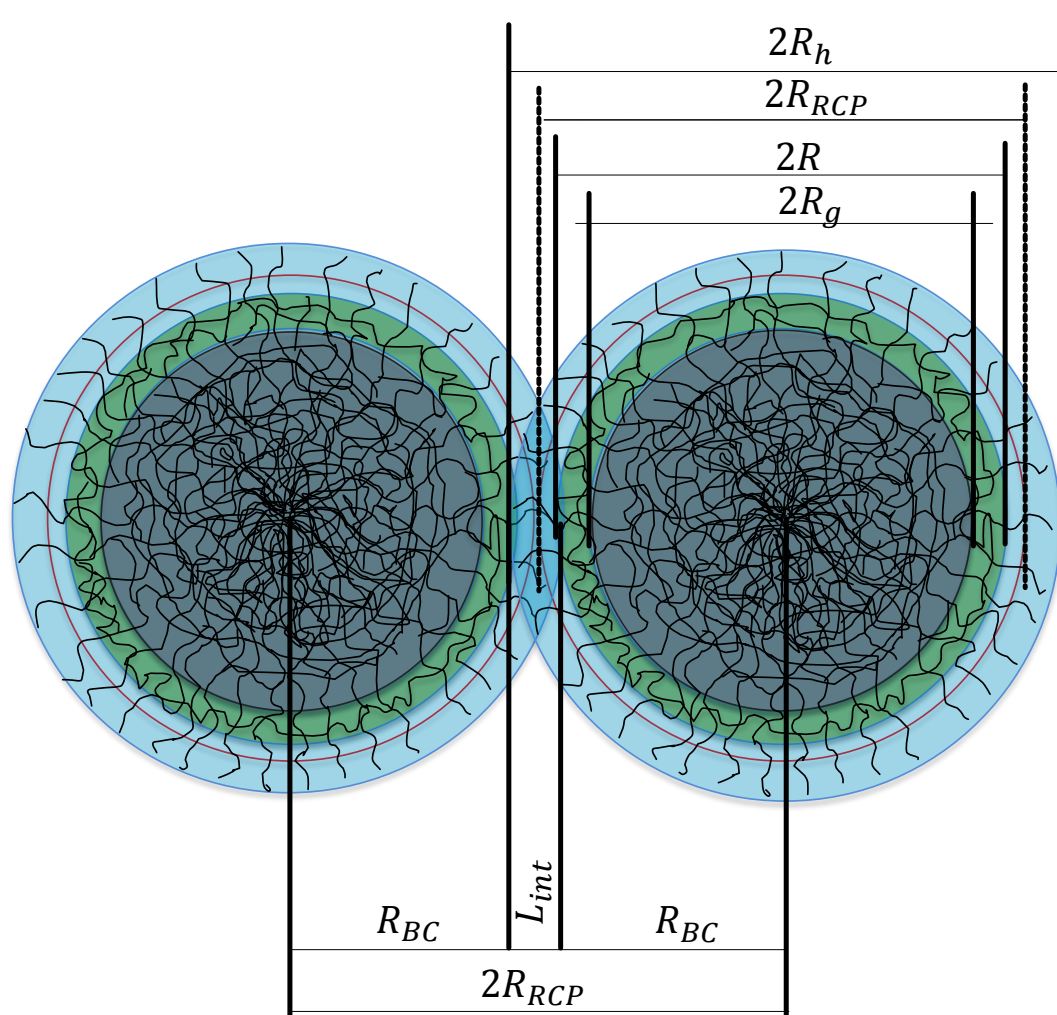


Figure 3.2: Schematic of the heterogeneous morphology of a microgel (drawn to scale) exhibiting various length scales in the system at high volume fraction ($\phi_{\text{eff}} \sim 0.98$), at 15 °C for $\rho = 2.67 \mu\text{m}^{-3}$. The highly crosslinked inner core R_g , the less crosslinked outer core region R and the loosely crosslinked brush region R_h are shown by the grey, green and blue circles respectively. The red circle represents R_{RCP} , the radius required for random close packing fraction ($\phi_{\text{RCP}} \sim 0.63$) in hard spheres at $\rho = 2.67 \mu\text{m}^{-3}$. L_{int} is the interpenetration region, $2R_{\text{RCP}}$ is the center-to-center distance and R_{BC} , is the distance between the brush of a microgel and the center of its neighbor.

The radius of gyration R_g was determined from SLS measurements in the low q region ($qR_g < 1$) using the Guineir approximation (see section 2.4.1). From the q dependent SLS data we determined the geometric radius R by fitting the corrected intensity $\Delta R(q)$, to a modified RGD form factor for sphere as given in equation 2.10 (Reufer *et al.* 2008). Figure 3.1(b) shows the form factor $P(q)$ for the bidisperse microgel suspension at 10 °C. The R_h , R and R_g were determined for few temperatures below and above the V_{PTT} . For other temperatures they were interpolated from the graph

of size vs. temperature. The measured and calculated size R_h , R and R_g for different temperatures are tabulated in Table 3.1 and schematically represented in Figure 3.2.

3.2.2 Preparation of dense suspensions

The synthesis when done without the surfactant gives large size particles ($\sim 1 \mu\text{m}$ in diameter) which can be seen under an optical microscope. The high crosslinker content (6.7 % by weight of the monomer) increases the crosslinking density and enhances the refractive index difference between the microgels and the suspending water phase. This in turn enhances the contrast when observed under the microscope. PNIPAm microgels are known to be highly monodisperse and thus tend to crystallize at volume fraction ~ 0.54 (Gao and Hu, 2002). Here, crystallization of the dispersion was suppressed by using a bi-disperse microgel suspension where the size difference of the two microgels is 20 %, and the ratio of their number densities is $\frac{\rho_{\text{small}}}{\rho_{\text{big}}} = 2.7$ (Eckert and Bartsch, 2006).

The hydrodynamic radii of the two microgels ($R_{h,\text{small}} = 340 \text{ nm}$ and $R_{h,\text{big}} = 510 \text{ nm}$ at 20°C), were determined by DLS. The number density ρ was determined by counting the number of microgels in a fixed volume. This was done by using a confocal microscope, where the 2D projections obtained from a 3D image were analyzed. Large numbers of sample volumes were scanned at different positions for good statistics. The number density of smaller microgels in their stock solution was determined to be $\rho_{\text{small}} = 2.25 \mu\text{m}^{-3} \pm 3.75 \%$ and that of the larger size particles in their stock solution was $\rho_{\text{big}} = 1.72 \mu\text{m}^{-3} \pm 3.8\%$. A stock solution containing a mixture of small and large microgels ($\frac{\rho_{\text{small}}}{\rho_{\text{big}}} = 2.7$) was prepared by mixing pre-determined volumes of the two individual stock solutions. This bidisperse stock solution of known number density and volume fraction of microgels was further used to prepare suspensions with number densities 2.08, 2.3 and $2.67 \mu\text{m}^{-3}$. This was done by centrifugation followed by removing water from the clear supernatant. All solutions were prepared in the presence of 10 mM NaSCN salt to screen the surface charges from the microgels.

Table 3.1: Various length scales in the heterogeneous morphology of PNIPAm microgel at high volume fractions: the impenetrable inner core of radius R_g , the outer core of intermediate crosslinked region of radius R and the loosely crosslinked brush of radius R_h . The radius for random close packing in hard spheres at a given number density is given as R_{rcp} . The interpenetration length is L_{int} and the brush to core distance R_{BC} is tabulated below at different temperatures with their corresponding ϕ_{eff} .

$\rho=2.08$ no./ μm^3 T ($^{\circ}\text{C}$)	ϕ	R_h	R	R_g	R_{rcp} for hard sphere ϕ 0.64	$L_{int} =$ $2(R_h - R_{rcp})$	$R_{BC} =$ $2 R_{rcp} - R_h$	Cage size = (MSD) $^{0.5}$	extra plateau
25	0.48	380	337	285	418	-76	456	liquid	-
20	0.67	425	346	284.7	418	14	411	liquid	-
18	0.7	432	349	286	418	28	404	47	-
16	0.74	439	356	299	418	42	397	33	-
15	0.76	444	357	303	418	52	392	25	-
14	0.77	446	362	323	418	56	390	20	-
13	0.79	449	367	325	418	62	387	16	-
12	0.8	452	372	327	418	68	384	15	-
11	0.83	456	367	330	418	76	380	13	8.5
10	0.84	459	382	333	418	82	377	12	8
$\rho=2.3$ no./ μm^3 T ($^{\circ}\text{C}$)	ϕ	R_h	R	R_g	R_{rcp} for hard sphere ϕ 0.64	$L_{int} =$ $2(R_h - R_{rcp})$	$R_{BC} =$ $2 R_{rcp} - R_h$	Cage size = (MSD) $^{0.5}$	extra plateau
22	0.72	421	334	289	404	34	387	48	-
21	0.73	424	343	288	404	40	384	46	-
20	0.74	425	346	284	404	42	383	18	-
19	0.77	430	348	285	404	52	378	14	-
18	0.78	432	349	286	404	56	376	11	-
15	0.84	444	357	303	404	80	364	9	4.6
12	0.89	452	372	327	404	96	356	7	3.2
$\rho=2.67$ no./ μm^3 T ($^{\circ}\text{C}$)	ϕ	R_h	R	R_g	R_{rcp} for hard sphere ϕ 0.64	$L_{int} =$ $2(R_h - R_{rcp})$	$R_{BC} =$ $2 R_{rcp} - R_h$	Cage size = (MSD) $^{0.5}$	extra plateau
24	0.68	392	342	282	385	14	378	35	-
23	0.77	410	345	293	385	50	360	25	-
22	0.79	413	334	289	385	56	357	18	-
21	0.8	416	343	288	385	62	354	13	-
20	0.83	420	346	284.7	385	70	350	10	-
17	0.87	427	353	292	385	84	343	7	4.2
16	0.89	431	356	299	385	92	339	6.5	3.5
15	0.93	436	357	303	385	102	334	6.2	2.8

3.2.3 DWS experimental protocol

Microgel dispersions of different number densities $\rho = 2.08, 2.3, \text{ and } 2.67 \mu\text{m}^{-3} \pm 5\%$, were filled in 5 mm square sample cuvettes of borosilicate glass. The cuvettes were stoppered by teflon caps and sealed with paraffin film and teflon tape to avoid evaporation. The samples were maintained at room temperature ($\sim 20^\circ\text{C}$) and then quenched to the desired experimental temperature for about 2 hours before the measurement. The experiments were performed at various temperatures below the $VPTT$ in the range of $15 - 25^\circ\text{C}$.

The results presented in this work are based on the data obtained from experiments performed on the DWS-Rheolab (LS Instruments, Switzerland). A laser beam $\lambda = 520 \text{ nm}$ was passed through a rotating ground glass before passing through the sample. Diffused light from the highly turbid sample was collected by a single mode optical fiber in the transmittance geometry. A digital correlator gave the autocorrelation function $G_2(\tau)$ over a large range of lag times ($10^{-9} - 10 \text{ s}$). The details of the DWS principle and setup could be found in section 2.4.3, and elsewhere (Pine *et al.* 1988; Zakharov *et al.* 2006). The $G_2(\tau)$ can be converted to ensemble average mean square displacement $\langle \Delta r^2(t) \rangle$, by an inverse Laplace transform of the field autocorrelation function by using equation 3.1 (Pine *et al.* 1988).

$$G_1(\tau) \propto \int_0^\infty P(s) \exp\left[-K_0^2 \langle \Delta r^2(t) \rangle \frac{s}{3l^*}\right] ds \quad 3.1$$

where $P(s)$ the probability of light travelling a path of length s , and is determined by solving the diffusion equation for the propagation of light for the relevant geometry and with the correct boundary conditions, K_0 is the wave vector of the incident light and l^* is the transport mean free path.

Experimental limitation for longer lag times: The current set-up used was not appropriate to give higher lag times. It is possible to get longer lag times, by using a camera in the backscattering geometry, which can give a good ensemble average. However, measurements here were done only in the transmission mode. To check the experimental range of working in the transmission mode, a solid block of teflon was measured. Being a solid, the teflon block is expected to give a straight line in the $G_2(\tau)$. However due to fluctuations, possibly from surrounding vibrations, $G_2(\tau)$ started to show a decay after 10 s. Thus, we show our data up to 10 seconds only.

3.3 Results and Discussions:

Each of the three suspensions of $\rho = 2.08, 2.3$ and $2.67 \mu\text{m}^{-3}$ was investigated by DWS at different temperatures (Figure 3.3), which was equivalent to varying the φ_{eff} of microgel suspension. At high effective volume fraction ($\varphi_{\text{eff}} \geq \varphi_{\text{RCP}}$) the brush-like surfaces of the microgel can be expected to interpenetrate. The interpenetrated length L_{int} was calculated using the fact that for a known number density, the particle radius (of an equivalent hard sphere) required for random close packing, R_{RCP} , can be calculated as $R_{\text{RCP}} = \left(\frac{0.63 \times 3}{4\pi\rho}\right)^{1/3}$. The interpenetration length is then calculated as $2(R_h - R_{\text{RCP}})$. Another length scale namely, the brush-to-centre distance is also estimated as $R_{\text{BC}} = 2R_{\text{RCP}} - R_h$. This indicates the distance between the surface of a microgel and the centre of a neighbouring microgel. When $R_{\text{BC}} \sim R$, the brush may be thought to interpenetrate and reach the outer core region of the neighbours. The R_g , R , R_h , L_{int} and the R_{BC} at different temperatures with the corresponding φ_{eff} are tabulated in Table 3.1 and represented schematically in Figure 3.2.

3.3.1 Glass transition

At higher temperatures, when the volume fraction is low ($\varphi_{\text{eff}} < \varphi_g \sim 0.7$) for soft spheres; c.f. Table 3.1, the brushes do not interpenetrate and the autocorrelation function $G_2(\tau)$ decays to zero indicating a fluid like behaviour, as seen for 25 °C and 20 °C in Figure 3.3(a), 23 °C in Figure 3.3(b) and 25 °C, in Figure 3.3(c). At lower temperatures, when $R_h \cong R_{\text{RCP}}$ ($0.7 < \varphi_{\text{eff}} < 0.8$) i.e. when the brushes of neighbouring particles start touching each other, the $G_2(\tau)$ does not decay to zero, instead it attains a plateau at longer lag times as seen for 18 – 12 °C in Figure 3.3(a), 21 – 19 °C in Figure 3.3(b) and 23 – 15 °C in Figure 3.3(c). This plateau is characteristic of a kinetically arrested glassy state, which is formed due to the ‘cage effect’ where the particle diffusion at high concentration is restricted within a cage formed by its nearest neighbors. In our study the plateau doesn’t decay to zero within the timescale of the experimental observation.

In this range of volume fractions, the loosely crosslinked brush-like surface swells to a larger extent relative to the highly crosslinked core, as can be seen from the values of R_h and R in Table 3.1. This results into interpenetration of the brushes, which in principle should reduce the flexibility of the brushes and make them stiffer.

As the brushes interpenetrate, the interpenetration length, L_{int} , increases and the brush to centre distance, R_{BC} , decreases, see Table 3.1. In this state the PNIPAm microgel suspension can be thought of as a heterogeneous system wherein highly crosslinked cores are embedded in a network of interpenetrated loosely crosslinked brushes.

3.3.2 Mixed characteristic of a glass and gel

Figure 3.3 shows a continuous increase in the values of the long-time plateau of $G_2(\tau)$ with decreasing temperature, or equivalently, increasing ϕ_{eff} . Such a continuous evolution of the plateau value appears in a low-density gel network, where the increase in the relative concentration of the sticky chains decreases the mesh size of the gel network (Chaudhuri et al. 2010; Hurtado et al. 2007; Michel et al. 2000). At still lower temperatures we see the appearance of a second plateau.

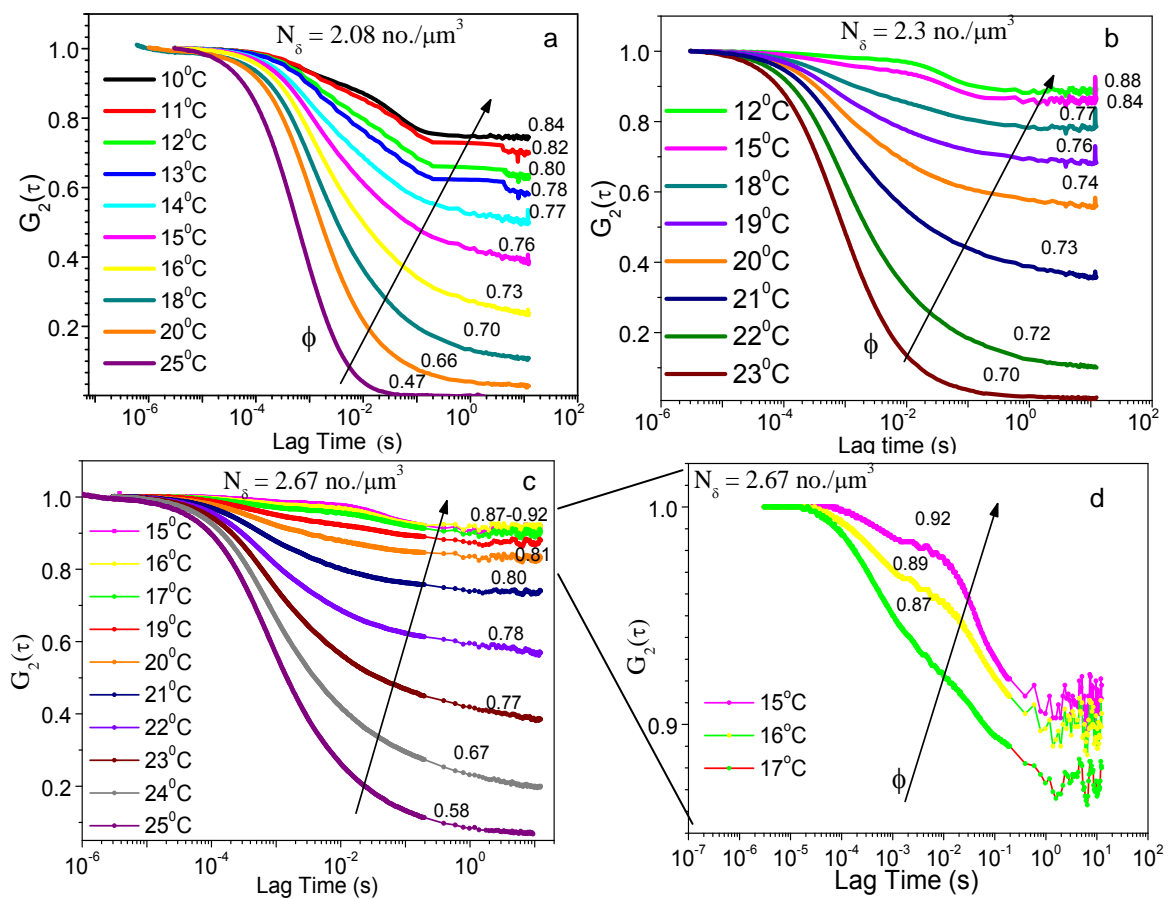


Figure 3.3: (a) Autocorrelation functions $G_2(\tau)$ at different temperatures for PNIPAm microgel suspension at number density ρ of (a) $2.08 \pm 5\% \mu\text{m}^{-3}$, (b) $2.18 \mu\text{m}^{-3}$ (c) $2.67 \mu\text{m}^{-3}$, and (d) shows zoomed-in view of the $G_2(\tau)$ of (d) for $\phi_{eff} > 0.8$.

In order to gain further insight into the additional plateau and the evolution of the cage, the $G_2(\tau)$ was transformed into the particle MSD by inverting the integral of the field correlation given in equation 2.17. At higher temperatures the MSD changes linearly with t , with a slope of 1, see Figure 3.4, indicating diffusive motion of the microgels. At lower temperatures the MSD deviates from the linear dependence and finally attains a plateau at longer times, as shown in Figure 3.4(a). The average maximum plateau value $\langle \Delta r_{max}^2 \rangle$ indicates the length scale over which particles display arrested dynamics due to the cage effect caused by core-core repulsion.

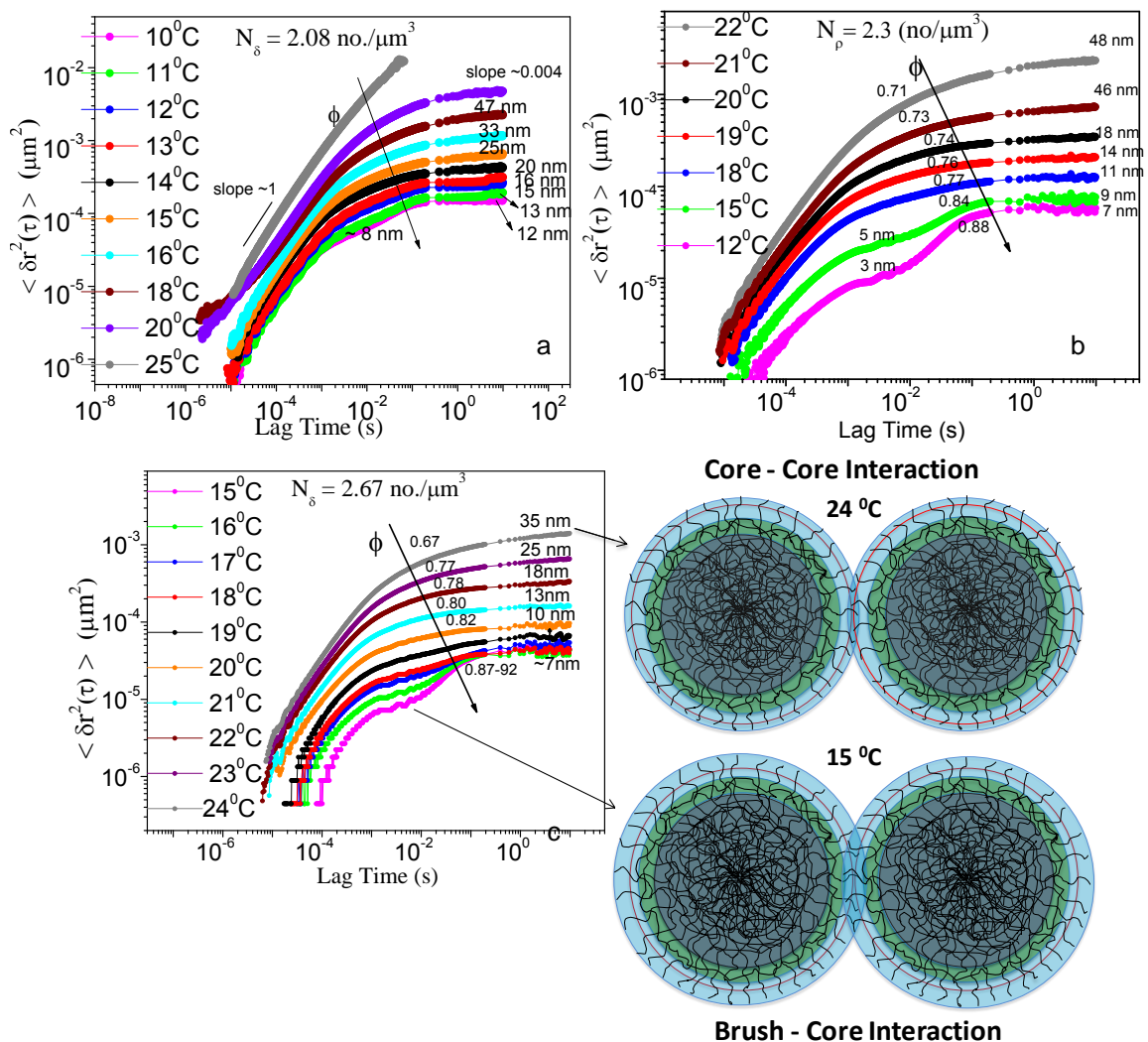


Figure 3.4: Mean square displacement as a function of lag time for PNIPAm microgel suspensions of concentrations (a) 2.08, (b) 2.3 and (c) 2.67 μm^{-3} at different temperatures. Schematic depiction of the microgel interpenetration in figure (c), drawn to scale using the different particle radii obtained by light scattering; the grey circle represents the radius of gyration; the green circle represents the geometric radius and the hydrodynamic radius is shown by the blue circle. Red circle represents the R_{RCP} .

In the volume fraction range $0.7 < \varphi_{eff} < 0.8$ the increase in the plateau value of $G_2(\tau)$ corresponds to a decrease in the MSD plateau. The cage size $[(\langle \Delta r_{max}^2 \rangle)^{0.5}]$, at low volume fraction is ~ 40 nm, ($\sim 0.05\sigma_h$, where $\sigma_h = 2R_h$), which continuously decreases with increasing volume fraction and saturates at $6 - 7$ nm, ($\sim 0.01\sigma_h$). These length scales are similar to that observed for glassy systems (Zaccarelli and Poon, 2009). Although the constant evolution of the plateau is a gel like characteristic, unlike gels which usually form due to attractive interactions, in case of PNIPAm suspensions, all the measurements were performed at temperatures much below the $VPTT$, where the microgels interact via excluded volume repulsion only (Wuet *al.* 2003; Huang and Hu, 2007). The absence of attractive interparticle interactions in dilute suspensions was confirmed by the positive value of the second virial coefficient $A_2 = 5 \times 10^{-7} \text{ mol.} \frac{\text{ml}}{\text{g}^2}$ at 20°C , calculated from the static light scattering data. This value is similar to that obtained by Huang and Hu, (2007). Earlier studies on star polymers claim that gelation is possible even for repulsive interactions (Loppinet *et al.* 2001). However the length scale obtained from their analysis was larger than the size of the star colloids. For gels usually the length scales are larger than that observed here (Chaudhuri *et al.* 2010; Zaccarelli and Poon, 2009; Loppinet *et al.* 2001). Thus, decrease in the cage size of the microgels have mixed characteristic which we believe is due to the softness of the brushes and the fact that they can become stiff when they interpenetrate.

3.3.3 Glass-Glass transition

Upon further lowering of the temperature when $\varphi_{eff} > 0.8$, similar to that of $G_2(\tau)$, the MSD also clearly shows the additional plateau at intermediate lag times. The additional plateau is observed in all the three suspensions and becomes prominent for the sample with the highest number density. Our analysis of the interpenetrated length scale, see Table 3.1, predicts that, at low temperatures such as 15°C for $\rho = 2.67 \mu\text{m}^{-3}$, the $R_g < R_{BC} \approx R$. This shows that at these temperatures the microgels swell to an extent where there is a complete interpenetration of the brushes to the extent where they start touching the outer core of the neighbouring microgel, or sometimes even penetrate it. This gives rise to a brush-core repulsive interaction which is responsible for this additional plateau. In this limit the centre-to-centre distance is such that $2R_{RCP} \sim R_h + R$. The volume fraction

calculated based on this centre-to-centre distance i.e., $(R_h + R)/2$ is 0.7, which confirms the inception of glass transition due to packing of microgel cores. Thus the presence of double plateau at lower temperatures predicts a glass-glass transition (Zaccarelli and Poon, 2009).

Figure 3.4 demonstrates the core-core and brush-core interactions with the help of a sketch showing various regions in the microgels drawn to scale using the experimental R_h , R , R_g and calculated R_{BC} . The appearance of double plateau is a signature of a higher order glass-glass transition which is usually observed in systems where there are two different interaction potentials like attractive and repulsive (Zaccarelli and Poon, 2009; Chenet *et al.* 2003). However, some recent studies have shown that glass-glass transition can also be obtained when both the potentials are repulsive, namely the square shoulder potential (Das *et al.* 2013; Sperl *et al.* 2010). In our system, although both the core-core interaction potential and brush-core interaction potential are repulsive, the degree of softness in these two potentials may be different.

3.3.4 Cage modulus

Since the origin of elasticity of a soft glass is entropic in nature, it is possible to relate the modulus of the glass to the cage size. The modulus of the cage is determined by equating the thermal energy $K_B T$ with the elastic energy $\frac{\kappa \langle \Delta r^2 \rangle}{2}$, where the spring constant κ is related to the modulus by $\kappa = Ga$, 'a' being the radius of a tracer particle. Thus the elastic modulus G is given by equation 3.2. In our case the microgels are large enough for themselves to act as tracer particles, thus a can be replaced by the R_h of the microgel.

$$G = \frac{K_B T}{\langle \Delta r^2 \rangle a} \quad 3.2$$

Figure 3.5 shows the modulus as a function of frequency, which is estimated from the lag time ($t = 2\pi/\omega$). At higher volume fractions there are two distinct plateau moduli; the low frequency plateau modulus corresponds to the core-core repulsion and the high frequency modulus represents the brush-core repulsion which is effective after complete interpenetration. Similar observations were made for a concentrated suspension of star colloids which in an oscillatory frequency sweep

experiment showed two plateau moduli, the higher frequency modulus being attributed to the interpenetrated stars (Helgeson *et al.* 2007).

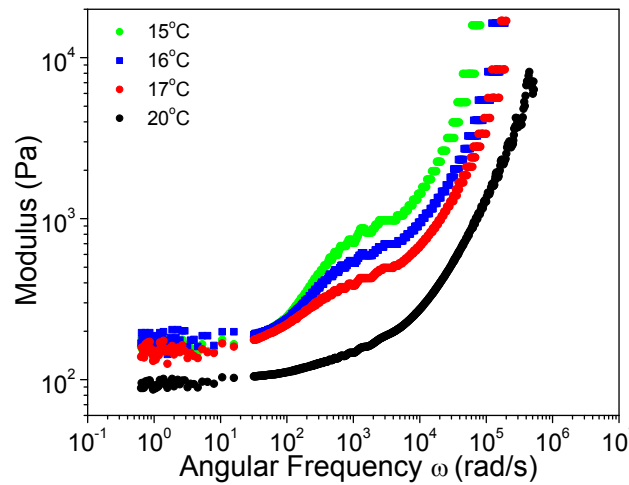


Figure 3.5: Modulus calculated by the MSD plateau value using equation 3.2 plotted as a function of angular frequency ($\omega = 2\pi/t$, here $t = \text{lag time}$). Data shown for PNIPAm microgels with $\rho = 2.67 \mu\text{m}^{-3}$.

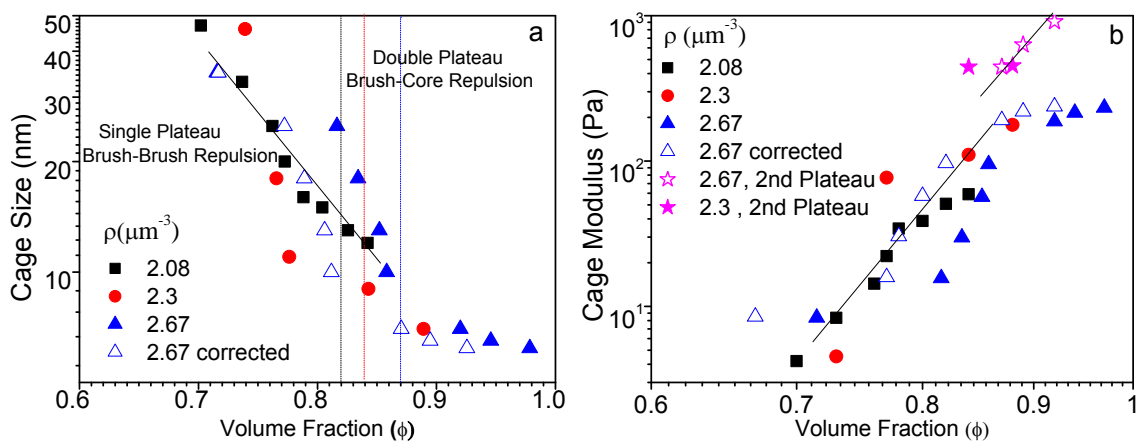


Figure 3.6: Master curves for (a) Cage size as a function of volume fraction and (b) Modulus as a function of volume fraction for PNIPAm suspensions at different number density. The solid line is a fit for (a) $\text{Cage size} \propto \varphi^{-8}$, (b) $G \propto \varphi^{15}$.

We find that for number densities of 2.08 and $2.3 \mu\text{m}^{-3}$, the cage size versus the φ_{eff} shows a master curve as seen in Figure 3.6(a). The sample with highest number density $2.67 \mu\text{m}^{-3}$ shows a discrepancy and does not fall on the master curve as seen in Figure 3.6(a). This we believe is due to the assumption that the hydrodynamic radius R_h , is same as that obtained from a dilute solution measurement. This may not be correct since the size of a PNIPAm microgel also depends on the availability of water. At a very high number density, availability of water for swelling may not be

enough and the microgel may not swell as much as it would swell in dilute solutions at a particular temperature. Thus, we back-calculated the expected R_h , for the highest number density $2.67 \mu\text{m}^{-3}$ by horizontally shifting the curve. The R_h so obtained is 98 % of the R_h measured under dilute solution conditions. The blue open symbols in Figure 3.6 is the shifted data.

The cage modulus calculated from the cage size by taking the plateau value of the MSD, $[\langle \Delta r_{max}^2 \rangle]^{0.5}$ in equation 3.2 also shows a master curve when plotted against the φ_{eff} as seen in Figure 3.6(b). Unlike hard spheres which show a divergence of viscosity/modulus at φ_g (Meeker *et al.* 1997), the cage modulus for microgels show a softer dependence on the volume fraction (Mattsson *et al.* 2009). Similar to that observed for star colloids (Wagner, 1993), this weak volume fraction dependence of the modulus is due to softness of the core-core interaction potential which leads to the interpenetration of the brushes at high volume fractions.

At even higher volume fractions ($\varphi_{\text{eff}} > 0.80 - 0.88$), the cage modulus shows a weaker dependence on the φ_{eff} , similar to that observed in core-shell like block copolymer systems at high concentrations (Charbonneau *et al.* 2011). The volume fraction at which the cage size saturates coincides with the volume fraction at which the second plateau appears. As discussed earlier, at this volume fraction, there is complete interpenetration of the brushes. Thus our study reveals that the saturation of the cage modulus is related to the complete interpenetration of the brushes.

The interpenetration of the brush-like surface of the microgels, suggests that the interparticle potential may be represented by two repulsive potentials at different length scales (core-core repulsion and the brush-core repulsion), something similar to the square-shoulder potential (Das *et al.* 2013; Sperl *et al.* 2010). However unlike the square shoulder potential the two different repulsive potentials can have different degrees of softness.

3.4 Summary

In this chapter, the decay of the temporal autocorrelation function, $G_2(\tau)$, was observed for different values of effective volume fractions φ_{eff} , which was controlled by varying the temperature. The rich dynamics observed in $G_2(\tau)$ can be attributed to the core-shell morphology of the microgels. At $\varphi_{\text{eff}} > \varphi_{\text{RCP}}$, the plateau in the correlation function is attributed to the core-core repulsive interaction. The continuous

increase in the plateau values with further increase in the volume fraction was attributed to the softness of the core-core interaction that allows them to interpenetrate and the interpenetration increases the stiffness of the brushes leading to a higher plateau value. At further low temperatures ($\varphi_{\text{eff}} \gg \varphi_{\text{RCP}}$), the $G_2(\tau)$ shows the presence of a second plateau, at a smaller length scale. We attribute this to the brush-core repulsive interactions which dominate when the brushes completely interpenetrate and touch the core of the neighbours.

However the length scales obtained from the plateau values are similar to that observed for glassy systems, and the continuous evolution of the plateau values is the feature observed in low density gels that are usually observed in attractive suspensions. Thus the dense suspension of the PNIPAm microgels show a mixed gel-glass like dynamical behaviour.

The cage modulus when plotted against φ_{eff} shows a master curve for all the densities with a weaker dependence on φ_{eff} which is a signature of a soft potential (Mattsson *et al.* 2009). The cage modulus at higher volume fraction shows a further softening, which has been observed earlier for core-shell like block copolymer systems at high concentrations (Charbonneau *et al.* 2011). We also find that the φ_{eff} at which this softening appears coincides with the volume fraction where the second plateau/modulus appears. Thus we predict that this softening is related to the complete interpenetration of the brushes.

Our experimental time window does not allow us to explore longer timescales where there may be a possibility that the correlation function will decay from the plateau. So from our experiment it was not possible to comment if the observed glass-glass transition is in the equilibrium or non-equilibrium region (Sperl *et al.* 2010). Although we discuss that the double repulsive potential and the softness of the potential leads to a mixed gel-glass like characteristics but we cannot quantify the exact origin of it. To quantify this behaviour we need to study model systems with various interaction potentials, which we propose as a future work.

Chapter 4

Yielding in Soft Colloidal Glass: Strain Rate Frequency Superposition under LAOS

In this chapter, we investigate the dynamics of SCGs under large amplitude oscillatory shear. The strain rate frequency superposition (SRFS), a technique proposed by (Wyss et al. 2007), was validated for a dense suspension of PNIPAm microgel and for other soft solids such as a Xanthan gum solution and a commercial hair gel. We investigate here the effect of the nonlinear strains on the higher harmonic moduli and show that the SRFS works identically for all of them. This further confirms that the time scale for structural relaxation in SCG's is set by the imposed deformation rate. We will use this important information in Chapter 5 as well.

4.1 Introduction

Linear viscoelastic response is limited to small strains or strain rates, and assumes a constant dynamic viscosity and constant normal stress difference coefficient. In order to probe their linear viscoelastic response, materials are frequently subjected to small amplitude oscillatory shear, wherein a sinusoidal strain is applied to the material as given by $\gamma(t) = \gamma_0 \sin(\omega t)$, here γ_0 is the strain amplitude, ω is the angular frequency, and t is the time. The resultant stress response is given by, $\sigma(t; \omega) = \gamma_0 [G'_1(\omega) \sin(\omega t) + G''_1(\omega) \cos(\omega t)]$ at the same angular frequency as the input. Here G'_1 and G''_1 are the “storage” modulus and “loss” modulus, and are functions of the angular frequency (Ferry, 1980).

By contrast, the resultant stress from a large-amplitude oscillatory shear (LAOS), has a non-linear response and contains higher harmonics which may be interpreted in terms of harmonic moduli G'_n and G''_n (subscript n refers to the n^{th} harmonic), which are functions of both the strain amplitude and the angular frequency.

$$\sigma(t; \omega \gamma_0) = \gamma_0 \sum_{n=1,3,5,\dots} [G'_n(\omega, \gamma_0) \sin(n\omega t) + G''_n(\omega, \gamma_0) \cos(n\omega t)] \quad 4.1$$

The n^{th} harmonic moduli is defined as

$$G'_n(\omega, \gamma_0) \equiv \frac{\sigma_n}{\gamma_1} \cos \phi_n$$

$$G''_n(\omega, \gamma_0) \equiv \frac{\sigma_n}{\gamma_1} \sin \phi_n$$
4.2

where $\phi_n(\omega, \gamma_0) = \phi_{n,\sigma} - n\phi_\gamma$ is the phase angle for the n^{th} harmonic moduli ($\phi_{n,\sigma}$ and ϕ_γ are the phase angles of the n^{th} harmonic in the stress and the first harmonic in the strain fourier series, respectively).

The shear rate in the processing of the materials on an industrial scale is usually large. Apart from their obvious utility in industrial processes, LAOS studies are of fundamental interest in rheology and may lead to the development of more representative constitutive models. Here we discuss the LAOS response preferentially to the yielding behaviour in soft colloidal glasses. The typical linear response, the need for investigation of large deformations and its effect on the relaxation processes is discussed.

Linear viscoelastic frequency response gives a direct measurement of the relaxation spectrum under quiescent conditions. The characteristic relaxation spectrum for soft glasses however is usually unable to probe the long-time structural relaxation indicated by a crossover of the viscoelastic moduli at lower frequency. The methods used to acquire the long-time dynamics of a glassy system include Time Temperature Superposition (TTS) (Li, 2000), Time Stress Superposition (Joshi and Reddy 2008), Stress relaxation (Ferry, 1980; Kapnistos *et al.* 1999) etc.

SRFS, a recent technique proposed by Wyss *et al.* (2007), probed the structural relaxation in the SCGs induced by an imposed large deformation rate. This technique showed that in a constant strain-rate frequency sweep measurement, the first harmonic of the viscoelastic moduli namely, G'_1 and G''_1 could be superimposed onto master curves. The utility of the SRFS procedure is that it provides a valuable relation between the structural relaxation time and the imposed deformation rate. Specifically, the authors showed that the structural relaxation time τ of the material showed an inverse power-law dependence (Leonardo *et al.* 2005) on the strain-rate amplitude $\dot{\gamma}$ (at high strain-rate amplitudes), $1/\tau(\dot{\gamma}) \propto \dot{\gamma}_0^v$ where $v > 0$ is the exponent in the power law.

The need to maintain a constant strain rate in a SRFS experiment requires imposition of non-linear strains in the low frequency regime. When subjected to LAOS, the resultant stress contains higher harmonics that are functions of both the strain amplitude and angular frequency in contrast to the Linear response where G'_1 and G''_1 were functions of the applied frequency alone.

This work prescribes a detailed experimental procedure to obtain the higher harmonic moduli and its role in the SRFS. In this work it is shown that higher harmonic moduli obtained from the constant strain-rate frequency sweep measurements on soft solids can be superimposed onto master curves with the same shift factors as for the first harmonic viscoelastic moduli. The moduli G''_1 which was physically interpreted in terms of the energy dissipated per unit volume per cycle of strain oscillation (Ganeriwala and Rotz, 1987), was experimentally verified for both linear and non-linear regimes with the help of surface plots for xanthan gum. It was also observed that the third harmonic moduli at low frequencies in a SRFS measurement is a mirror image of its strain sweep test.

4.2 Materials and experimental protocol:

4.2.1 Sample preparation for soft solids

PNIPAm microgels: The microgels were synthesized in the presence of a cross linker (2 wt% by wt of monomer) and surfactant (Senff and Richtering, 1999). The details of the reactants used and synthesis protocol followed are mentioned in section 2.3.2. The synthesis when done in the presence of the surfactant gives small size microgels ($R_h \sim 131$ nm at 25 °C). These microgels are soft and compressible; they seldom crystallize at very high concentrations. In this work a 14 wt.% PNIPAm microgel suspension was used.

Xanthan Gum: A 4 wt.% aqueous suspension of Xanthan gum gives a soft colloidal glass (Song et al. 2006). 98 ml of water is taken in a beaker and stirred at ~500 rpm with the help of an overhead stirrer. 4 g of Xanthan Gum powder was added very slowly to the already stirring water. This confirms complete and homogenous mixing of the powder. 7 mg of sodium azide (Merck) was added to prevent bacterial growth. The solution was continuously stirred for 30 mins after all the xanthan gum was added.

Hair Gel: BrylcreemWetlook Gel (Godrej Sara Lee Ltd., India) was purchased off-the-shelf and used as received.

4.2.2 Experiments

The experiments were carried out on the strain-controlled Advanced Rheometric Expansion System-2000 (ARES-2000, TA Instruments) rheometer. All experiments were done at $T = 25$ °C. After loading the sample on to the rheometer, a thin layer of silicone oil (SF 1000, GE Bayer Silicones), was applied at the edges of the sample to prevent drying. We used a cone-plate geometry with a cone diameter of 25 mm (cone angle=0.1 rad). The rheometer permits acquisition of dc voltage signals from the torque transducer (for measurement of torque) and the optical encoder (for measurement of the motor angular deflection) through BNC connectors in the rear panel of the instrument. These unprocessed voltage signals (in the range ± 5 volts) are neither noise filtered nor corrected for inertia and compliance of the torque transducer. Data was acquired at 16-bit analog input resolution through an analog-to-digital card (NI PCI-6014, National Instruments) coupled with a Labview (National Instruments) code at a sampling rate of 103 points per second. A small dc offset was subtracted from the acquired oscillatory signal and the same was filtered for noise using a Savitzky-Golay filter (Press *et al.* 2007). The signal was then calibrated to find formulae which were used to convert the voltage values to quantities of physical interest. The calibration curves used were $y = 0.046x$ (x in volts, y in Nm) for the torque and $y = 0.1x$ (x in volts, y in rads) for the deflection angle. Calibration was done using step rate tests in which the dc voltage signals for torque and angular deflection were compared with the values of torque and angular deflection measured by the inbuilt software of the rheometer. The values of the stress (in Pa) and the strain were calculated from the torque and the deflection angle, respectively, using conversion factors appropriate to the measuring system geometry and torque transducer employed.

4.2.3 Data analysis

The data analysis was carried out using Matlab programming software. We applied a discrete Fourier transform on the extracted signals, and use only the first half of the Fourier-transformed dataset (remainder of the dataset is redundant for real input data). Although in theory, the higher harmonic frequencies are integer multiples of the

fundamental frequency, in an experimental stress signal the measured harmonic frequencies located through peak values in the stress amplitude spectrum, differ by a small amount from the integer multiples. Hence, we use a code which locates peak values in the stress amplitude spectrum and explicitly finds the frequencies corresponding to the harmonics. Finally, we calculated the phase angles and thereafter the harmonic moduli of interest. It is important to note that there is no automated means of obtaining higher harmonic moduli from the ARES-2000 rheometer, therefore, each point in our graphs (with the exception of Figure 4.1 and Figure 4.2) were calculated from an independent oscillatory shear test with a fixed angular frequency and strain amplitude.

4.3 Results and Discussions:

4.3.1 First harmonic moduli

Figure 4.1(a) shows a typical yielding response observed for a soft colloidal glass, when it is subjected to increasing amplitude of oscillatory strain, at a fixed frequency. The linear viscoelastic regime in this case stays up to 5%. Figure 4.1(b), shows a linear viscoelastic frequency response, performed by ramping up the frequency of oscillation at a constant strain amplitude. The strain ($\gamma_0 = 0.01$) is chosen to be in the linear viscoelastic regime to obtain the relaxation spectrum under quiescent conditions.

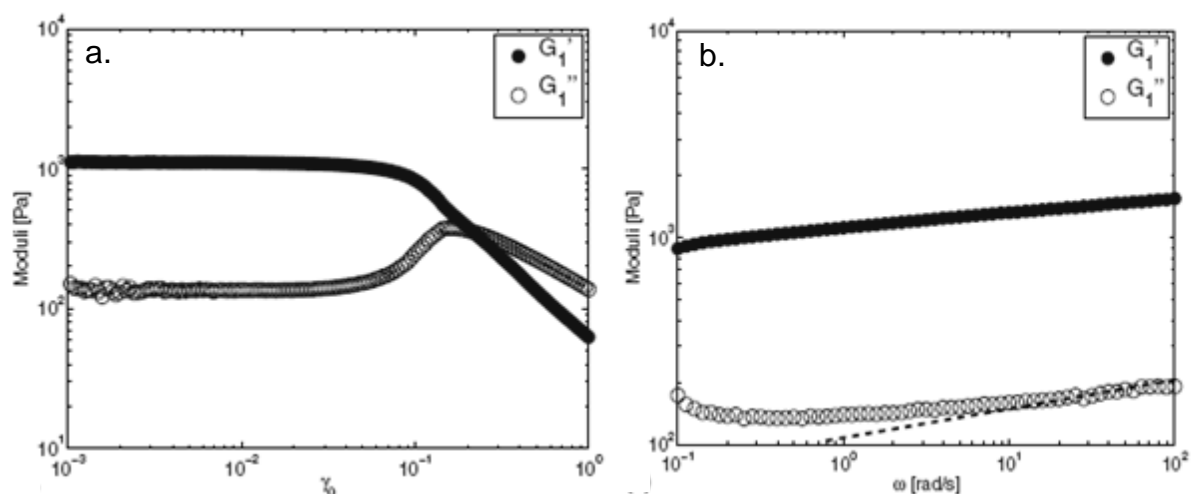


Figure 4.1:(a) Strain sweep at constant frequency $\omega = 1$ rad, $T = 25^\circ\text{C}$, for 14 wt. % PNIPAm microgel suspension and (b) Frequency sweep at constant strain $\gamma_0 = 0.01$. The dashed line is proportional to $\omega^{0.78}$.

Figure 4.1(b) suggest that, in the range of frequencies probed, the sample shows solid like behaviour with the first harmonic storage modulus G'_1 greater than the first harmonic loss modulus G''_1 . The small upturn in G''_1 at the smallest frequencies hints at the possibility of a crossover of the moduli at a much lower frequency. This crossover frequency represents the α -relaxation ($\omega_\alpha = 1/\tau_\alpha$), which is not observed due to inaccessibility of the lower frequency regime. Also, α -relaxation process is difficult to probe even if one waits long enough to probe lower frequencies. This is because such non-ergodic systems can age over the time scale of experiments thereby shifting the crossover to even lower frequencies.

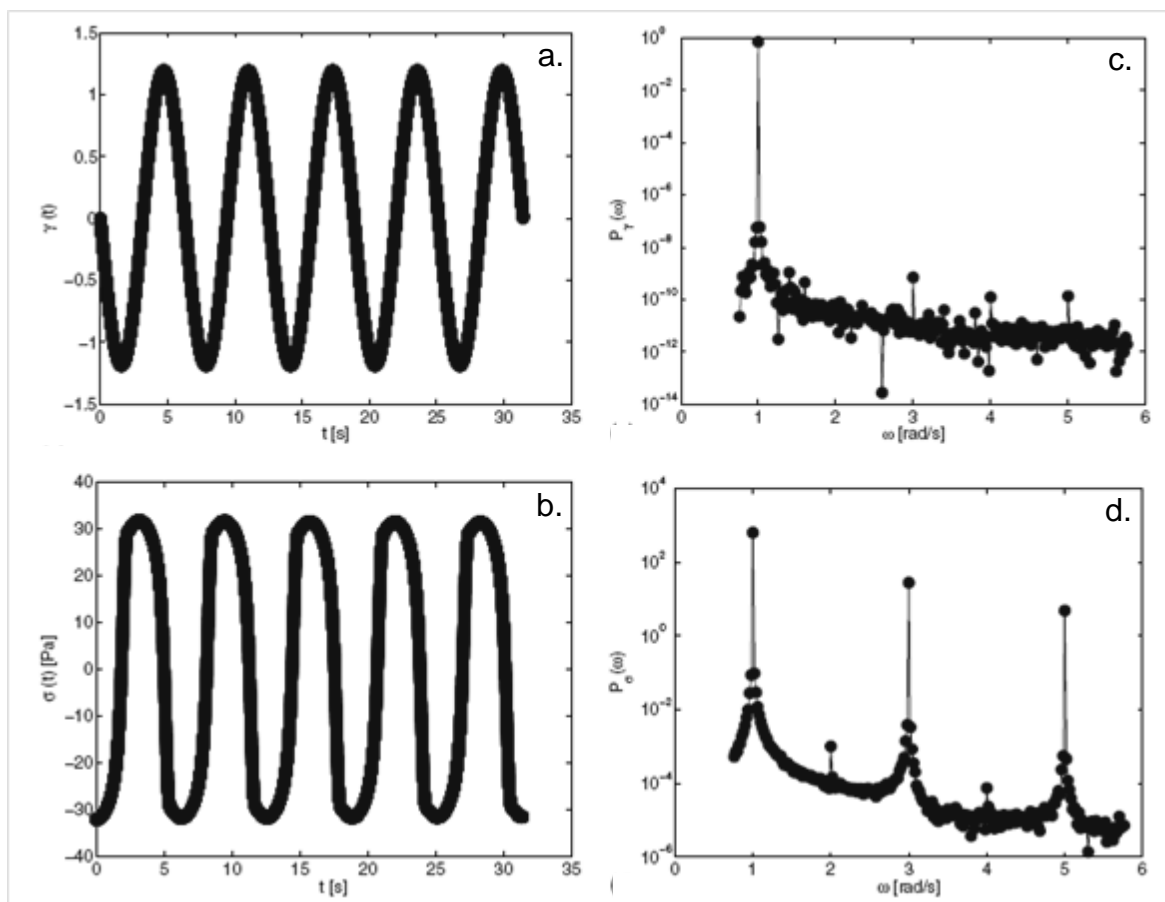


Figure 4.2:(a) A typical strain signal $\gamma(t)$ as a function of the time t from an oscillatory shear test with $\gamma_0 = 1.2$, $\omega = 1$ rad/s, (b) Plot of the resultant stress signal $\sigma(t)$ as a function of the time t with parameter values as in (a), (c) power spectrum P_γ of the strain signal and (d) power spectrum P_σ of the stress signal.

4.3.2 Higher harmonics

Figure 4.2(a), shows a few cycles of sinusoidal oscillations of the strain signal as a function of the time from a LAOS test at $\gamma_0 = 1.2$, $\omega = 1$ rad/s for PNIPAm. In Figure

4.2(b), the resultant stress signal as a function of time shows a non-sinusoidal nature, indicative of higher harmonics in the stress amplitude spectrum. The power spectrum of the strain P_γ as a function of ω for fifty oscillation cycles of the strain signal is shown in Figure 4.2(c). In Figure 4.2(d), we plot the response stress power spectrum P_σ as a function of ω . Prominent odd harmonics can be seen at frequencies which are close to integer multiples of the applied oscillation frequency $\omega = 1$ rad/s.

Figure 4.2(d), shows the third and fifth harmonic occurring at 3ω and 5ω , respectively, in addition to the normally observed first harmonics at the applied oscillating frequency $\omega = 1$ rad/s. In addition to these, small peaks at 2ω and 4ω were also observed, a result first noted by Krieger and Niu (1973). These even harmonics in the stress power spectrum have been hypothesized to occur in oscillatory shear flows because of wall slip, or due to secondary flows in the plate gap (Adrian and Giacomini, 1992). In our experiments, the ratio of the second to the first harmonic in the stress power spectrum is of the order 10^{-6} or smaller, therefore the even harmonics were neglected.

4.3.3 Strain rate frequency superposition under LAOS

As mentioned earlier, the SRFS test is a frequency sweep test performed at a constant strain rate. As the frequency is changed the strain is also changed correspondingly to maintain a constant strain rate, as $(\dot{\gamma}_0 = \gamma_0 \omega)$. Figure 4.3(a) shows the results of SRFS tests for PNIPAm suspension. Shown here are the first harmonic moduli as a function of ω for $\dot{\gamma}_0 = 0.9, 1.2, 2.1$ and 4.2 s^{-1} . The $\dot{\gamma}_0$ decreases the relaxation time and thus the crossover is observed in the range of frequencies probed. Note that the crossover was not visible in the linear viscoelastic frequency response, see Figure 4.1(b). The crossover frequency is shifted in the direction of increasing ω , for larger values of $\dot{\gamma}_0$, although the shapes of the moduli curves are similar. (Figure 4.3(a)). This allows for horizontal shifting of the data on to master curves. The curves for the highest value of $(\dot{\gamma}_0)$ are taken as the reference curves for the purpose of shifting. The resulting master curve is shown in Figure 4.3(b), where the rescaled moduli are plotted as a function of the rescaled angular frequency. The values of the shift factors, vertical $a_1(\dot{\gamma}_0)$ and horizontal $b_1(\dot{\gamma}_0)$ are listed in Table 4.1. The plot thus confirms the validity of the SRFS procedure for linear viscoelastic moduli, as reported in Wyss *et al.* (2007).

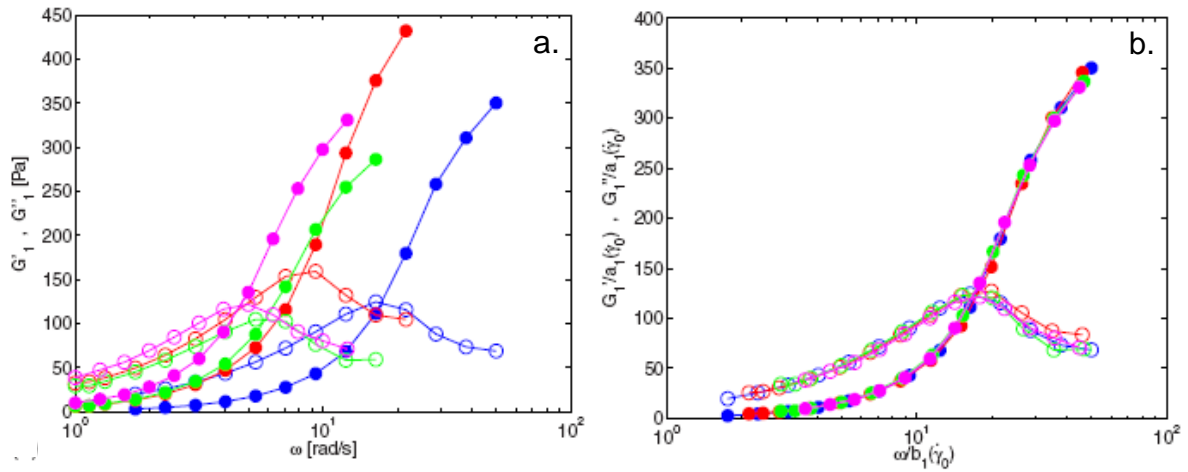


Figure 4.3:(a) Plot of the first harmonic moduli G'_1 (solid circles) and G''_1 (open circles) as a function of the angular frequency ω from constant strain-rate frequency sweep measurements at strain-rate amplitudes of $\dot{\gamma}_0 = 4.2 \text{ s}^{-1}$ (blue), 2.1 s^{-1} (red), 1.2 s^{-1} (green), 0.9 s^{-1} (pink) using PNIPAm and (b) master curve obtained by shifted the data to highest strain rate.

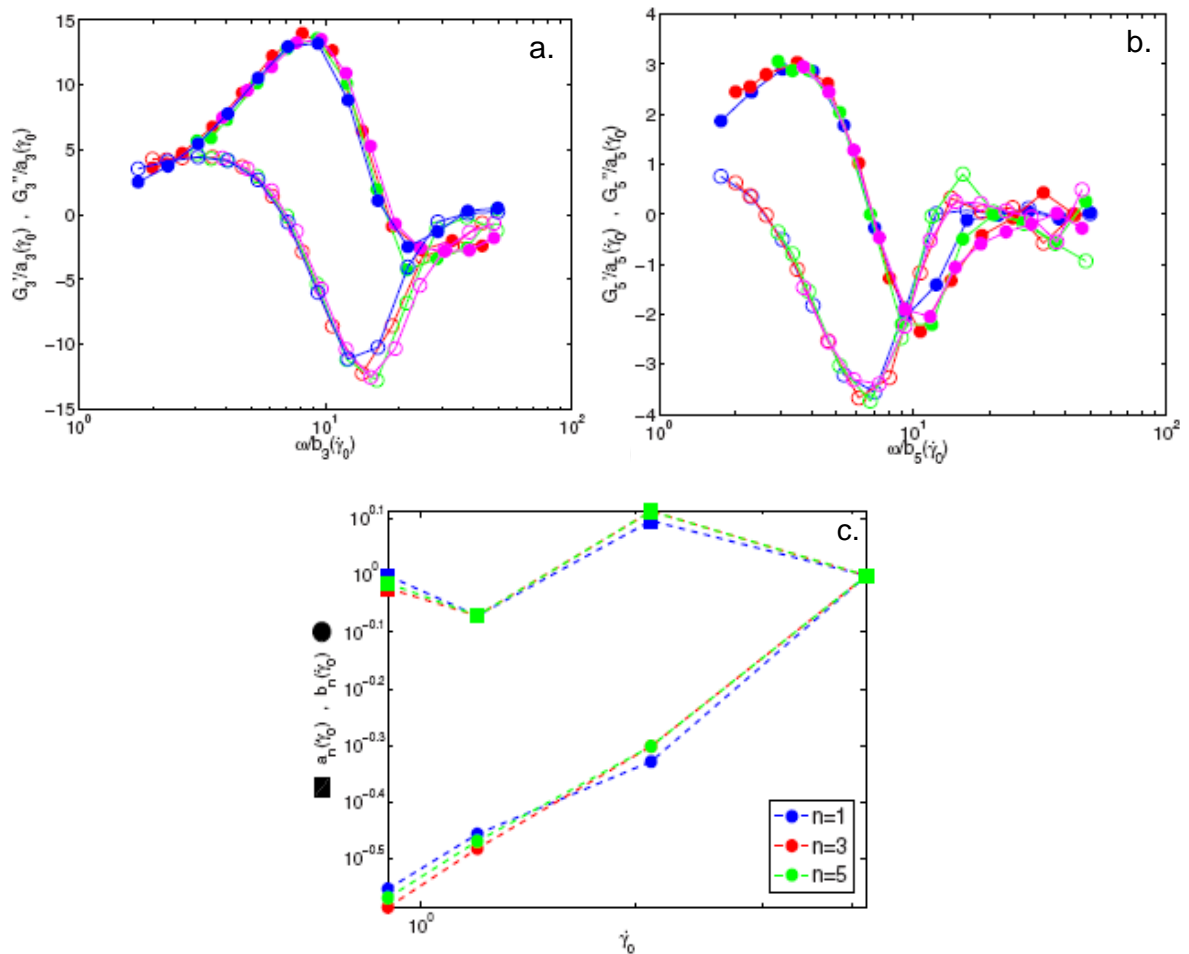


Figure 4.4: Higher harmonic moduli for PNIPAm microgel suspension(14 wt %, $T = 25 \text{ }^\circ\text{C}$).(a)Master curve for third harmonic moduli, (b) master curve for fifth harmonic moduli and (c) shift factors for first third and fifth harmonic moduli.

Figure 4.4(a) and (b) shows the master curves of the corresponding rescaled third and fifth harmonic moduli as a function of the rescaled angular frequency from the same test as reported in Figure 4.3(a). The values of the shift factor of these non-linear moduli are listed in Table 4.1

Table 4.1: Vertical $a_n(\dot{\gamma}_0)$ and horizontal $b_n(\dot{\gamma}_0)$ shift factors for the harmonic moduli G'_n and G''_n for $n = 1, 3, 5$ for different values of $\dot{\gamma}_0$ using PNIPAm, xanthan gum, and hair gel.

Material	$\dot{\gamma}_0 (s^{-1})$	a_1	b_1	a_3	b_3	a_5	b_5
PNIPAm	0.9	1	0.28	0.95	0.26	0.97	0.27
	1.2	0.85	0.35	0.85	0.33	0.85	0.34
	2.1	1.25	0.47	1.3	0.5	1.3	0.5
	4.2	1	1	1	1	1	1
Xanthan Gum	0.3	1.1	0.12	0.85	0.095	1	0.095
	1.2	1.1	0.38	0.9	0.35	1	0.34
	2.1	1.1	0.5	0.8	0.5	0.79	0.48
	4.2	1	1	1	1	1	1
Brylcreem	0.5	0.83	0.05	0.85	0.05	0.91	0.07
	1	0.75	0.09	0.74	0.1	0.8	0.12
	5	0.83	0.45	0.83	0.5	0.83	0.55
	10	1	1	1	1	1	1

The vertical shift factors $a_n(\dot{\gamma})$ for all the harmonics were found to be of the order of unity, (Note the subscript n denotes the n th harmonic as $n = 1, 3, 5$), while the horizontal shift factors $b_n(\dot{\gamma})$ ($n = 1, 3, 5$) showed a power law dependence $b_n(\dot{\gamma}_0) \propto \dot{\gamma}_0^\nu$, with an exponent $\nu = 0.89 \pm 0.01$. The shift factor ($b_1(\dot{\gamma}_0)$) is postulated to depend inversely on the structural relaxation time, viz. $b_1(\dot{\gamma}_0) \propto \frac{1}{\tau(\dot{\gamma}_0)}$ and our results for $b_n(\dot{\gamma}_0)$ (for $n=1, 3, 5$) are in agreement with the exponent $\nu = 0.9$ reported in (Wyss *et al.* 2007). This suggests that

$$b(\dot{\gamma}_0) = \frac{\tau_0}{\tau(\dot{\gamma}_0)} = 1 + K\dot{\gamma}_0^{0.9} \text{ or } \frac{1}{\tau(\dot{\gamma}_0)} = \frac{1}{\tau_0} + K(\omega\gamma_0)^{0.9} \quad 4.3$$

where, τ_0 is some microscopic relaxation time and $\tau(\dot{\gamma}_0)$ is the structural relaxation time that is dependent on the effective strain rate $\omega\gamma_0$.

4.3.4 Relation between SRFS and strain sweep

The shape of the SRFS master curves in Figure 4.3(b), suggests that the low frequency behaviour of the moduli is similar to the higher strain behaviour of the moduli in a strain sweep experiment shown in Figure 4.1(a). This analogy holds true for the higher harmonic moduli also as shown in Figure 4.5(a). In this figure, third harmonic moduli G'_3 and G''_3 obtained from an SRFS test at $\dot{\gamma}_0 = 1.2 \text{ s}^{-1}$ for xanthan gum solution is plotted as a function of ω . Adjacent to it in Figure 4.5(b) is shown a strain sweep test at a frequency $\omega = 5 \text{ rad/s}$. The plots are a remarkable demonstration of the “reversed” nature of the higher harmonic moduli as reported from SRFS tests and from a strain sweep test.

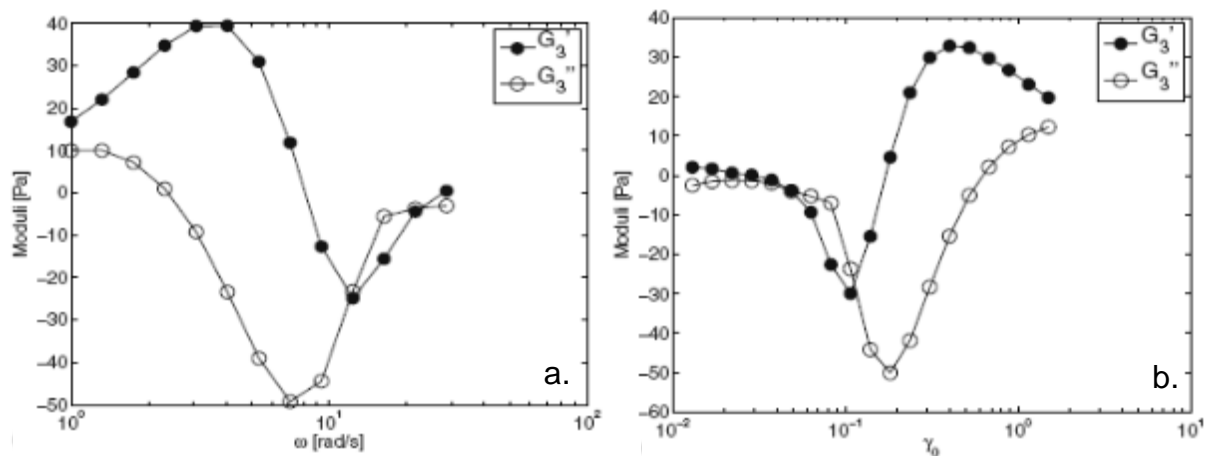


Figure 4.5:(a) SRFS curve showing the third harmonic moduli as a function frequency ω with constant strain-rate amplitude $\dot{\gamma}_0 = 1.2 \text{ s}^{-1}$, using xanthan gum and (b) strain sweep showing the third harmonic moduli at $\omega = 5 \text{ rad/s}$.

4.3.5 Energy dissipation rate

The energy dissipated per unit volume per cycle of strain oscillation as shown by Onogi, *et al.* (1970) is

$$\varepsilon(t; \omega, \gamma_0) \equiv \int_0^{2\pi/\omega} \sigma d\gamma \quad 4.4$$

Ganeriwala and Rotz,(1987)have shown that on substituting the one-dimensionalGreen-Rivlin constitutive equation[†], for the stress intothis formula and assuming a sinusoidal strain one obtainsan expression

$$\varepsilon = \Pi\gamma_0^2 G_1''(\omega\gamma_0) \tag{4.5}$$

which is true for arbitrary values of γ_0 . The second law of thermodynamics requires that $\varepsilon \geq 0$, i.e., G_1'' is strictly positive, but places no restriction onthe sign of the other moduli.

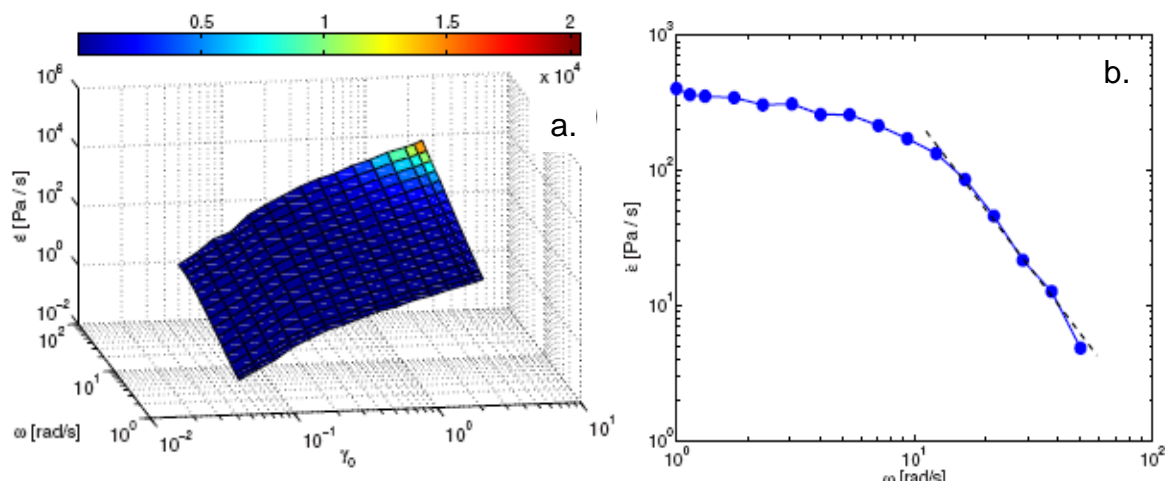


Figure 4.6: (a) Surface plot of the energy dissipation rate per unit volume as a function of the angular frequency ω , and the strain amplitude γ_0 , using xanthan gum. The color bar indicates the magnitude of energy dissipation rate $\dot{\varepsilon}$ in units of Pa/s. (b) Curve of intersection of the surface $\dot{\gamma}_0 = \gamma_0 \omega = 2.1s^{-1}$ with the surface plot in (a).The dashed line is proportional to $\omega^{-2.36}$.

It is plausible that the otherharmonic moduli are involved in reversible exchanges of energyin LAOS.InFigure 4.6(a), we show the surface plot of the energy dissipation rateper unit volume for xanthan gum. It is interesting to notethat the $\dot{\varepsilon}$ surface grows monotonically with, γ_0 and ω , despitethe material showing a

[†]Green Rivlin equation in one dimension is $\sigma(t) = \int_{-\infty}^t K_1(t - t_1)\dot{\gamma}(t_1)dt_1 + \iiint_{-\infty}^t K_3(t - t_1, t - t_2, t - t_3) \times \dot{\gamma}(t_1)\dot{\gamma}(t_2)\dot{\gamma}(t_3)dt_1 dt_2 dt_3 + \dots$, where $K_1, K_3 \dots$ are the stress relaxation modulus

solidlike response at higher frequencies. On account of the logarithmic scaling used for the axes and the orientation of the surface in Figure 4.6(a), it may not be directly apparent that $\dot{\epsilon}$ is in fact a *decreasing* function at large ω , along the curve of intersection of the surface at $\dot{\gamma}_0 = \gamma_0 \omega = 2.1 s^{-1}$. Thus the surface for energy dissipation rate is shown in Figure 4.6(b). We may rewrite the expression for the energy dissipation rate per unit volume as $\dot{\epsilon} = \omega \gamma_0^2 G_1'' / 2$. In linear viscoelasticity, G_1'' is directly proportional to ω at small ω , implying that energy dissipation rate $\dot{\epsilon}$ is constant along the SRFS curve which accords with Figure 4.6(b) for $\dot{\gamma}_0 = 2.1 s^{-1}$. The dashed-line fit to the high-frequency (corresponding to *low* strain amplitude) portion of the energy dissipation rate curve was found to be proportional to $\omega^{-2.36}$.

4.4 Summary

In this chapter, we show that the SRFS technique is generally applicable to soft solids, specifically, that the SRFS curves for higher harmonic moduli also can be superimposed onto master curves with the same shift factors as for the first harmonic modulus. It was also confirmed that the crossover obtained in the SRFS technique is not the actual relaxation of the material but is a strain induced relaxation time set by the strain rate. This result will be used in the next chapter. Another outcome of this work is that the third harmonic moduli at low frequencies in a SRFS measurement is a mirror image of its strain sweep test. From the analysis of the surface plots of Xanthan gum solutions it was confirmed that energy dissipated per unit volume in an oscillatory shear is governed by the first harmonic loss modulus alone.

The next chapter extends the study of the yielding in soft colloidal glasses with specific attention to the characteristic peak in the loss modulus appearing in the strain sweep test. Since the higher harmonic moduli shift factors are identical to the first harmonic, it is reasonable to consider only the first harmonic while considering a routine strain sweep tests, for the purpose of the work investigated further in this thesis.

Chapter 5

Universal attributes of yielding in soft materials under Large Amplitude Oscillatory Shear

This chapter deals with yielding of soft materials subjected to large amplitude oscillatory flows. In particular, the phenomenon of a peak in loss modulus, followed by yielding observed in strain sweep experiments was investigated at different frequencies for a variety of soft materials, having different microstructures and thermodynamic states. The experimental observations were explained by a simple phenomenological model, which predicted the nonlinear response qualitatively and showed that all soft materials when probed in appropriate frequency-concentration-temperature windows will exhibit universal features of yielding.

5.1 Introduction

The non-linear mechanical response of many materials when subjected to large deformation or stress changes from being predominantly elastic (solid like) to predominantly plastic (liquid like) (Stokes and Frith, 2008). This transition is called yielding. One of the experimental techniques to investigate the non-linear response of soft materials involves subjecting them to oscillatory shear flow in which the shear strain $\gamma = \gamma_0 \sin(\omega t)$ is varied by ramping its amplitude γ_0 at a constant frequency. For an arbitrary strain amplitude, the measured stress $\sigma(t)$ can be de-convoluted into an in-phase response characterized by the elastic modulus G' , and an out-of-phase response, characterized by the viscous modulus G'' . An accurate representation of the stress response would consist of Fourier harmonics of the elastic and viscous moduli (Ewoldt *et al.* 2008). However, harmonics higher than the first can be neglected for moderate γ_0 at which yielding is most often seen in soft materials. Thus in strain sweep test, the mechanical response of soft materials changes from being elastic ($G' > G''$) at small strain to viscous ($G' < G''$) at large strain.

At intermediate strain, many metastable soft materials show a characteristic response in which the viscous modulus increases from its linear value up to a maximum value G''_{max} before falling off, while the elastic modulus decreases monotonically with strain and crosses below the viscous modulus at the yield point. This non-monotonic G'' response, also called the Type-III LAOS behavior (Hyun *et al.*, 2002), has been reported earlier for carbon composites of butyl rubber (Payne, 1963), soft colloidal glasses (Brader *et al.* 2010), emulsions (Mason *et al.* 1995; Bower *et al.*,1999), gels (Altmann *et al.* 2004), electrorheological fluids (Parthasarathy and Klingenberg, 1999; Sim *et al.* 2003), associating polymer solutions (Tirtaatmadja *et al.* 1997a; Tirtaatmadja *et al.*1997b) and weakly structured materials such as xanthan gum solutions (Song *et al.* 2006). On the other hand, polymeric fluids such as solutions and melts, which are ergodic, are typically known to exhibit strain-softening response (Doi and Edwards, 1986) in which chain orientation causes both moduli to decrease monotonically with increasing shear strain.

Recently, Miyazaki *et al.* (2006) proposed an elegant qualitative argument for explaining the origin of the non-monotonic G'' response based on the reasoning that yielding involves a strain-induced decrease in the characteristic relaxation time of the material. The authors proposed that the non-monotonic G'' behavior should be observable in all complex fluids. In this work, we validate this hypothesis by demonstrating experimentally the universality of the yielding response. We also extend the argument further to infer an interesting dynamical feature.

Modified Maxwell model

Following Miyazaki *et al.* (2006) we may represent any viscoelastic fluid by a parallel combination of N Maxwell elements each comprising linear springs[†] in series with non-linear dashpots so that the relaxation times (τ_i) of the Maxwell elements are given by some decreasing function of the strain amplitude such as

$$\frac{1}{\tau_i(\gamma_0)} = \frac{1}{\tau_i^{LVE}} + k(\omega\gamma_0)^m \quad 5.1$$

[†]Non-linear springs can be used without loss of generality. Strain softening springs will cause a reduction in the prediction of the magnitude of G''_{max} .

In equation 5.1, τ_i^{LVE} represents the characteristic relaxation time for the i^{th} mode in the linear regime, i.e. under small imposed strain. The validity of equation 5.1 with $m \approx 1$ for non-linear deformations of metastable materials was demonstrated by (Wyss *et al.* 2007) and (Yamamoto and Onuki, 1998; Leonardo *et al.* 2005; Kalelkar *et al.* 2010). Incidentally, equation 5.1 also describes the so-called convective constraint release mechanism of stress relaxation in entangled polymer melts subjected to high shear (Marrucci, 1996). Thus, the use of equation 5.1 for describing the strain dependence of relaxation times of many soft materials in the non-linear regime appears justified. Indeed, equation 5.1 is a simplified version of the model proposed by Derec *et al.* (2001), who in addition to considering the strain dependence of relaxation times, have also taken into account the influence of possible aging effects.

The elastic and viscous moduli for the Maxwell model can be written as

$$G'(\omega, \gamma_0) = \sum_i^N \frac{g_i [\omega \tau_i(\gamma_0)]^2}{1 + [\omega \tau_i(\gamma_0)]^2}; G''(\omega, \gamma_0) = \sum_i^N \frac{g_i [\omega \tau_i(\gamma_0)]}{1 + [\omega \tau_i(\gamma_0)]^2} \quad 5.2$$

Here $\tau_i(\gamma_0)$ is given by equation 5.1. Miyazaki *et al.* (2006) explained the strain dependence of G'' by considering a single mode ($N = 1$) in equation 5.2. The frequency regime of interest is one in which the material is predominantly elastic at small strains so that the Deborah number is given by $\omega \tau_c^{\text{LVE}} \gg 1$, where τ_c^{LVE} is a strain independent characteristic time of the material that is experimentally measured as the inverse of the cross-over frequency. At small strain amplitudes, $G' \sim g$ and $G'' \sim g / \omega \tau_c^{\text{LVE}}$ so that $G' > G''$ and both are independent of the applied strain. At moderate strain amplitudes just after the linear regime, the Deborah number is still $\omega \tau_c(\gamma_0) > 1$ but the relaxation time decreases upon increasing strain so that $G'' \sim g / \omega \tau_c(\gamma_0)$ is an increasing function of strain. For large strain amplitudes the effective strain rate reduces the relaxation time to the extent where $\omega \tau_c(\gamma_0) \ll 1$, so that the moduli in equation 5.2 can be approximated as $G'' \sim g_i [\omega \tau(\gamma_0)]$; $G' \sim g_i [\omega \tau(\gamma_0)]^2$ indicating both G' and G'' to be decreasing functions of strain, with $G'' > G'$. Further, the model also predicts the crossover point i.e., the macroscopic yield point at

$$\omega \tau_c(\gamma_{0,y}) = 1, \text{ where } G' = G''_{\text{max}} = g / 2 \quad 5.3$$

In equation 5.3, $\gamma_{0,y}$ is the yield strain, which is unity when normalized as $\tilde{\gamma}_{0,y} = k\gamma_{0,y} \cong 1$ [c.f. equation 5.1]. Since equation 5.1 invokes neither the microstructural details of soft materials nor their dynamical details, the Miyazaki argument presented above should be equally valid for all viscoelastic fluids as long as they are probed in an appropriate frequency window. In what follows, we demonstrate this experimentally for different complex fluids, which are chosen such that under near-quiescent conditions some of them are in equilibrium state (polystyrene melt, surfactant lamellar phase) and some in metastable state (microgel dense suspension, hair gel, xanthan gum, and gelatin). The chosen materials also have very different microstructures.

Further, we study the complex yielding behavior of PNIPAm microgel suspensions in greater detail. Specifically, when the strain amplitude sweeps were performed at higher frequencies, a complex yielding behavior comprising two peaks in the G'' was observed. The phenomenon of double yielding in colloidal suspension has been observed in the past for suspensions of weakly attractive particles, the two peaks were attributed to cage breaking and bond breaking events (Pham *et al.* 2006; Kramb and Zukoski, 2010), or due to the presence of an additional timescale from the star arm relaxation in the case of star colloidal polymer suspensions (Helgeson *et al.* 2007). In our present study of PNIPAM microgel suspension we believe that the secondary yielding occurs due to the melting of a strain induced structure formed at higher strains, as will be discussed later in this chapter.

5.2 Materials and experiments:

5.2.1 PNIPAm: Synthesis and characterization

PNIPAm microgels were synthesized in the presence of a crosslinker (2 % by weight of monomer) and surfactant. Details of the reactants and synthesis protocol were mentioned in section 2.3.2. The synthesis was done in the presence of a surfactant which gives small size microgels ($R_h \sim 131$ nm at 20 °C). After the purification of the microgels by extensive dialysis for about 14 days they were freeze dried and stored in the form of powder. Concentrated suspensions were then prepared by dispersing known amount of polymer in deionized water. As these microgels are soft and compressible they seldom crystallize at very high concentrations. The suspensions were mixed and equilibrated at low (5 °C) and high (28 °C) temperatures. These

alternate heat–cool cycles were repeated for a week to ensure complete mixing and homogenization of the suspensions. Air bubbles trapped during mixing were removed by centrifugation. Aqueous suspensions of 4, 6, 8, 9 and 12 wt. % were prepared as described above and were then stored at 5 °C.

Characterization: Dilute microgel suspensions were used to determine the hydrodynamic radius R_h of the PNIPAm microgel. This was done by standard dynamic light scattering experiments on the 3DDLS instrument (LS Instruments Switzerland).

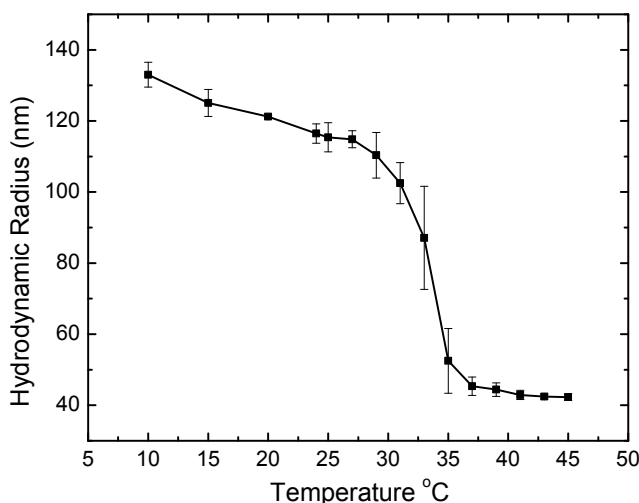


Figure 5.1: Hydrodynamic radius of PEG-diacrylate crosslinked PNIPAm microgels as a function of temperature showing VPTT at ~ 32 °C.

Determination of effective Volume fraction φ_{eff} : The microgel suspension behaves like a soft solid only when $\varphi_{\text{eff}} > \varphi_g$, where φ_g is the volume fraction at which glass transition occurs. Thus it is important to determine the φ_{eff} of the PNIPAm microgel suspension. Unlike the large microgels described in Chapter 3, the microgels used here are small in size and therefore they cannot be observed under the microscope. Hence the φ_{eff} cannot be calculated as $\varphi_{\text{eff}} = \rho * \frac{4}{3} \pi R_h^3$, ρ being the number density measured directly by microscopic observations. Thus the effective volume fraction was determined by measuring the relative viscosity in dilute solutions and using the Einstein equation which is related to the volume fraction as below

$$\left(\frac{\eta_s}{\eta_0} \right) = 1 + 2.5kc \quad 5.4$$

Here, c is the mass concentration of microgels in suspension, k denotes the conversion factor from c to ϕ_{eff} , ($\phi_{\text{eff}} = kc$) and is approximately given by $k = \alpha (\rho_g)^{-1}$ where ρ_g is the bulk density of PNIPAm, and α is the swelling ratio given by $\alpha = (R_{h(\text{swollen})})^3 / (R_{h(\text{dry})})^3$.

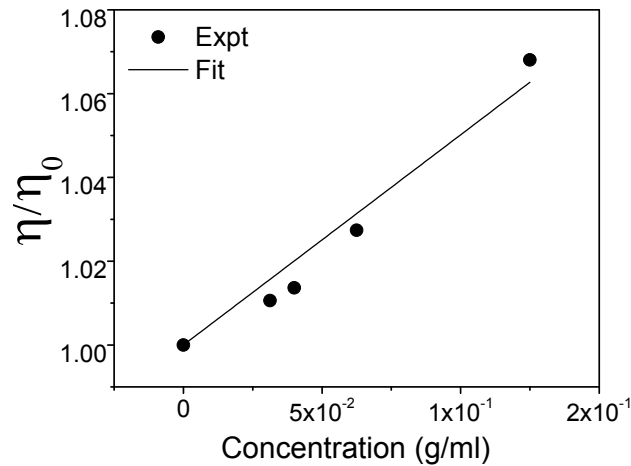


Figure 5.2: Relative viscosity as a function of concentration for PNIPAm microgel suspension.

We followed the method described by Senff and Richtering, (1999) in which a series of dilute aqueous solutions of PNIPAm microgels of known mass concentrations were prepared and their relative viscosities were measured using an automatic viscometer (CT 1650, Schott-Gerate, Germany) at 24 °C. The relative viscosity measurement as a function of concentration for various dilute aqueous suspensions of PNIPAm is shown in Figure 5.2. The symbols are experimental data points and the line is a fit of the equation 5.4 to the experimental data. The factor k was calculated by fitting the data to the Einstein's equation. The volume fraction at 24 °C was then calculated as kc . The volume fractions at other temperatures were determined by equation 5.5

$$\phi_{\text{eff}}(T) = \phi_{\text{eff}}(24^\circ\text{C}) \times \left(\frac{R_h(T)}{R_h(24^\circ\text{C})} \right)^3 \quad 5.5$$

For a 6 wt.% PNIPAm suspension, the calibration constant ' k ', ϕ_{eff} at different temperatures as determined from equation 5.5, and the R_h are tabulated in Table 5.1. It can be seen that $\phi_{\text{eff}} > \phi_g$ for $T < V_{\text{P}TT}$ indicating that the 6 wt.% suspension is a SCG. However for $T > V_{\text{P}TT}$, we see that $\phi_{\text{eff}} < \phi_g$. Above the $V_{\text{P}TT}$ the suspension

becomes a gel due to attractive interparticle interactions. Thus all the experiments on PNIPAm microgels were performed at $T < VPTT$.

Table 5.1: Hydrodynamic radius ' R_h ', calibration constant ' k ' and effective volume fraction φ_{eff} at different temperatures.

Temperature °C	15	20	24	32	33	35
R_h (nm)	125	131	116	87	74	52
k	25	28	20	8	5	1.8
φ_{eff} (6 wt.%)	1.8	1.5	1.2	0.5	0.3	0.1

5.2.2 Preparation of other complex fluids

Xanthan Gum: A 2 wt. % aqueous suspension of xanthan gum gives a soft colloidal glass (Song *et al.* 2006). 98 ml of water is taken in a beaker and stirred at ~500 rpm with the help of an overhead stirrer. 2 g of xanthan gum powder was added very slowly to the already stirring water. This confirmed complete and homogenous mixing of the powder. Stirring was continued for 30 mins after all the xanthan gum is added. The suspension was stored at 5 °C in a screw cap container.

Surfactant Lamellar Phase: A 90wt. % aqueous suspension of a non-ionic surfactant C₁₂E₉ (Rylo) was prepared using deionized water. The suspension was heated above the isotropic temperature (~40 °C) on a water bath. This warm solution was then mixed vigorously using a vibrato meter. Bubbles trapped were removed by sonication and multiple cycles of heating and cooling above the isotropic melting temperature. A thermodynamically stable homogenous lamellar phase was formed at room temperature (~25 °C) as confirmed by small angle x-ray scattering (Kulkarni *etal.* 2011).

Gelatin: A 14 wt. % Gelatin solution was prepared in deionized water. Heating the solution above 40°C homogenized the gelatin powder. On cooling the solution to room temperature, a gel was formed, which took the shape of the container at room temperature (~25 °C).

Hair Gel: A commercial hair gel (Brand –Park Avenue) was used as received.

Polystyrene Melt: Polystyrene ($M_w \sim 550,000 \frac{\text{g}}{\text{mol}}$, PDI~1.05) was purchased from Sigma Aldrich, (GPC grade) and disk samples (25 mm diameter) were prepared by compression moulding at 170 °C (Pandey, 2012).

5.2.3 Experimental protocol:

5.2.3.1 PNIPAm suspensions

All rheology experiments were done on a stress controlled rheometer (MCR301, Anton Paar). The geometry used was a cone and plate (cone angle 1 degree, diameter 25 mm). A humidity chamber was used around the sample to minimize the evaporation of water during the rheological experiments. The schematic representation of the experimental protocol specifically for PNIPAm suspensions is shown in Figure 5.3.

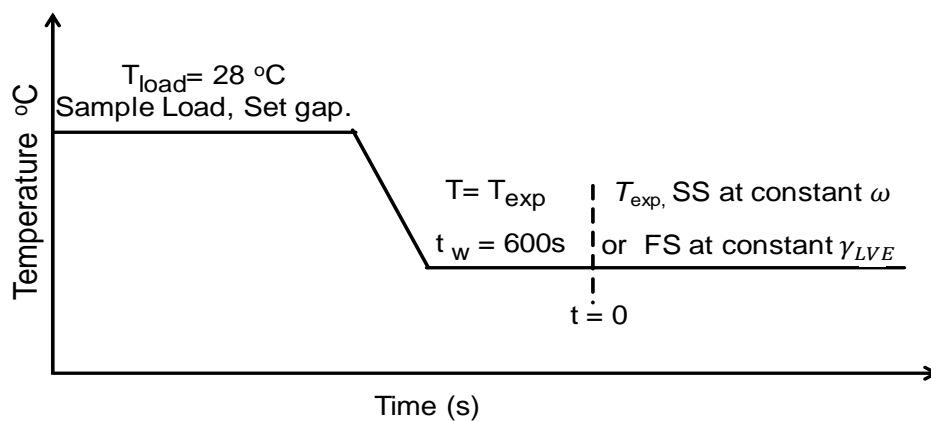


Figure 5.3: Schematic of experimental protocol used for measuring the rheology of PNIPAm microgel suspensions. SS and FS denote strain sweep and frequency sweep experiments, which were performed at constant frequency ω and constant strain γ_{LVE} respectively.

The sample was loaded onto the rheometer plate, and the gap was set at temperature $T_{load} = 28\text{ }^{\circ}\text{C}$. The sample was then cooled down to the desired experimental temperature T_{exp} and left isolated for around 10 mins before starting the experiment. This procedure is chosen to erase the thermal and/or deformation history in the samples which could occur during sample preparation, sample loading etc. At $T_{load} = 28\text{ }^{\circ}\text{C}$, the microgels are of slightly smaller size as compared to the experimental temperature (typically $T_{exp} = 20\text{ }^{\circ}\text{C}$). Thus loading at a higher temperature and then lowering the temperature swells the particles and this is found to give the samples a controlled history. We also avoided loading the sample above VPTT in order to prevent aggregation.

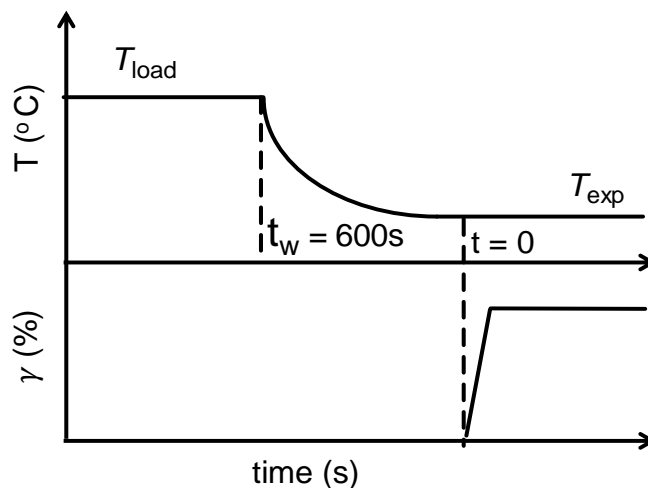


Figure 5.4: Schematic of the experimental protocol for the step strain -stress relaxation experiments.

Stress relaxation experiments were performed to determine the relaxation modulus $G(t)$, the Laplace transform of which gave the frequency dependent storage (G') and loss moduli (G''). The experimental protocol is represented schematically in Figure 5.4. The sample was loaded as explained previously and then subjected to a step strain ($\gamma = 1\%$ in the LVE regime) and stress relaxation is observed up to 3 hrs. The data when transformed to G' and G'' allowed for probing the low frequency region where the relaxation time of the interpenetrated brushes of the microgel surface could be estimated.

5.2.3.2 Other soft materials

The strain sweep and frequency sweep measurements on all the other soft materials namely xanthan gum solution, surfactant lamellar phase, gelatin and hair gel were also performed in a cone and plate geometry (cone angle 1 degree, diameter 25 mm) on a stress controlled rheometer (MCR301, Anton Paar), except for the polystyrene melt which was performed in a parallel plate geometry (25 mm diam) on a strain controlled rheometer (ARES-G2, TA Instruments). The samples were loaded onto the rheometer plate at the experimental temperature. The experiments were performed after a waiting time of 15 mins to ensure equilibration of temperature and to erase stress history during the sample loading.

5.3 Results and Discussions:

5.3.1 Yielding in PNIPAm microgel suspension

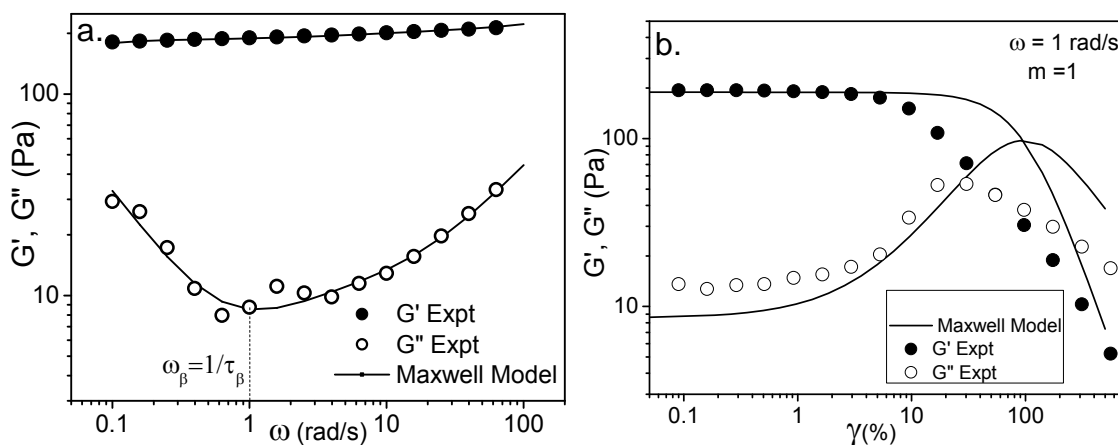


Figure 5.5: (a) Frequency sweep data at low strain amplitude ($\gamma_{LVE} = 0.6 \%$) of a 6 wt. % ($\phi_{\text{eff}} \sim 1.5$, at 20 °C) PNIPAm microgel suspension along with fit of the multi-mode Maxwell model and (b) strain sweep data for sample along with the Maxwell model fits.

Figure 5.5(a) shows a dynamic frequency sweep experiment performed on a 6 wt. % PNIPAm microgel suspension at a constant small amplitude strain, $\gamma_{LVE} = 0.6 \%$, at 20 °C. It may be noted from Table 5.1 that at 20 °C, the ϕ_{eff} for a 6 wt. % suspension is greater than one. This suggests that the microgels are tightly packed with their brushes penetrating neighbouring particles. As a result the 6 wt. % suspension of PNIPAm microgels is a SCG wherein particles are effectively trapped in a cage formed by their nearest neighbours. The predominantly elastic response of the SCG can be seen in Figure 5.5(a) where, in the range of frequencies probed, the storage modulus G' is higher than the loss modulus G'' as would be expected for a SCG. In the range of frequencies probed here the storage modulus increases monotonically but weakly with frequency. The loss modulus shows non-monotonic frequency dependence with a shallow minimum at an intermediate frequency. The value of the storage modulus at the frequency where the G'' shows a minimum is often called the plateau modulus G_p .

The linear viscoelastic frequency response characterises the microstructural timescales of the material. The G'' minimum occurs at the so-called β -relaxation frequency, ω_β , corresponding to the local fast dynamics of the particle with relaxation

time, t_β . For the 6 wt.% suspension we see that $\omega_\beta = 1\text{rad/s}$. The $\omega_\beta = 1/t_\beta$, is defined here in the context of the mode coupling theory (MCT) as discussed earlier in the introduction section of Chapter 2.

Table 5.2: Thirteen mode relaxation spectrum for a 6 wt.% PNIPAm microgel suspension at 20 °C obtained from the Rheometer software by fitting the Maxwell model to the experimental Linear viscoelastic frequency response shown in Figure 5.5(a).

nth mode	1	2	3	4	5	6	7	8	9	10	11	12	13
τ_i	0.0004	0.001	0.003	0.0081	0.022	0.059	0.16	0.43	1.15	3.11	8.38	22.59	60.9
g_i	317.59	100.9	33.832	13.382	7.228	6.013	6.79	5.17	1.83	0.95	1.52	9.265	175.2

At frequencies lower than the ω_β , we observe a small upturn of the G'' indicating a possible crossover with G' , which corresponds to the slower structural relaxation arising from the escape of a particle from its cage. The crossover frequency ω_α corresponds to the α -relaxation time t_α . At frequencies $\omega > \omega_\beta$ the G''_{LVE} increases again due to dissipation related to the local particle motion over length scales of the cage. At ω_β the cage effect is the largest giving rise to minimum in G''_{LVE} .

The decrease in the α -relaxation time is possible if the cage structure is affected by the application of large amplitude strain. Figure 5.5(b) shows a strain sweep experiment performed on a 6 wt.%PNIPAm microgel suspension at 20 °C, and $\omega_\beta = 1\text{rad/s}$. At small values of strains both G' and G'' are independent of the applied strain and the material is predominantly elastic with $G' > G''$. With further increase in the strain amplitude a monotonic decrease in the G' and a non-monotonic behaviour of the G'' are observed. In particular, the loss modulus increases from its linear viscoelastic value, crosses the elastic modulus and then decreases with further increase in strain amplitude. The peak in the G'' represents the dissipation of energy in the form of heat and is a characteristic rheological feature of a soft solid (Hyun et al. 2002). The strain at which $G' = G''$, is defined here as the yield point; above this strain $G'' > G'$ implying that the material is predominantly viscous in nature. This transition from a solid-like ($G' > G''$) to liquid like $G'' > G'$ behaviour under the influence of large amplitude oscillatory flows illustrates the yielding phenomenon and is likely caused by the breakdown of the microstructure(in this case, the cage structure) in the SCG.

5.3.2 Universal features of yielding

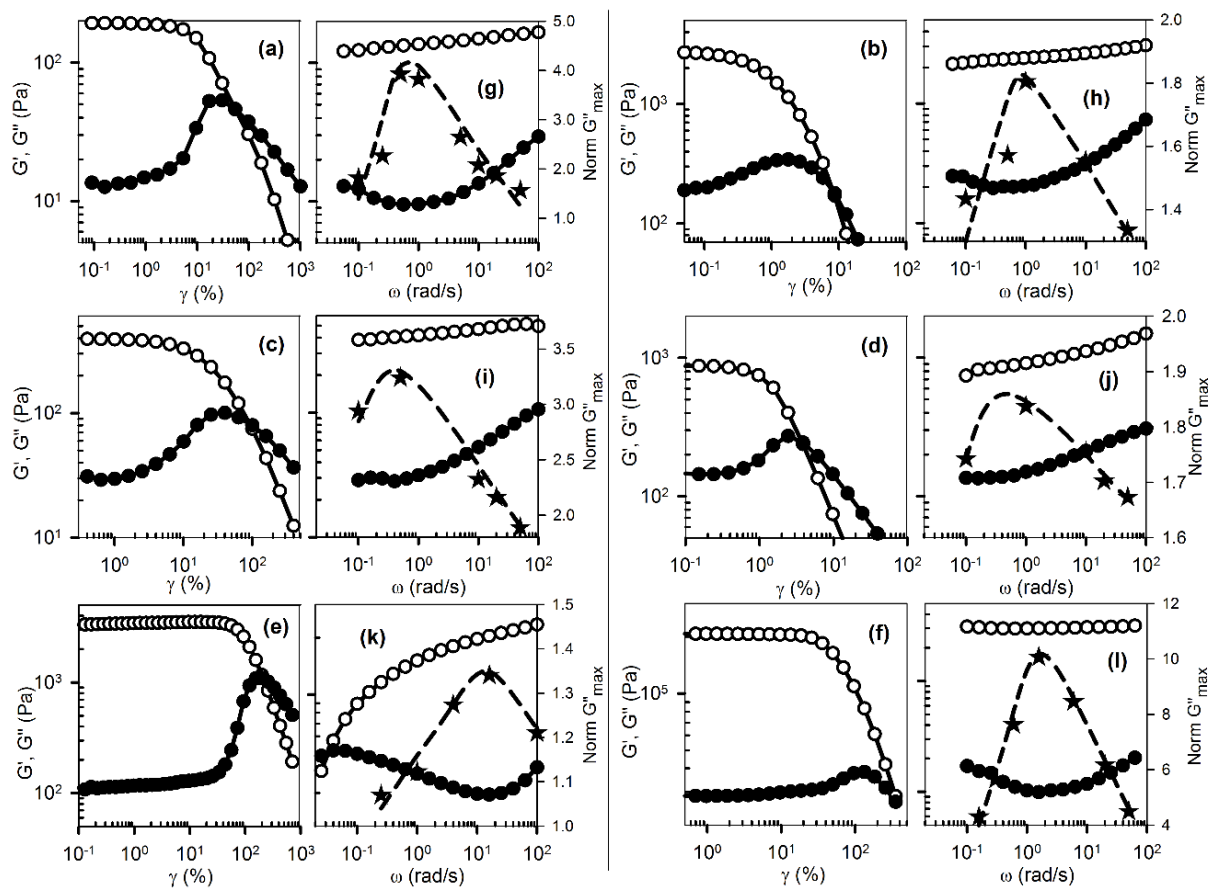


Figure 5.6: Strain sweep data at frequency where maximum in normalized G'' is observed (a-f). Frequency sweep (in LVE) and normalized G'' as a function of frequency for different materials (g-l). PNIPAm suspension (6 wt.%) at 20 °C and frequency of 1 rad/s (a, g); Lamellar phase of C_nH_{2n+1} surfactant at 25 °C and frequency of 1 rad/s (b, h); Hair gel at 25 °C and frequency of 0.5 rad/s (c, i); Xanthan gum solution at 25 °C and frequency of 1 rad/s (d, j); Gelatin at 25 °C and frequency of 1.6 rad/s (e, k) and Polystyrene at 170 °C and frequency of 16 rad/s [Adopted from, Pandey et.al, 2012] (f, l). G' is represented by open circles, G'' by filled circles, maximum normalized G'' (\tilde{G}''_{max}) by filled stars and dotted lines are guides to the eye.

Figure 5.6(a-f) shows that all materials, including the entangled polystyrene melt and the lamellar surfactant phase, show a non-monotonic G'' response followed by a crossover of the moduli, i.e. the macroscopic yielding event. Figure 5.6(g-l) shows that the linear viscoelastic frequency response of all these materials, irrespective of their microstructure and thermodynamic state, is qualitatively similar. In a particular frequency-temperature-concentration window of observation, $G'_{LVE} > G''_{LVE}$ suggesting that the material is predominantly elastic. G'_{LVE} increases monotonically but weakly with frequency, whereas the G''_{LVE} shows non-monotonic frequency

dependence with a minimum at intermediate frequency. Thus the data corroborates the simple arguments presented in the model, and underlines the similarity of patterns observed in the yielding process in complex fluids.

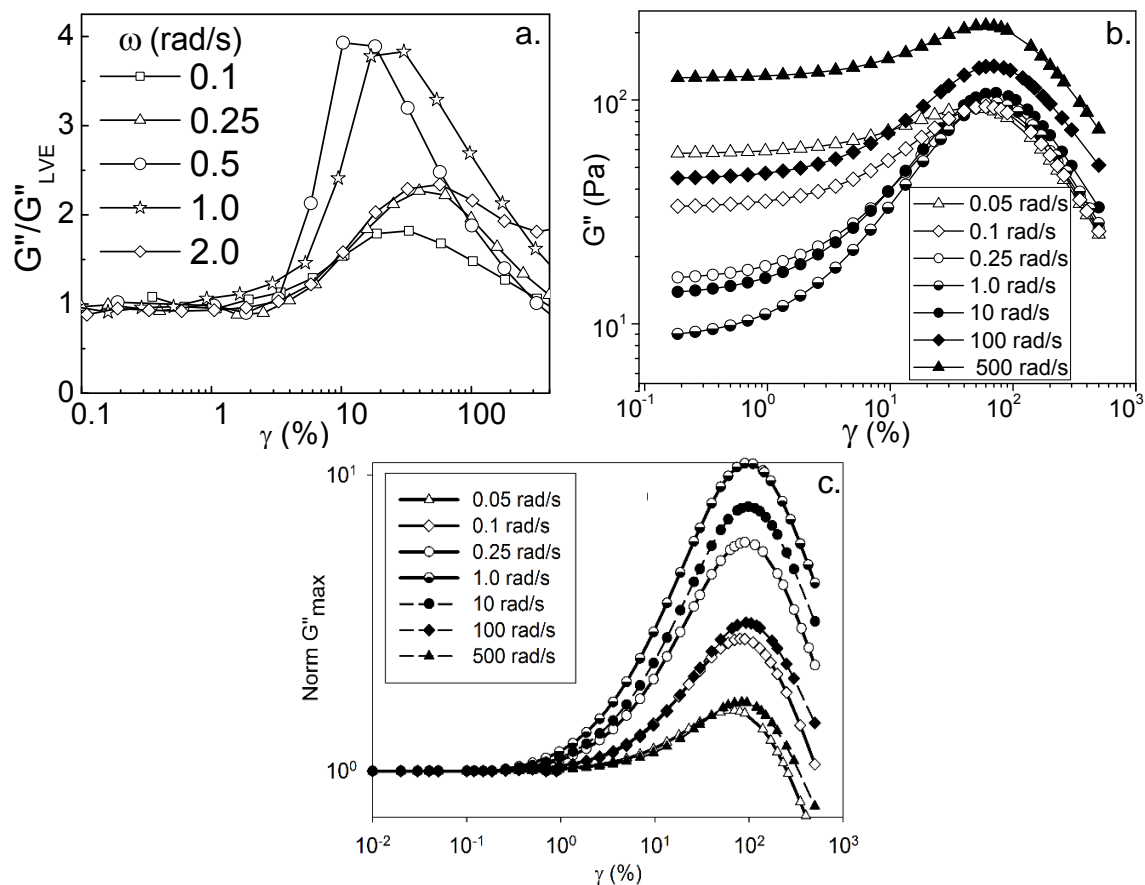


Figure 5.7: (a) Loss moduli G'' normalized with its values in the LVE regime as a function of the applied strain, probed at different frequencies $\omega = 0.1, 0.25, 0.5, 1.0$ and 2 rad/s (6 wt.% PNIPAm suspension $T = 20^\circ\text{C}$), (b) Maxwell model predictions of the strain dependence of G''_{max} for various frequencies and (c) Maxwell model predictions of the strain dependence of normalized G'' for various frequencies.

The predictions of the multi-mode Maxwell model [equation 5.2] are shown in Figure 5.5 for the representative case of the PNIPAm microgel suspension. For this calculation, a thirteen-mode relaxation spectrum was obtained in Table 5.2 by fitting the model to the experimental linear viscoelastic frequency response shown in Figure 5.5(a). The prediction of the multi-mode Maxwell model for a strain sweep experiment carried out at a representative frequency of 1 rad/s is compared with experimental data in Figure 5.7(b). Different values of the parameter m in equation 5.1 were tried and it was found that $m = 1$ gave the best fit to the experimental data. Previous experimental investigations have also suggested the value of $m = 1$ (Wyss *et al.* 2007; Kalelkar *et al.* 2010). The model provides a qualitative prediction of the non-

monotonic G'' response. In the present work, our interest is in seeking broader understanding of the phenomenon rather than quantitative predictions, for which more sophisticated models will be required. Hence, we concern ourselves with only the trends predicted by the Maxwell model.

While the multi-mode Maxwell model predicts similar non-linear response as the single-mode version of Miyazaki *et al.* (2006), it allows us to interrogate what happens to the dissipation component when the strain sweep experiments are done at different frequencies. To answer this, we define the normalized viscous modulus $\tilde{G}_{\max}'' = G_{\max}''/G_{\text{LVE}}''(\omega)$ so that the dissipation can be compared for different frequencies relative to the linear limit. Figure 5.7 (a) shows the experimental data of the strain dependence for various frequencies ($\omega = 0.1, 0.25, 0.5, 1$ and 2 rad/s).

It can be seen that \tilde{G}_{\max}'' shows a non-monotonic dependence on frequency. Specifically, \tilde{G}_{\max}'' increases with frequency, reaches a maximum and then decreases with further increase in frequency. This happens because G_{\max}'' has a weaker dependence on frequency, see Figure 5.7(b) relative to $G_{\text{LVE}}''(\omega)$; the latter has a frequency dependence shown in Figure 5.7(a). The Maxwell model predictions for \tilde{G}'' also show the same trend as seen in Figure 5.7(c). These results show that the normalized viscous modulus \tilde{G}_{\max}'' has a maximum at the characteristic frequency at which the $G_{\text{LVE}}''(\omega)$ shows minimum. To illustrate this further, Figure 5.8 shows the predictions of \tilde{G}_{\max}'' at different frequencies as calculated from the multi-mode Maxwell model for the case of the PNIPAm microgel suspension. Also shown are experimentally determined values of \tilde{G}_{\max}'' and the linear frequency response for this material. Indeed the maximum in \tilde{G}_{\max}'' is seen to occur at the frequency where $G_{\text{LVE}}''(\omega)$ shows minimum. That this is a common feature of yielding for all soft materials is seen from Figure 5.6(g-l), which shows \tilde{G}_{\max}'' at various frequencies for all materials investigated here. In each case the maximum in \tilde{G}_{\max}'' is seen at the frequency where $G_{\text{LVE}}''(\omega)$ shows minimum.

In order to better understand this phenomenon, we show in Figure 5.9 the predictions of Maxwell model for frequency dependence of viscoelastic moduli at various strain amplitudes starting from small strain (linear response) to large strains (non-linear response). The relaxation spectrum used here as an example is that for the PNIPAm suspension, see Table 5.2, however, similar features will be predicted for any other complex fluid.

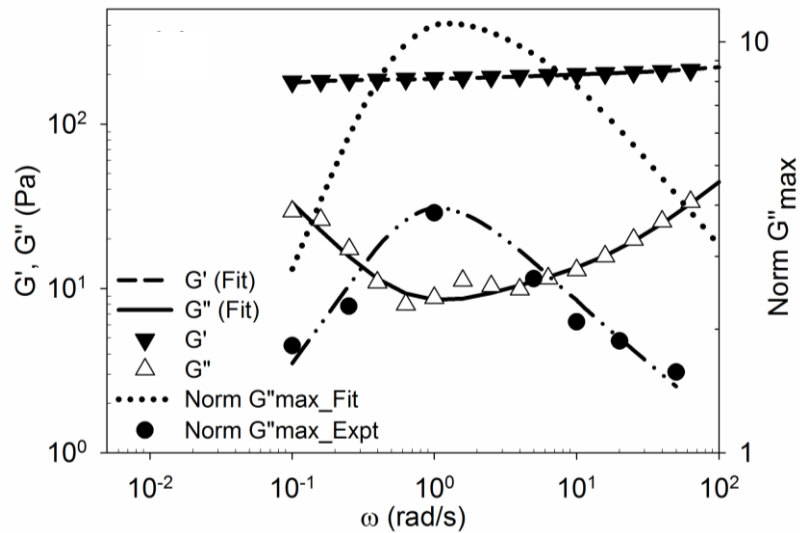


Figure 5.8: Comparison of experimentally determined normalized \tilde{G}''_{\max} (filled circles) as a function of frequency with predictions of the Maxwell model (dotted line) for the normalized \tilde{G}''_{\max} . The dash-dot line through the experimental data only serves as guide to the eye. The figure also shows the experimental linear viscoelastic frequency response (triangles) and model fit for the same (bold and dashed lines).

The calculations are extrapolated to low frequencies where the Maxwell model predicts a crossover of moduli corresponding with the structural relaxation time τ_c^{LVE} . For increasing strain amplitude several features are worth noticing in the Figure 5.8: In the low frequency region $\omega < \omega_c^{\text{LVE}}$, both moduli decrease with increasing strain suggesting strain softening behavior with $G'' > G'$. At higher frequencies $\omega > \omega_c^{\text{LVE}}$, while the G' decreases with strain, the G'' increases with strain. This corresponds with the upturn in G'' seen in the amplitude sweep predictions. It can be seen that the ratio $\tilde{G}'' = G''(\omega, \gamma_0) / G''_{\text{LVE}}(\omega)$, i.e. the normalized loss modulus, is always the highest for the frequency corresponding to the minimum in $G''_{\text{LVE}}(\omega)$ indicating maximum dissipation at this frequency.

The crossover frequency $\omega_c(\gamma_0)$ increases with strain amplitude indicating a decrease in the structural relaxation time in accordance with equation (5.1). Thus the slow structural relaxation time scale approaches the fast time scale monotonically with increasing strain amplitude. At 90 % strain for this material, the ω_c approaches the frequency at which $G''_{\text{LVE}}(\omega)$ shows a minimum and at a slightly higher strain we get $\omega_c = \omega_\beta$.

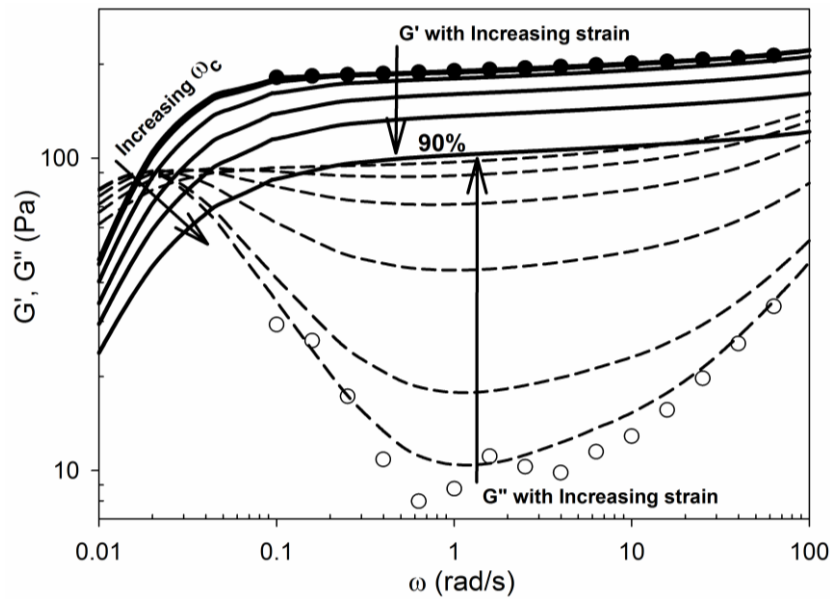


Figure 5.9: Prediction of the Maxwell model for the frequency dependence of G' and G'' at different strains $\gamma_0 = 1\%$ (LVE), 5, 20, 40, 60 and 90% (arrows indicate increasing strain amplitudes). The closed symbols and the open symbols represent the experimental G' and G'' respectively for $\gamma_{LVE} = 0.6\%$.

Above this strain, G' decreases below G'' (indicating yielding), and G'' also decreases over the entire frequency range. Thus the maximum normalized dissipation is obtained at slightly higher than 90% strain for this fluid and at frequency equal to ω_β , which is the frequency corresponding to the minimum in G''_{LVE} and is referred to as the beta relaxation frequency of cage dynamics in the framework of the Mode Coupling Theory (Mason and Weitz, 1995).

The above observations together with equation 5.3 imply that the maximum relative dissipation (\tilde{G}''_{max}) just before macroscopic yielding will occur in an amplitude sweep experiment when the imposed frequency satisfies $\omega = 1/\tau_c = 1/\tau_\beta$; here $\tau_c(\gamma_0)$ is the strain dependent structural relaxation time and $\tau_\beta = 1/\omega_\beta$ is the β -relaxation time. For soft glassy materials comprising particles trapped in a local 'cage', τ_c represents the time scale over which a trapped particle would escape its cage, while τ_β corresponds to the cooperative motion of the particles within the cage (Roldan-Vargas *et al.* 2010). Thus, the maximum relative dissipation prior to macroscopic yielding is seen to occur when the dynamics of structural relaxation are accelerated by the imposed shear to an extent where they become equal to the beta relaxation dynamics so that, effectively, a particle in the fluid does not *feel* the presence of topological constraints.

For entangled polymers, whose dynamics may be understood using the tube model, Marucci (1996) argued that the tube renewal time scale τ_c will decrease upon imposition of large and rapid deformation by the so-called convective constraint release process in which neighbouring entangled chains are convected away from the test chain releasing entanglements locally along its contour. Under sufficiently strong flows, if the rate of CCR is of the same order as the relaxation of a disentangled polymer then the polymer chain would not experience the presence of topological constraints (tube) in a dynamical sense. The latter is approximately given by the Rouse reorientation time τ_R of half the chain in its tube. Hence when the imposed frequency of a large amplitude oscillatory flow approaches τ_R , a complete destruction of the tube is possible. This is akin to the destruction of the cage structure in a soft glassy material. It is well known that the Rouse frequency $\omega_R = 1/\tau_R$ is slightly lower than the frequency at which G''_{LVE} shows minimum (Rubinstein and Colby, 2003; Doi and Edwards, 1986). If the imposed frequency equals the Rouse frequency, a polymer chain would not feel the presence of topological constraints of the entanglements. Therefore the criterion $\omega = 1/\tau_c = 1/\tau_R$ results in maximum dissipation in the case of entangled polymers as well.

5.3.3 Effect of concentration on G'' peak

Figure 5.10(a) and (b) shows the strain dependence of the storage modulus and loss modulus of PNIPAm microgel suspensions performed at a constant frequency ($\omega = 1 \text{ rad/s}$) for three different concentrations namely 4, 8 and 12 wt. % at 25 °C. Figure 5.10(c) shows the normalized storage modulus (G'/G'_{LVE}) and loss modulus (G''/G''_{LVE}) for the same suspensions. As the concentration is increased, the cage size decreases as indicated by rise in the storage modulus, see Figure 5.10(a). The extent of the relative dissipation as a function of concentration seen in Figure 5.10(c) shows that the maximum relative dissipation occurs for the highest concentration. This can be explained by the single mode Maxwell model given in equation 5.2., which suggests that $\tilde{G}''_{max} = g/G''_{LVE}$. Figure 5.10(a) shows that g (as $G'_{LVE} \sim g$) increases with the increase in concentration. However, G''_{LVE} doesn't increase as much as the g with increase in concentration. Thus the maximum relative dissipation \tilde{G}''_{max} , increases with increase in concentration.

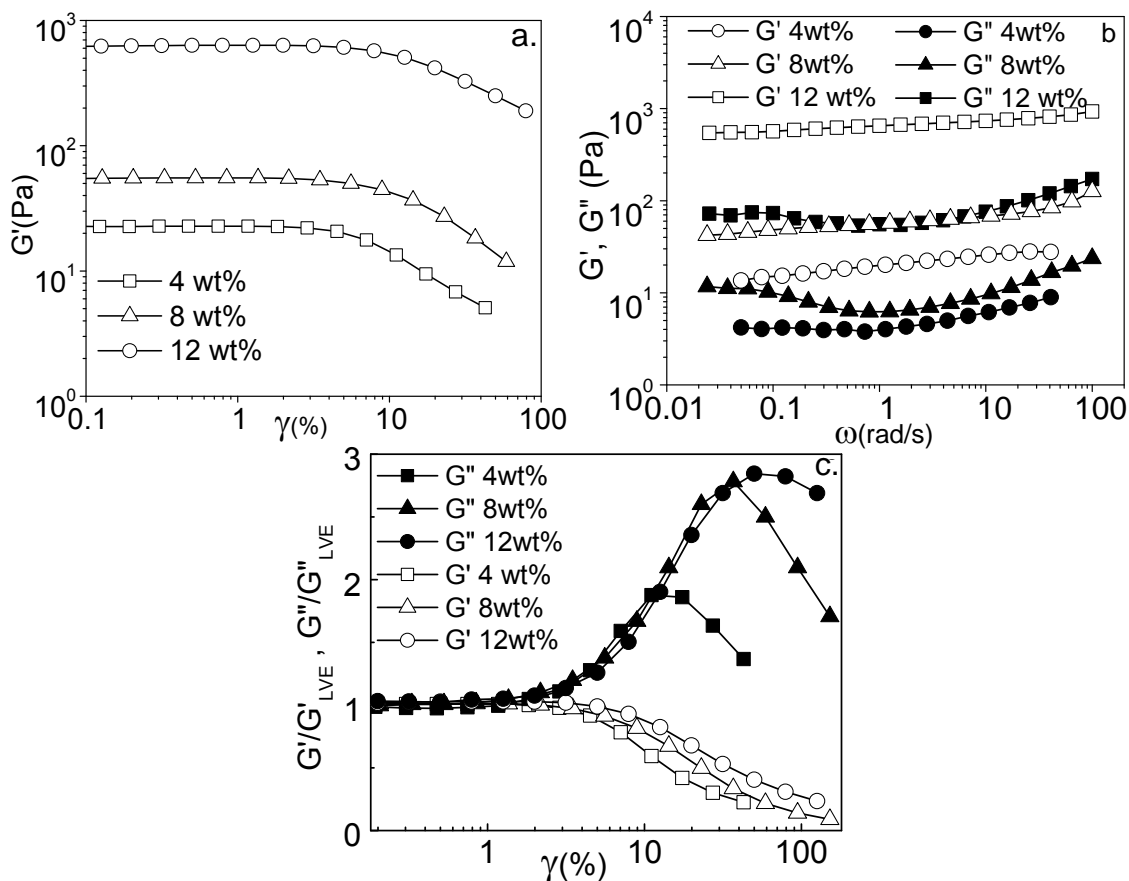


Figure 5.10: (a) Storage modulus G' as a function of strain ($\omega = 1$ rad/s), (b) storage modulus G' and loss modulus G'' as function of frequency ($\gamma_{LVE} = 0.5\%$) and (c) normalized storage (G'/G'_{LVE}) and loss (G''/G''_{LVE}) modulus as a function of strain.

5.3.4 Double yielding in PNIPAm suspensions

When strain sweep experiments were performed at higher frequencies ($\omega > \omega_{\beta}$), a complex yielding behavior with two peaks in the loss modulus G'' were observed as seen in Figure 5.11(a). At these frequencies ($\omega = 5, 10, 20$ and 50 rad/s) the intensity of the second G'' peak is greater than the intensity of the first G'' peak. There is also an occurrence of a weak but clear peak in the storage modulus G' at higher strains as shown in Figure 5.11(b). The intensity of strain induced G' peak becomes prominent with increasing frequency, with the corresponding prominence of the second G'' peak with frequency, see Figure 5.11. Thus, it is clear that the appearance of the G' and G'' peaks are frequency dependent.

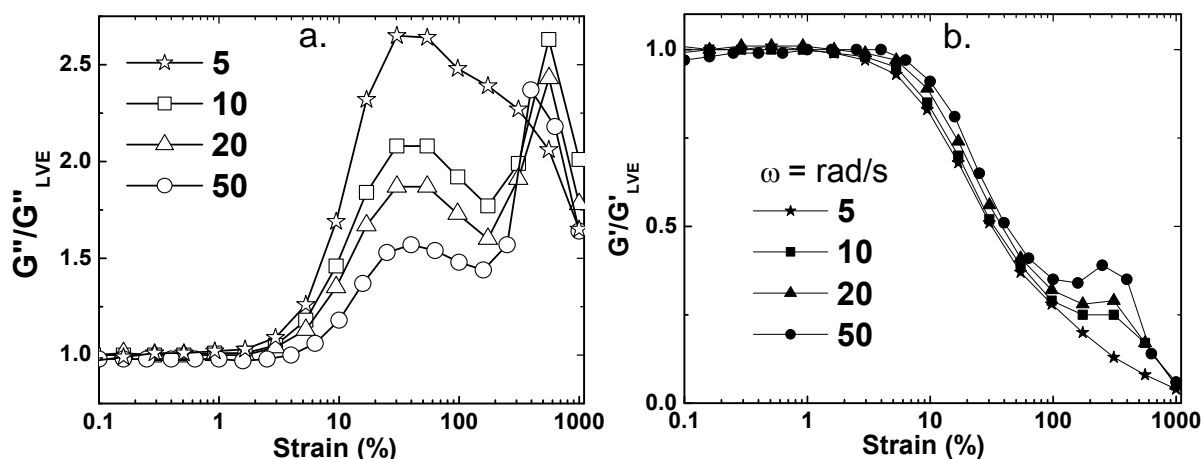


Figure 5.11: Effect of frequency on the height of the G' and $2^{\text{nd}} G''$ peak (a) Normalised G' as function of strain for different frequencies $\omega = 5, 10, 20$ and 50 rad/s and (b) Normalized G'' as function of strain for different frequencies.

The phenomenon of double yielding in colloidal suspension has been observed in the past and found to occur in suspensions of weakly attractive particles, in which the two peaks were attributed to cage breaking and bond breaking events (Pham *et al.*, 2006; Kramb and Zukoski, 2010). However, in case of PNIPAm suspensions, all the experiments were performed at 20°C which is much below the VPTT, where the microgels interact via excluded volume repulsion. We have discussed this in detail in chapter 3. Thus, in case of PNIPAm microgel suspensions the double peak cannot be due to weak attractive potentials.

The double peak has also been observed in soft repulsive systems such as star polymer colloids, where the additional plateau is attributed to an additional timescale from the star arm relaxation (Helgeson *et al.* 2007). As discussed earlier the microgels have morphology similar to star colloids. We attempted to analyze the double yielding phenomenon in our system similar to that done for star colloidal glasses by Helgeson *et al.* (2007). In their work they observed the double yielding below and above the beta relaxation frequency. The second yielding at the lower frequencies was attributed to the star arm relaxation process t_μ occurring at longer time scales. The yielding was attributed to the disengagement of star arms followed by the usual cage breaking process. Detailed analysis was done by constructing an operating curve called the effective Pipkin diagram.

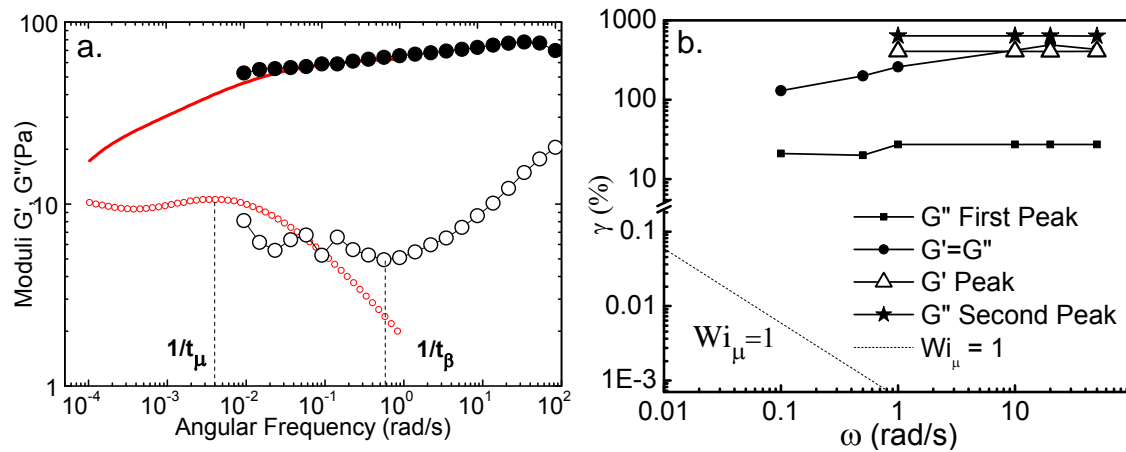


Figure 5.12: (a) Linear Viscoelastic Spectrum for a 5 wt.% ($\varphi_{\text{eff}} = 1.5$, at 10 °C) PNIPAm microgels suspension. Black filled circles and open circles represent the storage and loss modulus obtained from a frequency sweep test. The red filled and open circles are storage and loss modulus determined by a Laplace transform of a relaxation modulus $G(t)$, obtained from the stress relaxation experiment. (b) Pipkin diagram showing strain-frequency space, depicting various yielding transitions for a 5 wt.% ($\varphi_{\text{eff}} = 1.5$, at 10 °C) PNIPAm microgels suspension.

This is a strain-frequency plane and specifies the critical strains and frequencies for yielding transitions. The critical yielding is established by drawing an effective shear rate line which uses the characteristic relaxation times (t_{μ} or t_{β}), of the system under investigation. Thus the dimensionless effective Weissenberg number $Wi_{\mu,\beta} = (\gamma_0 \omega) t_{\mu,\beta}$ compares the effective shear rate ($\gamma_0 \omega$) with the characteristic relaxation time t_{μ} or t_{β} .

Figure 5.12(b) shows the Pipkin space for a 5 wt.% PNIPAm suspension at 10 °C ($\varphi_{\text{eff}} = 1.5$). The characteristic relaxation times are shown in the Figure 5.12(a) which is an extended linear viscoelastic frequency response of the material. The lower frequency response shown by the red curve is determined by the Laplace transformation of the relaxation modulus $G(t)$ obtained from the stress relaxation experiments performed in the LVE strain ($\gamma = 1\%$). The black curve is the usual FS obtained in a dynamic oscillatory response in the LVE regime.

In the Pipkin diagram the $Wi_{\mu} = 1$ line is shown by a dotted line, and is an operating line where the characteristic relaxation time t_{μ} matches the applied effective shear rate ($\gamma_0 \omega$). For the PNIPAm suspension we find that all yielding processes (first G'' peak, second G'' peak and G', G'' crossover) occur well above the $Wi_{\mu} = 1$ line.

Hence we conclude that the double yielding observed for PNIPAm does not have the same origin as double yielding seen for the star polymer colloid.

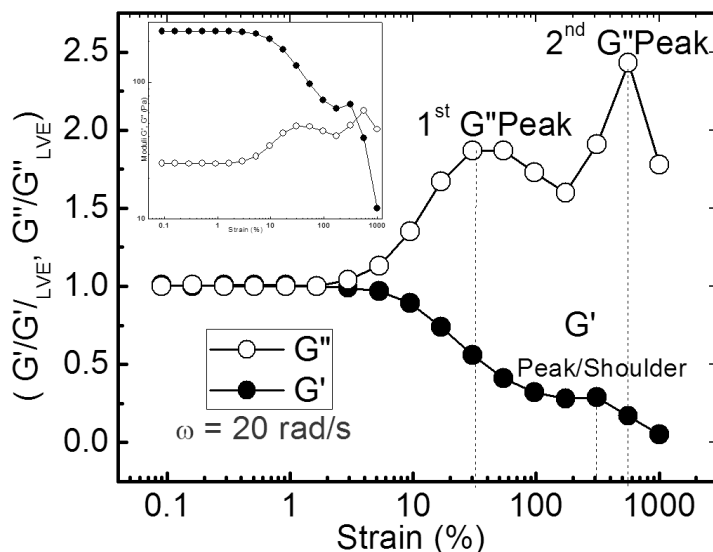


Figure 5.13: Strain sweep performed on a 6 wt.% ($\varphi_{\text{eff}} = 1.5, 20^\circ\text{C}$) PNIPAm microgels suspension at $\omega = 20 \text{ rad/s}$. The moduli G' and G'' are normalized by their absolute values in the linear viscoelastic regime. The inset shows the absolute G' and G'' as a function of strain for the same sample.

We now discuss the origin of the second peak in G'' observed at frequencies higher than the ω_β . Figure 5.13 shows normalized moduli in strain sweep experiments performed at $\omega = 20 \text{ rads}$ on a 6 wt.% PNIPAm suspension at 20°C . The inset shows the same data with its absolute values of G' and G'' . As shown in the Figure 5.13 there is occurrence of a weak but clear peak in the storage modulus G' at higher strains. The G' peak occurs after the first peak of G'' and just before the second peak of G'' . Also note that the crossover does not happen just after the first peak of G'' (Figure 5.13 inset) as was observed for lower frequency, see Figure 5.7(a). We believe that the occurrence of the G' peak could be due to formation of a strain induced structure at higher strains similar to that observed in concentrated shear thickening colloidal suspensions along the compression axis (Wagner and Brady, 2009; Kalman and Wagner, 2009).

To confirm the formation of a strain induced structure we have looked at the Lissajous curves which show the raw stress- strains curves at a constant strain and frequency for few periods of oscillation. The characteristic shapes of this curve change with the change in the viscoelastic behavior and gives useful information of the response of the viscoelastic sample under LAOS. For this purpose we used a 12

wt % sample to get good torque resolution and to obtain noise free raw data. Figure 5.14(a) shows a strain sweep test with the interesting features highlighted by colored data points and their corresponding stress-strain curves.

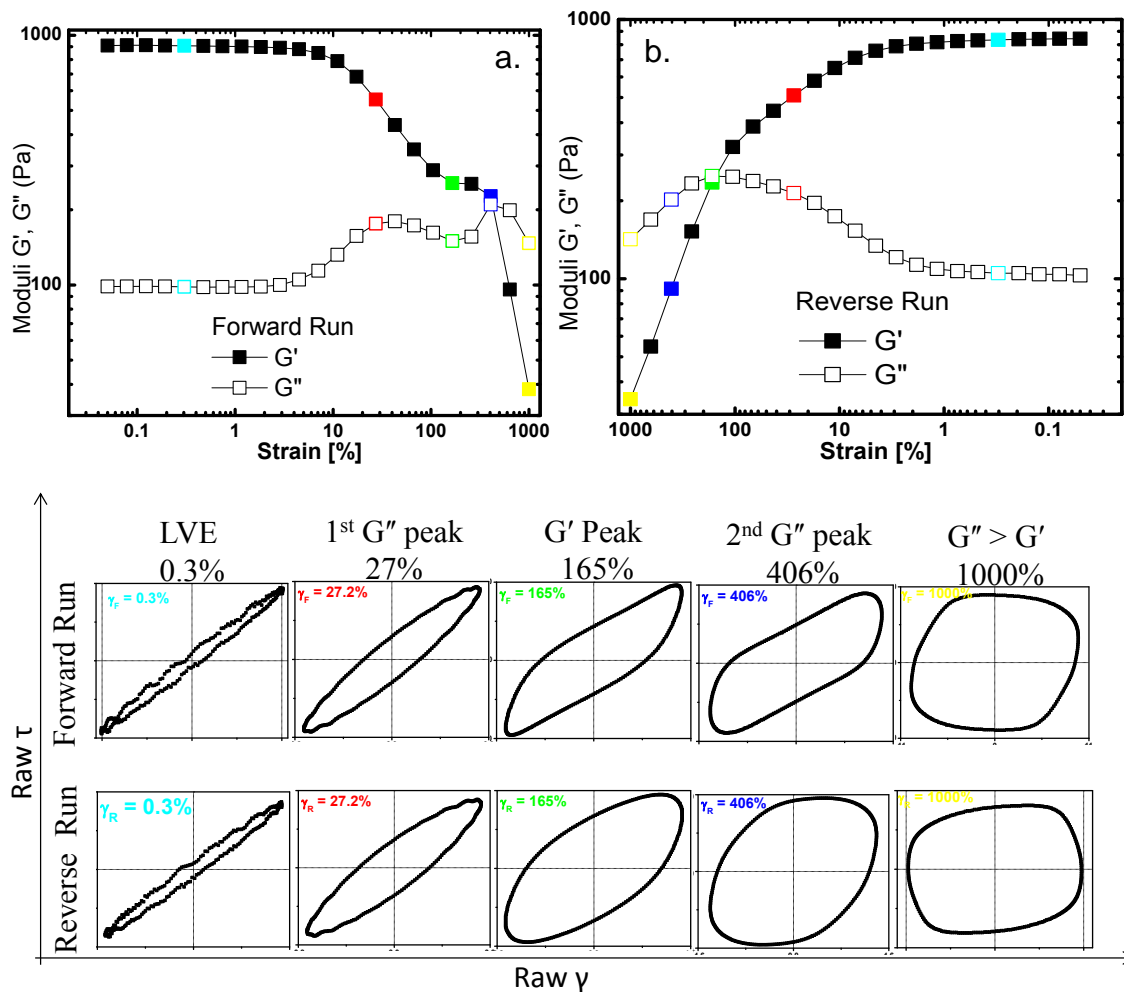


Figure 5.14: (a) Forward and (b) Reverse strainsweep test done on the same sample at a constant frequency of $\omega = 10 \text{ rad/s}$ for a 12 wt.% suspension of PNIPAm at 20 °C, comparing the stress-strain curves of some important features in the forward and reverse strain sweep runs.

The light blue data point indicates the LVE region at $\gamma = 0.3 \%$. In this region the material is solid like with the $G' > G''$ and the stress is proportional to strain. Thus the Lissajous plot appears as an ellipse with two mirror planes (the major and minor axes of the ellipse). This thin ellipse represents a viscoelastic material with high elasticity. The red data point indicates the first localized yielding event at $\gamma = 27 \%$ which is the strain value at which the first G'' peak appears. In this case the ellipse has an increased minor axis indicating a viscous component to the viscoelastic nature.

Further, the green data point at $\gamma = 165\%$ represent the G' peak. The shape of the ellipsoid loses its symmetrical nature and gets distorted. This typical shape is shown by strain hardening materials or shear thickening fluids (Ewoldt *et al.* 2008) and therefore suggests the formation of strain induced structures possibly leading to the peak in G' . The blue data point at $\gamma = 406\%$ represents the crossover point and the second G'' peak where the minor axis of the ellipse increases and also reduces the distortion.

Finally, after the crossover when the viscous component takes over the elastic component we see an ellipse regaining its symmetrical nature with much larger minor axes at $\gamma = 1,000\%$ (yellow data point). This circular feature of the Lissajous curve indicates a viscous behavior confirming a macroscopic yielding event.

A backward strain sweep was also performed immediately after the forward run Figure 5.14(b). The G' peak disappears but the loss modulus shows a broad dissipation. This suggests a thixotropic behavior of the suspension.

The formation of the strain induced structure has been shown mainly by weakly attractive particles and is driven by hydrodynamics which take over the Brownian dynamics at high strains (Wagner and Brady, 2009). However, in case of PNIPAm microgels which interact only via excluded volume repulsion at the experimental temperatures, it is not entirely clear as to what would drive the formation of structure at higher strains. Breaking of this strain induced structure adds to the dissipation and thus the secondary G'' peak occurs just after the G' peak. The macroscopic yielding i.e. the crossover of G' and G'' takes place after the G' peak, although dissipation associated with structural rearrangement has likely occurred along with the first peak in G'' . Thus the yielding process at high frequency probably involves multiple complex events.

5.4 Summary

In summary, we have shown that soft materials exhibit universal features of yielding in an oscillatory shear test when conducted in an appropriate frequency-temperature-concentration window. Specifically, the linear frequency response and the non-linear strain response are related such that the maximum relative dissipation prior to macroscopic yielding is obtained when the imposed frequency resonates with the β -relaxation time scale of the material. Under this condition of high shear, the

microscopic structural entities that make up the material do not feel topologically constrained any more. Lastly, the double yielding phenomena observed for the PNIPAm microgels at high frequencies was attributed to the melting of a shear induced structure formed at high strains.

Chapter 6

Conclusions and Future Work

6.1 Conclusions:

This thesis reports investigations on structure-property relations in dense aqueous suspensions of PNIPAm microgels, which are model systems to study structure and dynamics of soft colloidal glasses. Large (micron-sized) and small (sub-micron) microgels were synthesized and characterized by light scattering techniques. Dense suspensions of microgels were studied by DWS, which provides information about their structure and dynamics under quiescent conditions, and by non-linear rheology, which provides information about their flow properties.

Monodisperse PNIPAm microgels were synthesized by precipitation polymerization in the presence of a cross-linker as described by Pelton and Chibante,(1986). The size of the microgel was controlled by adding an anionic surfactant during the polymerization. The synthesis of highly cross-linked and larger size microgels was done in the absence of surfactant and by adding ~6.7 % (by weight of monomer) cross-linker. The faster reaction rate of the cross-linker resulted in a core-shell like morphology of the microgel with a highly cross-linked inner core and a loosely cross-linked brush-like surface. SLS and DLS experiments were performed to measure the hydrodynamic radius R_h , geometric radius R and the radius of gyration R_g , which together represent the radial density gradients in the microgel, see Figure 3.2.

Dense disordered suspensions were prepared by mixing large sized microgels with predetermined amount of smaller sized microgels. The number density of the suspension was determined by confocal microscopy. The effective volume fraction (defined as $\varphi_{\text{eff}} = \rho * \frac{4}{3}\pi R_h^3$, ρ being the number density) of the suspensions could be varied by simply changing the measurement temperature; this was possible due to the thermoresponsive nature of the PNIPAm polymer. All studies in this work were

done at temperatures below the VPTT of PNIPAm (VPTT \sim 32 °C). The structure and dynamics of these suspensions in the concentration range of $0.6 < \varphi_{\text{eff}} < 0.9$ were interrogated using DWS.

Dense suspensions of sub-micron size PNIPAm microgels with lower cross-linker content (2 %by weight of monomer) were used for rheological studies. These suspensions remained disordered at high concentrations. Since the microgels were much smaller, their number density could not be determined by microscopy. Instead, the φ_{eff} was determined directly by measuring the relative viscosity in dilute solutions and using the Einstein's relation, see equation 5.4. The rheology of dense suspensions of these microgels was investigated by performing oscillatory shear experiments. In particular, non-linear flow properties were studied by performing strain rate frequency superposition experiments and strain sweep experiments at constant frequencies.

The salient conclusions of the DWS studies and the non-linear rheological studies are described below.

6.1.1 DWS studies

Dynamics of dense suspensions of larger sized microgels was investigated close to and above the random close packing fraction $\varphi_{\text{RCP}} = 0.63$ (of equivalent hard spheres) by using diffusing wave spectroscopy. The decay of the temporal autocorrelation function $G_2(\tau)$ was measured for different values of φ_{eff} , which was controlled by varying the temperature. For $\varphi_{\text{eff}} < \varphi_{\text{RCP}}$, the autocorrelation function decayed to zero, however for $\varphi_{\text{eff}} > \varphi_{\text{RCP}}$, when the brushes touch each other, the correlation function reached a non-zero plateau from where it did not decay within the experimental time window. Interestingly, a continuous increase in the plateau value was observed with increase in φ_{eff} , see Figure 3.3. This kind of evolution of the $G_2(\tau)$ plateau is usually seen in systems which forms gels where the increase in the number of sticky strings lead to a denser network giving rise to a higher plateau value (Chaudhuri *et al.* 2010). However unlike gels, in which the length scales for dynamical arrest obtained from the plateau value are typically of the order of particle size or larger, the length scales observed for the PNIPAm microgel dense suspensions were much smaller than particle size ($\sim 0.1R_h$), which are typical of glasses and represent the size of a local cage (or a local energy minima) in which

particles are trapped. Moreover unlike gels, where there is an attractive interaction between the constituents, the interaction between the microgels was dominated by excluded volume repulsion. Thus the continuous evolution of the plateau in the PNIPAm microgel suspension suggests an interesting mixed gel-glass characteristic of the dynamics. In this thesis we have proposed that the ability of the soft brush like surfaces of the microgels to interpenetrate and thereby stiffen provides a soft repulsive core-core interaction, which is the origin of this kind of mixed dynamical behaviour.

At still lower temperatures where $\varphi_{\text{eff}} \gg \varphi_{\text{RCP}}$, yet another interesting feature was observed namely that the $G_2(\tau)$ showed a logarithmic decay at intermediate lag times for suspensions of lower number density, and a well-defined additional plateau at intermediate lag times for suspensions of higher number density, see Figure 3.3 and Figure 3.4. These features translated similarly for the average mean square displacement of particles in the suspensions. The appearance of a double plateau is a signature of a higher order glass-glass transition. Usually glass-glass transition is observed in systems where there are two different interaction potentials like attractive and repulsive (Zaccarelli and Poon, 2009; Chen *et al.* 2003). However, some recent studies showed that glass-glass transition can also be obtained when both the potentials are repulsive, namely the square shoulder potential (Das *et al.* 2013; Sperl *et al.* 2010). Our analysis of the structure of the microgel suspension shows that the second plateau appears when the brushes penetrate to an extent where they now start touching or slightly penetrating the outer region of the highly cross-linked cores of the neighboring particle. This gives rise to an additional brush-core repulsion, which is expected to be stronger than the core-core repulsion due to the impenetrable nature of the core. At these volume fractions the cage size saturates to values of $\sim 0.1R_{\text{RCP}}$, indicating that the cores of the microgels reach close to random close packing arrangement.

The cage size when plotted against the effective volume fraction shows a master plot for suspensions of different number densities, see Figure 3.6. The cage modulus, as calculated from the cage size using entropic arguments, shows a weaker φ_{eff} dependence compared to the hard sphere system. This kind of weak dependence is a signature of a soft potential (Mattsson *et al.* 2009). At higher volume fraction where the second plateau in $G_2(\tau)$ was observed, the modulus shows further

softening similar to that observed for core-shell like block copolymer systems at high concentrations (Charbonneau *et al.* 2011).

6.1.2 Non-linear-rheology

In this work, the strain rate frequency superposition (SRFS) technique, first proposed by Wyss *et al.* (2007) for the first harmonic viscoelastic moduli, was validated for dense suspensions of PNIPAm microgels, see Figure 4.3 and 4.4 and for other soft solids such as a Xanthan gum solution and a commercial hair gel (Kalelkaret *al.* 2010). Furthermore, the SRFS principle was also checked for the higher harmonics of the viscoelastic moduli and found to work identically for all of them. Specifically, it was shown that the SRFS curves for higher harmonic moduli also could be superimposed onto master curves with the same shift factors as for the first harmonic moduli, see Table 4.1. Further, it was shown that the frequency dependences of the third and the fifth harmonic moduli obtained from SRFS measurements are mirror images of their strain dependences obtained from strain sweep tests, see Figure 4.5. It was also confirmed that the energy dissipated per unit volume in an oscillatory shear experiment is governed by the first harmonic loss modulus alone, see Figure 4.6. Most importantly, this study confirmed that under large deformation conditions the time scale for structural relaxation in soft solids is set by the imposed deformation rate, see equation 4.3.

As a follow up on the SRFS work we studied the phenomenon of yielding of soft materials in large amplitude oscillatory shear flows. In particular, the PNIPAm microgel suspension and several other soft materials representing widely different microstructures and thermodynamic states (equilibrium and non-equilibrium) were subjected to strain sweep experiments at different frequencies. For each of these materials, a frequency-density-temperature window was selected in which the material was predominantly elastic ($G' > G''$) at a small strain. With increasing strain, all the materials investigated here showed a monotonic decrease in the elastic modulus and a non-monotonic change in the viscous modulus (the so-called Type III LAOS response) followed by a crossover of the viscoelastic moduli ($G'' > G'$), which is defined here as a macroscopic yielding event. Particular attention was given to the phenomenon of a peak observed in the loss modulus followed by macroscopic yielding. Our experimental results unambiguously validate the hypothesis of universal features of yielding proposed by Miyazaki *et al.* (2006) namely, that all soft materials

whose characteristic time scale for structural relaxation is set by the imposed shear rate will show Type III LAOS response. Additionally, our data suggests that the linear frequency response and the non-linear strain response are related such that the maximum relative dissipation in a strain sweep experiment is observed when the imposed frequency resonates with the characteristic β -relaxation time scale τ_β of the material, see Figure 5.6. The characteristic τ_β is defined as the inverse of the frequency at which the linear viscous moduli (G''_{LVE}) shows a minimum ($\tau_\beta = 1/\omega_\beta$). Under this condition of high shear, the microscopic structural entities that make up the material do not feel topologically constrained anymore. This is because the topological constraints are removed by the imposed shear at the same frequency at which the structural entities explore the length scale of the constraints. A simple multi-mode extension of Miyazaki's (Miyazaki *et al.* 2006) phenomenological Maxwell model is able to predict qualitatively all the universal features of yielding in soft materials, see Equation 5.1 and 5.2.

For the PNIPAm suspensions, in addition to the yielding phenomenon described above, a more complex yielding behavior comprising two peaks in the G'' was observed when the strain amplitude sweeps were performed at high frequencies, see Figure 5.11. The phenomenon of double yielding in colloidal suspensions has been observed in the past for suspensions of weakly attractive particles, in which the two peaks were attributed to cage breaking and bond breaking events (Pham *et al.* 2006; Kramb and Zukoski 2010), or due to the presence of an additional timescale from the star arm relaxation in the case of star colloidal polymer suspensions (Helgeson, Wagner, and Vlassopoulos 2007). However, in our case the experiments were done below the VPTT where the PNIPAm microgels interact via excluded volume repulsion. Furthermore, a Pipkin diagram representation, see Figure 5.12, showed that unlike star colloidal suspensions, the double plateau for the PNIPAm suspension cannot arise from relaxation of the interpenetrated brushes of the microgels. Thus the double yielding observed for PNIPAm suspensions couldn't be attributed to similar reasons proposed in earlier works (Helgeson *et al.* 2007).

Our experimental data for the PNIPAm microgel suspensions showed that the occurrence of the second peak in the viscous modulus is preceded by a weak peak in the storage modulus which becomes prominent at higher frequency, see Figure 5.13. We believe that the peak in G' occurs as a result of strain-induced structure formation

at higher strains and the second peak in G'' occurs due to the shear-melting of this strain induced structure. Lissajous plots of the raw stress-strain data showed distinct features that support the hypothesis of formation of a strain induced structure, see Figure 5.14.

6.2 Recommendation for future work:

The results of the work presented in this thesis opens up several interesting opportunities for future investigations, some of which are listed below.

6.2.1 Dynamics of homogeneously cross-linked microgels at $\varphi_{\text{eff}} > \varphi_{\text{RCP}}$

In this work, the gel-like evolution of $G_2(\tau)$ with increasing φ_{eff} and the appearance of a double plateau in $G_2(\tau)$ at $\varphi_{\text{eff}} > \varphi_{\text{RCP}}$ was attributed to the core-core and brush-core repulsive interactions of different potentials. These arose because of the core-shell morphology of the microgel that was created due to the different reactivity of the monomer and the crosslinker. It would be interesting to study the dynamics of a suspension of microgels which are devoid of the core-shell morphology. Recently, Acciaro and coworkers (2011) prescribed a synthesis protocol which gave microgels of uniform crosslinking density. DWS studies on dense suspensions of uniformly cross-linked microgels at $\varphi_{\text{eff}} > \varphi_{\text{RCP}}$ can provide a useful check on the hypothesis presented in this work.

6.2.2 Dynamics of polymer grafted hard sphere suspensions at $\varphi_{\text{eff}} > \varphi_{\text{RCP}}$

As discussed earlier the PNIPAm microgels have a radial density gradient resulting in a core-shell like morphology. For the sake of simplicity we have assumed that R_g , R and R_h represent the radial density gradients in the microgel. However, the absence of a sharp boundary of the density makes it difficult to determine the interaction potential for these particles. To address this issue, we suggest the use of suspensions formed by polymer grafted silica hard spheres (Wang *et al.* 2005; Liu and Pan, 2007). The advantage of using these core-shell particles is that the size of the core and the brush can be selected and/or controlled accurately. Silica particles of controlled size can be easily prepared or procured. Similarly, polymer brushes of controlled surface grafting density and molecular weights can be synthesized by either grafting-from or grafting-to approaches. The final core-shell structure can also

be confirmed by complimentary techniques like the dynamic light scattering and small angle neutron scattering (Harrak *et al.* 2005). The polymer grafted hard spheres, allow for precise tuning of the interaction potential by changing the grafting density, length (Harrak *et al.* 2005; Choi *et al.* 2013) and flexibility of the grafted polymer (Choi *et al.* 2010). Such core-shell structure is different than that of the star-colloids in which the 'core' is practically missing. Investigation of these core-shell particles, having a well characterized size and interparticle potential, would provide further insights in the dynamics of dense suspensions, particularly at $\varphi_{\text{eff}} > \varphi_{\text{RCP}}$.

The core-shell microgels described above might also throw more light on the phenomenon of softening of shear modulus at $\varphi_{\text{eff}} \gg \varphi_{\text{RCP}}$ as reported in this work and for other soft systems on the basis of the idea discussed below. It is likely that the strong interpenetration of brushes will in fact osmotically reduce the size of the microgel particles relative to that measured in dilute suspensions. This is akin to the reduction in coil size of a polymer chain dissolved in a good solvent as the concentration of the polymer increases. This happens because with increase in polymer concentration the good solvent is effectively rendered 'relatively poor' as monomers increasingly see other monomers around them rather than solvent molecules. Thus if the modulus were to be plotted against the effective volume fraction calculated from the corrected value of R_h the real extent of softening will be known. In case of the core-shell particles, if a few particles are made using deuterated polymer grafts and suspended with other 'identical' core-shell particles then the size of the tracer particles in dense suspensions can be measured using neutron scattering techniques. DWS studies at high volume fractions of these suspensions might then provide the corrected relation between shear modulus and effective volume fraction.

6.2.3 Application of microgels in biomaterials

In addition to its use as model systems for soft colloidal glasses, PNIPAm finds a large number of applications in the field of biology; examples include drug delivery vehicles, controlled release drug delivery multi responsive scaffolds used in tissue engineering etc. We have made initial attempts to prepare thermoresponsive scaffolds from PNIPAm microgels and our study suggests possible use in future as Biomaterials.

Cho and co workers(2008) proposed a simple method to make 3-dimensional macroscopic scaffolds by covalently connecting PNIPAm microgels. Following their method we prepared macroscopic scaffolds by covalently connecting the microgels using a condensation reaction. The scaffold formed is shown in Figure 6.1, which shows the response in terms of volume change to changes in the environmental temperature. We observed a threefold volume change from swollen state at 20 °C to collapsed state at 60°C. The response time of this scaffold was faster as compared to that of a bulk gel formed by linear PNIPAm (Cho *et al.* 2008).

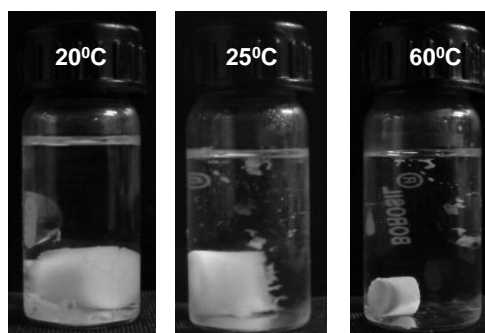


Figure 6.1: Cross-linked microgels of PNIPAm-co-Acrylic acid (10wt.%aqueous suspension)forming thermoresponsive scaffold.

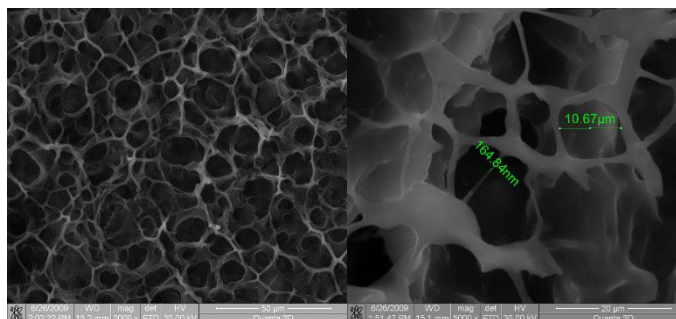


Figure 6.2: Porous network formed by freeze drying of microgel suspension of PNIPAm

A porous scaffold could be made by simply freeze drying the PNIPAm microgel suspension (Deville *et al.* 2006). When an aqueous suspension is frozen, the suspended particles get phase separated in the boundaries between the ice crystals. When the frozen suspension is lyophilized the self-assembled particles form a porous network. The pores formed were $\sim 10\mu\text{m}$, which were comparable to the dimension of the cells. Figure 6.2 shows a scanning electron microscopy image of a porous scaffold formed by PNIPAm microgel suspension.

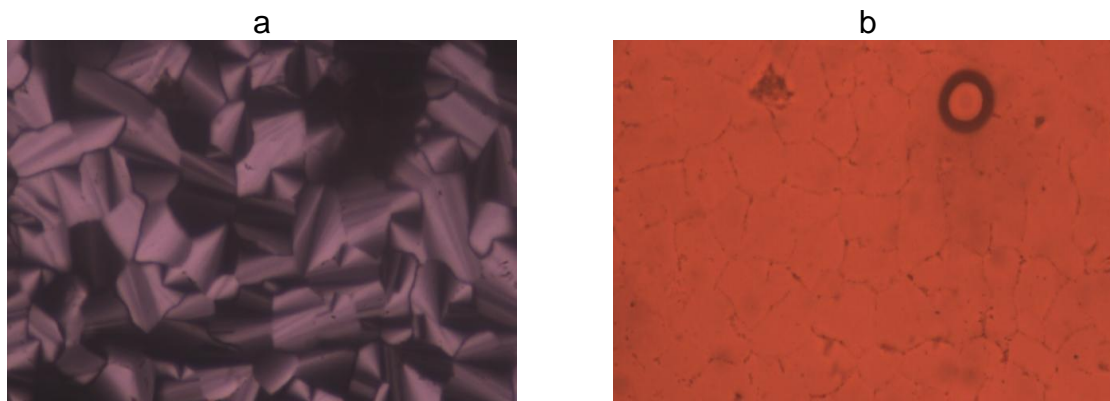


Figure 6.3: Self-assembly of PNIPAm microgels in a hexagonal meso-phase of a surfactant–water system at room temperature; (a) Optical micrograph images showing the hexagonal phase under cross polarizers and (b) parallel polarizers.

The porous scaffolds can also be prepared by self-assembly of particles at the grain boundaries of a lyotropic hexagonal surfactant mesophase (Bouchama *et al.*, 2004 and Sharma *et al.*, 2009). The advantage of this method is that the size of the pores can be tuned (Sharma *et al.* 2009). Figure 6.3 shows the optical micrographs showing the network structure formed by the PNIPAm microgels at the grain boundaries of the hexagonal meso-phase. Since the characteristic of the single particle response transfers to a macroscopic response, we suggest the use of the above mentioned protocols to develop a range of multi-responsive scaffolds.

References

- Aastuen, D.J., Clark, N.A., and Cotter, L.K.,(1986), "Nucleation and Growth of colloidal crystals",*Physical Review Letters* 57, (14), 1733–1737.
- Acciaro, R., Gilányi, T., and Varga, I.,(2011), "Preparation of monodisperse poly(N-isopropylacrylamide) microgel particles with homogenous cross-link density distribution",*Langmuir*(27)-12, 7917–25.
- Adrian, D.W., and Giacomin, A.J.,(1992), "The quasiperiodic nature of a polyurethane melt in oscillatory shear", *Journal of Rheology*(36), 1227–1243.
- Altmann, N., Cooper-white, J.J., Dunstan,D.E., and Stokes, J.R.,(2004), "Strong through to weak ' sheared ' gels",*Journal of Non-newtonian Fluid Mechanics*(124), 129–136.
- Andersson, M., and Maunu, S.L.,(2006), "Structural studies of poly (N-isopropylacrylamide) microgels : Effect of SDS surfactant concentration in the microgel synthesis",*Polymer*(44)-23, 3305–3314.
- Angell, C.A., Ngai, K.L., McKenna,G.B., McMillan,P.F.,and Martin, S.W.,(2000), "Relaxation in Glass Forming Liquids and Amorphous Solids",*Journal of Applied Physics*(88), 3313–3357.
- Antl, L., Goodwin, R.D., Hill,J.W., Ottewill, R.H., Owens,S.M., and Papworth, S.,(1986), "The Preparation of Poly(Methyl Methacrylate) Latices In Non-Aqueous Media",*Colloids and Surfaces*(17), 67–78.
- Arleth, L., Xia, X., Hjelm, R.P., Wu, J., and Hu, Z.,(2005), "Volume Transition and Internal Structures of Small Poly(N -isopropylacrylamide) Microgels",*Journal of Polymer Science Part B: Polymer Physics* (43), 849–860.
- Auer, S., and Frenkel, D.,(2001), "Suppression of Crystal Nucleation in Polydisperse Colloids Due to Increase of the Surface Free Energy",*Nature*(413), 711–713.

References

- Badiger, M.V., Lele, A.K., Bhalerao, V.S., Varghese, S., and Mashelkar, R.A., (1998). "Molecular Tailoring of Thermoreversible Copolymer Gels: Some New Mechanistic Insights", *Journal of Chemical Physics* (109), 1175–1184.
- Berne, B.J., and Pecora, R., (1976), "*Dynamic Light Scattering: With Applications to Chemistry, Biology and Physics*", Wiley, New York.
- Blaaderen, A.V., and Vrij, A., (1992), "Synthesis and Characterization of Colloidal Dispersions of Fluorescent, Monodisperse Silica Spheres", *Langmuir* (8)-12, 2921–2931.
- Bolhuis, P.G., and Kofke, D.A., (1996), "Monte Carlo Study of Freezing of Polydisperse Hard Spheres", *Physical Review E* (54)-1, 634–643.
- Bosma, G., Pathmamanoharan, C., Hoog, E.H.D., Kegel, W.K., Blaaderen, A.V., and Lekkerkerker, H.N.W., (2002), "Preparation of Monodisperse, Fluorescent PMMA Latex Colloids by Dispersion Polymerization", *Journal of Colloid and Interface Science* (245), 292–300.
- Bower, C., Gallegos, C., and Mackley, M.R., (1999), "The Rheological and Microstructural Characterisation of the Non-linear Flow Behaviour of Concentrated Oil-in-water Emulsions", *Rheologica Acta* (38)-2, 145–159.
- Brader, J.M., Siebenbürger, M., Ballauff, M., Reinheimer, K., Wilhelm, M., Frey, S.J., Weysser, F., and Fuchs, M., (2010), "Nonlinear Response of Dense Colloidal Suspensions Under Oscillatory Shear: Mode-coupling Theory and Fourier Transform Rheology Experiments", *Physical Review E* (82), 061401.
- Brown, R., (1985), "The Miscellaneous Botanical Works of Robert Brown", In *Philosophical Journal*, edited by Bennett, J.J., (1), R. Hardwicke, London.
- Burns, J.L., Yan, Y.D., Jameson, G.J., and Biggs, S., (1997), "A Light Scattering Study of the Fractal Aggregation Behavior of a Model Colloidal System", *Langmuir* (13)-24, 6413–6420.

- Campbell, A.I., and Bartlett, P.,(2002), “Fluorescent Hard-Sphere Polymer Colloids for Confocal Microscopy”,*Journal of Colloid and Interface Science*(256), 325–330.
- Chambon, F., Petrovic, Z.S., Macknight, .J., and Winter, H.H., (1986), “Model Polyurethanes at the Gel Point”,*Macromolecules*(2149)-24, 2146–2149.
- Charbonneau, C., Chassenieux, C., Colombani, O., and Nicolai, T.,(2011), “Controlling the Dynamics of Self-Assembled Triblock Copolymer Networks via the pH”,*Macromolecules*(44), 4487–4495.
- Chaudhuri, P., Berthier, L., Hurtado, P.I., and Kob, W.,(2010), “When Gel and Glass Meet: A Mechanism for Multistep Relaxation”,*Physical Review E*(81)-4, 1–4.
- Chen, S.H., Chen,W.R., and Mallamace, F.,(2003), “Observation of Liquid-to-Glass and Glass-to-Glass Transitions in L64/D₂O Triblock Copolymer Micellar System”,*Molecular Simulation* (29)-10, 611–618.
- Cho, E.C., Kim, J.W., Fernandez, N.A., and Weitz, D.A.,(2008a), “Highly Responsive Hydrogel Scaffolds Formed by Three-dimensional Organization of Microgel Nanoparticles”,*Nano Letters*(8)-1, 168–72.
- Choi, J., Dong, H., Matyjaszewski, K., and Bockstaller, M.R.,(2010), “Flexible Particle Array Structures by Controlling Polymer Graft Architecture”,*Journal of American Chemical Society*(132), 12537–12539.
- Choi, J., Hui, C.M., Schmitt, M., Pietrasik, J., Margel, S., Matyjaszewski, K., and Bockstaller, M.R.,(2013), “Effect of Polymer-Graft Modification on the Order Formation in Particle Assembly Structures”,*Langmuir*(29), 6452–6459.
- Cola, E.D., Sztucki, M., Narayanan, T.,and Zaccarelli, E.,(2009), “Correlation Between Structure and Rheology of a Model Colloidal Glass”,*The Journal of Chemical Physics*(131), 144903.
- Conrad, J.C., Dhillon, P.P., Weeks, E.R., Reichman, D.R., and Weitz, D.A.,(2006), “Contribution of Slow Clusters to the Bulk Elasticity Near the Colloidal Glass Transition”,*Physical Review Letters* (265701), 1–4.

- Courtland, R.E., and Weeks, E.R.,(2003), “Direct Visualization of Ageing in Colloidal Glasses”,*Journal of Physics: Condensed Matter*(15)-1, S359–S365.
- Das, G., Gnan, N., Sciortino, F., and Zaccarelli, E.,(2013), “Unveiling the Complex Glassy Dynamics of Square Systems: Simulations and Theory”,*Archive- Cond Mat Soft.* 1–12.
- Derec, C., Ajdari,A., and Lequeux, F.,(2001), “Rheology and Aging: A Simple Approach”,*The European Physical Journal. E, Soft Matter*(4), 355–361.
- Derjaguin, B., and Landau, L.,(1941), “Theory of the Stability of Strongly Charged Lyophobic Sols and of the Adhesion of Strongly Charges Particles in Solution of Elctrolytes”,*Acta Physicochim. USSR*(14), 633.
- Deville, S., Saiz, E., Nalla, R.K., and Tomsia, A.P.,(2006), “Freezing as a Path to Build Complex Composites”,*Science* (311)-5760, 515–8.
- Doi, M., and Edwards, S.F.,(1986),“*The Theory of Polymer Dynamics*”, Clarendon, Oxford.
- Du, H., Wickramasinghe, R., and Qian, X.,(2010), “Effects of Salt on the Lower Critical Solution Temperature of Poly (N-isopropylacrylamide)”,*The Journal of Physical Chemistry. B*(114)-49, 16594–16604.
- Eckert, T., and Bartsch, E.,(2002), “Re-entrant Glass Transition in a Colloid-Polymer Mixture with Depletion Attractions”,*Physical Review Letters*(89)-12, 20–23.
- Eckert, T., and Richtering, W.,(2008), “Thermodynamic and Hydrodynamic Interaction in Concentrated Microgel Suspensions: Hard or Soft Sphere Behavior?”,*The Journal of Chemical Physics*(129), 124902.
- Einstein, A.,(1905), “Uber Die Von Der Molekularkinetischen Theorie Der Warme Geforderte Beegung Von in Ruhenden Flussigkeiten Suspendierten Teilchen”,*Ann Phys*(17), 549–560.
- Elsesser, M.T, and Hollingsworth A.D.,(2010), “Revisiting the Synthesis of a Well-Known Comb-Graft Copolymer Stabilizer and Its Application to the Dispersion

References

- Polymerization of Poly (Methyl Methacrylate) in Organic Media”,*Langmuir*(26)-23, 17989–17996.
- Erwin, B.M., Vlassopoulos, D., and Cloitre, M.,(2010), “Rheological Fingerprinting of an Aging Soft Colloidal Glass”,*Journal of Rheology*(54), 915-939.
- Ewoldt, R.H., Hosoi, A.E., and Gareth H.M.,(2008), “New Measures for Characterizing Nonlinear Viscoelasticity in Large Amplitude Oscillatory Shear”,*Journal of Rheology*(52)-6, 1427-1458.
- Farage, T., and Brader J.M.,(2012), “Three Dimensional Flow of Colloidal Glasses”,*Journal of Rheology*(56)-2, 259.
- Fasolo, M., and Sollich, P.,(2003), “Equilibrium Phase Behavior of Polydisperse Hard Spheres”,*Physical Review Letters*(91)-6, 068301.
- Fernández-Barbero, A., Suárez, I.J., Sierra-Martín, B., Fernández-Nieves, A., Nieves, F.J.L., Marquez, M., Rubio-Retama, J., and López-Cabarcos, E., (2009), “Gels and Microgels for Nanotechnological Applications”,*Advances in Colloid and Interface Science*(147-148), 88–108.
- Ferry, J.D.,(1980),"*Viscoelastic Properties of Polymers*", Third. Wiley, New York.
- Fujishige, S., Kubora, K., and Ando, I.,(1989), “Phase Transition of Aqueous Solutions of Poly(N-isopropylacrylamide) and Poly(N-isopropylmethacrylamide)”,*The Journal of Physical Chemistry*, (93)-8, 3311–3313.
- Ganeriwala, S., and Rotz, C.,(1987), “Fourier Transform Mechanical Analysis for Determining the Nonlinear Viscoelastic Properties of Polymers,” *Polymer Engineering & Science*(27)-2, 165–178.
- Gao, J., and Hu, Z.,(2002), “Optical Properties of N-Isopropylacrylamide Microgel Spheres in Water”,*Langmuir*(18)-4, 1360–1367.
- Goodwin, J.W.,(2004),"*Colloids and Interfaces with Surfactants and Polymers-An Introduction*", Vol. 7, John Wiley and Sons Ltd.

- Grasso, D., Subramaniam, K., Butkus, M., Strevett, K., and Bergendahl, J.,(2002), "A Review of non-DLVO Interactions in Environmental Colloidal Systems", *Reviews in Environmental Science & Biotechnology*(1), 17–38.
- Harrak, A., Carrot, G., Oberdisse, J., and Boue, F.,(2005), "Control of the Colloidal Stability of Polymer-Grafted-Silica Nanoparticles Obtained by Atom Transfer Radical Polymerization", *Macromolecule Symposium*(226), 263–278.
- Hartl, W.,(2001), "Colloidal Glasses." *Current Opinion in Colloid & Interface Science*(6), 479–483.
- Helgeson, M.E., Wagner, N.J., and Vlassopoulos, D.,(2007), "Viscoelasticity and Shear Melting of Colloidal Star Polymer Glasses." *Journal of Rheology*(51)-2, 297–316.
- Heimenz, P.C., and Rajagopalan, R.,(1997), "*Principles of Colloid And Surface Chemistry*", Third. New York: Marcel Dekker.
- Hiltner, P.A., Papir, Y.S., and Krieger, I.M., (1971), "Diffraction of Light by Nonaqueous Ordered Suspensions", *Journal of Physical Chemistry*(76)-12, 1881–1886.
- Hodge, I.M.,(1995), "Physical Aging in Polymer", *Science*, (267), 1945-1947.
- Huang, G., and Hu, Z.,(2007), "Phase Behavior and Stabilization of Microgel Arrays", *Macromolecules*(40)-10, 3749–3756.
- Hurtado, P.I., Berthier, L., and Kob, W.,(2007), "Heterogeneous Diffusion in a Reversible Gel", *Physical Review Letters*(98)-13, 135503.
- Hynninen, A., and Dijkstra, M.,(2003), "Phase Diagrams of Hard-core Repulsive Yukawa Particles", *Physical Review E*(68)-021407, 1–8.
- Hyun, K., Kim, S.H., Ahn, K.H., and Lee, S.J.,(2002), "Large Amplitude Oscillatory Shear as a Way to Classify the Complex Fluids", *Journal of Non-newtonian Fluid Mechanics*(107), 51–65.

References

- Ilett, S.M., Orrock, A., Poon, W.C.K., and Pusey, P.N.,(1995), “Phase Behavior of Model Colloid-polymer Mixture”,*Physical Review E*(51)-2, 1344–1353.
- Jang, J.H.,Jhaveri, S.J., Rasin, B., Ober, C.K., Thomas, E.L.,and Koh, C.,(2008), “Three-Dimensionally-Patterned Submicrometer-Scale Hydrogel / Air Networks That Offer a New Platform for Biomedical Applications”,*Nano Letters*(8)-5, 1456–1460.
- Jijo, V.J., Sharma, K.P., Mathew, R., Kamble, S., Rajamohanan, P.R., Ajithkumar, T.G., Badiger, M.V., and Kumaraswamy, G., (2010), “Volume Transition of PNIPAM in a Nonionic Surfactant Hexagonal Mesophase”,*Macromolecules*(43), 4782–4790.
- Joshi, Y.M., and Reddy, G.R.K.,(2008), “Aging in a Colloidal Glass in Creep Flow: Time-stress Superposition”,*Physical Review E*(77)-2, 021501– 021505.
- Kalelkar, C., Lele, A.K., and Kamble, S.,(2010), “Strain-rate Frequency Superposition in Large-amplitude Oscillatory Shear”,*Physical Review E*(81)-3, 1–10.
- Kalman, D.P., and Wagner, N.J.,(2009), “Microstructure of Shear-thickening Concentrated Suspensions Determined by flow-USANS”,*Rheologica Acta*(48), 897–908.
- Kapnistos, M., Semenov, A.N., Vlassopoulos, D., and Roovers, J., (1999), “Viscoelastic Response of Hyperstar Polymers in the Linear Regime”,*The Journal of Chemical Physics*(111)-4, 1753.
- Kob, W., and Barrat, J.L., (1997), “Aging Effects in a Lennard-Jones Glass”, *Physical Review Letters*(78)-24, 4581–4584.
- Kramb, R.C., and ZukoskiC.F.,(2010), “Yielding in Dense Suspensions: Cage, Bond, and Rotational Confinements.” *Journal of Physics. Condensed Matter: an Institute of Physics Journal*(23)-3, 035102.
- Krieger, I.M, and Niu, T.F.,(1973), “A Rheometer for Oscillatory Studies of Nonlinear Fluids”,*Rheologica Acta*(12),: 567–571.

- Krieger, I.M., Hiltner, P.A., and Krieger, I.M.,(1969), “Diffraction of Light by Ordered Suspensions.” *Journal of Physical Chemistry*(78)-1, 2386–2389.
- Kulkarni, C.V., Wachter, W., Iglesias-salto, G., Engelskirchen, S., and Ahualli, S.,(2011), “Monoolein : a Magic Lipid ?”, *Physical Chemistry Chemical Physics : PCCP*(13), 3004–3021.
- Kumar, A., and Wu, J.,(2004), “Jamming Phase Diagram of Colloidal Dispersions by Molecular Dynamics Simulations”, *Applied Physics Letters*(84)-22, 4565.
- Kunugi, S., Takano, K., and Tanaka, N.,(1997), “Effects of Pressure on the Behavior of the Thermoresponsive Polymer Poly(N-vinylisobutyamide)(PNVIBA).” *Macromolecules*(30), 4499–4501.
- Leonardo, D., Ianni, F., and Ruocco, G.,(2005), “Aging Under Shear: Structural Relaxation of a non-Newtonian Fluid.” *Physical Review E*(71), 011505.
- Li, R., (2000), “Time-temperature Superposition Method for Glass Transition Temperature of Plastic Materials”, *Materials Science and Engineering A*(278), 36–45.
- Lin, M.Y., Lindsay, H.M, Weitz, D.A., Ball, R.C., Klein, R., and Meakin, P.,(1989), “Universality in Colloidal Aggregation.” *Nature*(339), 360–362.
- Liu, A.J., and Nagel, S.R.,(1998), “Jamming Is Not Just Cool Any More”, *Nature*(396), 21.
- Liu, C., and Pan, C., (2007), “Grafting Polystyrene onto Silica Nanoparticles via RAFT Polymerization”, *Polymer*(48), 3679–3685.
- Loppinet, B., Stiakakis, E., Vlassopoulos, D., Fytas, G., and Roovers, J.,(2001), “Reversible Thermal Gelation in Star Polymers: An Alternative Route to Jamming of Soft Matter”, *Macromolecules*(34), 8216–8223.
- Lu, P.J., and Weitz, D.A.,(2013), “Colloidal Particles: Crystals, Glasses, and Gels”, *Annual Review of Condensed Matter Physics*(4)-9, 1–17.

- Marrucci, G.,(1996), “Dynamics of Entanglements : A Nonlinear Model Consistent with the Cox-Merz Rule”,*Journal of Non-newtonian Fluid Mechanics*(62), 279–289.
- Martinez, V.A., Bryant, G., and Megen, W.V.,(2008). “Slow Dynamics and Aging of a Colloidal Hard Sphere Glass.” *Physical Review Letters*(101), 135702.
- Mason, T.G., Bibette, J., and Weitz, D.A., (1995), “Elasticity of Compressed Emulsions”,*Physical Review Letters*(75)-10, 2051–2054.
- Mason, T.G, and Weitz, D.A.,(1995), “Optical Measurements of Frequency-Dependent Linear Viscoelastic Moduli of Complex Fluids”,*Physical Review Letters*(74)-7, 1250–1253.
- Mason, T.,(2000), “Estimating the Viscoelastic Moduli of Complex Fluids Using the Generalized Stokes-Einstein Equation”,*Rheologica Acta*(39)-4, 371–378.
- Mason, T.G, and Weitz, D.A.,(1995),“Linear Viscoelasticity of Colloidal Hard Sphere Suspensions Near the Glass Transition”,*Physical Review Letters*(75)-14, 2770–2773.
- Mattsson, J., Wyss,H.M., Fernandez-Nieves, A., Miyazaki,K., Hu, Z., Reichman, D.R., and Weitz, D.A.,(2009), “Soft Colloids Make Strong Glasses.” *Nature*(462)-7269, 83–86.
- Medebach, M., Moitzi, C., Freiburger, N., and Glatter, O.,(2007), “Dynamic Light Scattering in Turbid Colloidal Dispersions : A Comparison Between the Modified Flat-cell Light-scattering Instrument and 3D Dynamic Light-scattering Instrument”,*Journal of Colloid and Interface Science* (305)-1, 88–93.
- Meeker, S.P., Poon,W.C.K., and Pusey,P. N.,(1997), “Concentration Dependence of the Low-shear Viscosity of Suspensions of Hard-sphere Colloids”,*Physical Review E*(55)-5, 5718–5722.
- Megen, W.V., and Underwood, S.M., (1993), “Dynamics Light Scattering Study of Glasses of Hard Colloidal Spheres”,*Physical Review E*(47)-1, 248–261.

References

- Michel, E., Filali, M., Aznar, R., Porte, G., and Appell, J.,(2000), "Percolation in a Model Transient Network: Rheology and Dynamic Light Scattering",*Langmuir*(16)-23, 8702–8711.
- Miyazaki, K., Wyss, H.M., Weitz, D.A., and Reichman, D.R., (2006), "Nonlinear Viscoelasticity of Metastable Complex Fluids",*Europhysics Letters*(75)-6, 915.
- Nayak, S., and Lyon, L.A.,(2005), "Soft Nanotechnology with Soft Nanoparticles",*Angewandte Chemie*(44)-47, 7686–708.
- Nyffenegger, R., Quellet, C., and Rick, J.,(1993)., "Synthesis of Fluorescent, Monodisperse, Colloidal Silica Particles",*Journal of Colloid and Interface Science*(159), 150–157.
- Onogi, S., Masuda, T., and Matsumoto, T.,(1970),"Non-linear Behavior of Viscoelastic Materials. I. Disperse Systems of Polystyrene Solution and Carbon Black",*Journal of Rheology*(14),-2, 275–294.
- Pusey, P.N.,(1999)., "Suppression of Multiple Scattering by Photon Cross-correlation Techniques",*Current Opinion in Colloid and Interface Science*(4), 177–185.
- Pusey,P.N., and Megen, W.V.,(1986), "Phase Behaviour of Concentrated Suspensions of Nearly Hard Colloidal Spheres",*Nature*(320), 340–342.
- Parthasarathy, M., and Klingenberg, D.J.,(1999), "Large Amplitude Oscillatory Shear of ER Suspensions",*J.Non-Newtonian Fluid Mech*(81), 83–104.
- Payne, A.R.,(1963), "Dynamic Properties of Heat-treated Butyl Vulcanizates",*Journal of Applied Polymer Science*(7)-3, 873–885.
- Pelton, R.H., and Chibante, P., (1986), "Preparation of Aqueous Latices with N-Isopropylacrylamide",*Colloids and Surfaces*(20), 247–256.
- Pelton, R.H., Pelton,H.M., Morphesis, A., and Rowells,R.L.,(1989), "Particle Sizes and Electrophoretic Mobilities of Poly(N-isopropylacrylamide) Latex",*Langmuir*(51)-1, 816–818.

References

- Pham, K.N., Puertas, A.M., Bergenholtz, J., Egelhaaf, S.U., Moussaïd, A., Pusey, P.N., Schofield, A.B., Cates, M.E., Fuchs, M., and Poon, W.C.K., (2002), "Multiple Glassy States in a Simple Model System." *Science*(296), -5565, 104–106.
- Pham, K.N., Petekidis, G., Vlassopoulos, D., Egelhaaf, S.U., Pusey, P.N., and Poon, W.C.K., (2006), "Yielding of Colloidal Glasses." *Europhysics Letters* (75)-4, 624–630.
- Pine, D.J., Weitz, D.A., Chaikin, P.M., and Herbolzheimer, E., (1988), "Diffusive Wave Spectroscopy", *Physical Review Letters*(60)-12, 1134–1137.
- Prasad, V., Semwogerere, D., and Weeks, E.R., (2007), "Confocal Microscopy of Colloids", *Journal of Physics: Condensed Matter*(19)-11, 113102.
- Press, W., Teukolsky, S., Vetterling, W., and Flannery, B., (2007), "*The Art of Scientific Computing*", Cambridge: Cambridge University Press.
- Rahola, J.C., (2007), "Elasticity and Dynamics of Weakly Aggregated Colloidal Systems", Dissertation, University of Fribourg, Department of Physics.
- Reufer, M., Díaz-Leyva, P., Lynch, I., and Scheffold, F., (2008), "Temperature-sensitive poly(N-Isopropyl-Acrylamide) Microgel Particles: A Light Scattering Study", *The European Physical Journal. E, Soft Matter*(25), 8–10.
- Roldan-Vargas, S., De, V.J., Barnadas-Rodriguez, R., Quesada-Perez, J., Estelrich, M., and Callejas-fernández, J., (2010), "Suspensions of Repulsive Colloidal Particles Near the Glass Transition: Time and Frequency Domain Descriptions", *Physical Review E*(82), 021406.
- Romer, S., Scheffold, F., and Schurtenberger, P., (2000), "Sol-Gel Transition of Concentrated Colloidal Suspensions", *Physical Review Letters*, (85)-23, 4–7.
- Roovers, J., Paul, L.Z., Zwan, M.V.D., Iatrou, H., and Hadjichristidis, N., (1993), "Regular Star Polymers with 64 and 128 Arms. Models for Polymeric Micelles", *Macromolecules*(26), 4324–4331.
- Rubinstein, M., and Colby, R.H., (2003), *Polymer Physics*. Oxford University Press, USA.
-

- Saunders, B.R., Laajam,N., Daly,E., Teow,S., Hu,X., and SteptoR.,(2009), "Microgels: From Responsive Polymer Colloids to Biomaterials",*Advances in Colloid and Interface Science*(147)-148, 251–62.
- Saw, S., Ellegaard,N.L., Kob,W., and Sastry,S.,(2011), "Computer Simulation Study of the Phase Behavior and Structural Relaxation in a Gel-former Modeled by Three-body Interactions",*The Journal of Chemical Physics*(134)-164506, 1–13.
- Scheffold, F., Díaz-Leyva,P., and Reufer,M., (2010), "Brushlike Interactions Between Thermoresponsive Microgel Particles",*Physical Review Letters*(104)-12, 128304.
- Sciortino, F., Tartaglia, P., and Zaccarelli, E.,(2003), "Evidence of a Higher-Order Singularity in Dense Short-Ranged Attractive Colloids",*Physical Review Letters*(91)-26, 268301–4.
- Senff, H., and Richtering W.,(1999), "Temperature Sensitive Microgel Suspensions: Colloidal Phase Behavior and Rheology of Soft Spheres",*The Journal of Chemical Physics*(111)-4, 1705.
- Sharma, K., Kumaraswamy, G., Ly, E., and Monval M,M., (2009), "Self Assembly of Silica Particles in a Nonionic Surfactant Hexagonal Mesophase", *The Journal of Physical Chemistry B* (113)-11, 3423.
- Shibayama, M., Ikkai, F., Inamoto,S., Nomura,S., and Han, C.C.,(1996). "pH and Salt Concentration Dependence of the Microstructure of Poly(N Isopropylacrylamide-co-acrylic Acid) Gels." *Journal of Chemical Physics*(105)-10, 4358–4366.
- Sim, H.G., Ahn,K.H., and Lee,S.J.,(2003), "Three-dimensional Dynamics Simulation of Electrorheological Fluids Under Large Amplitude Oscillatory Shear Flow." *Journal of Rheology*(87), 879.
- Sirota, E.B., Yang-Qu,H.D., Sinha,S.K., and Chaikin, P.M.,(1989), "Complete Phase Diagram of a Charged Colloidal System: A Synchrotron X-Ray Scattering Study",*Physical Review Letters*(62)-13, 1524–1527.
- Smoluchowski, V.M.,(1906), "Zur Kinetischen Thoery Der Brownschen Molekular Beegung Und Der Suspensionen." *Ann Phys*(21), 756–780.

- Song, K.W., Kuk, H.Y., and Chang, G.S.,(2006), “Rheology of Concentrated Xanthan Gum Solutions: Oscillatory Shear Flow Behavior”,*Korea-Australia Rheology Journal*(18)-2, 67–81.
- Sperl, M., Sapienza,L., Moro,P.A., and Stanley, H.E.,(2010), “Disconnected Glass-Glass Transitions and Diffusion Anomalies in a Model with Two Repulsive Length Scales”,*Physical Review Letters*(104), 145701.
- Stieger, M., Pedersen,J.S., Lindner,P., and Richtering, W.,(2004), “Are Thermoresponsive Microgels Model Systems for Concentrated Colloidal Suspensions? A Rheology and Small-angle Neutron Scattering Study”,*Langmuir : the ACS Journal of Surfaces and Colloids*(20), 7283–7292.
- Stieger, M., Richtering,W., Pedersen,J.S., and Lindner,P.,(2004), “Small-angle Neutron Scattering Study of Structural Changes in Temperature Sensitive Microgel Colloids.” *The Journal of Chemical Physics*(120)-13, 6197–206.
- Stokes, J.R., and Frith,W.J.,(2008), “Rheology of Gelling and Yielding Soft Matter Systems”,*Soft Matter*(4), 1133–1140.
- Sutherland, A.,(1905), “A Dynamical Theory of Diffusion for Non-electrolytes and the Molecular Mass of Albumin.” *Philosophical Magazine* (9), 781–785.
- Tirtaatmadja, V., Tam,K.C., and Jenkins, R.D.,(1997a), “Superposition of Oscillations on Steady Shear Flow as a Technique for Investigating the Structure of Associative Polymers.” *Macromolecules*(30)-5, 1426–1433.
- Tirtaatmadja, V., Tam,K.C., and Jenkins, R.D.,(1997b), “Rheological Properties of Model Alkali-soluble Associative (HASE) Polymers: Effect of Varying Hydrophobe Chain Length”,*Macromolecules* 30 (11): 3271–3282.
- Trappe, V., Prasad, V., Cipelletti, L., Segre,P.N., and Weitz,D.A.,(2001), “Jamming Phase Diagram for Attractive Particles”,*Nature*(411)-6839, 772–5.
- Urban, C., Scheffold, F., and Schurtenberger, P.,(2000), “Static and Dynamics Light Scattering in Turbid Suspensions”,*Macromolecular Symposia*(162), 235–247.

- Urban, C., and Schurtenberger, P.,(1998),“Characterization of Turbid Colloidal Suspensions Using Light Scattering Techniques Combined with Cross-Correlation Methods”,*Journal of Colloid and Interface Science*(158), 150–158.
- Varghese, S., Lele, A.K., and Mashelkar, R.A., (2000), “Designing New Thermoreversible Gels by Molecular Tailoring of Hydrophilic-hydrophobic Interactions”,*The Journal of Chemical Physics* 112 (6): 3063.
- Verwy, E.J.W., and Overbeek, J.G.,(1948),"*Theory of Stability of Lyophobic Colloids*", Amsterdam: Elsevier.
- Vlassopoulos, D.,(2004), “Colloidal Star Polymers : Models for Studying Dynamically Arrested States in Soft Matter”,*Journal of Polymer Science Part B: Polymer Physics*(42), 2931–2941.
- Wagner, N.J.,(1993), “The High-frequency Shear Modulus of Colloidal Suspensions and the Effects of Hydrodynamic Interactions”,*Journal of Colloid and Interface Science*(161), 169–181.
- Wagner, N.J., and Brady, J.F.,(2009), “Shear Thickening in Colloidal Dispersions”,*Physics Today* (October): 27–32.
- Wang, Y., Pei,X., He,X., and Yuan, K.,(2005), “Synthesis of Well-defined, Polymer-grafted Silica Nanoparticles via Reverse ATRP”,*European Polymer Journal*(41), 1326–1332.
- Weeks, E., and Weitz, D.A.,(2002), “Properties of Cage Rearrangements Observed Near the Colloidal Glass Transition”,*Physical Review Letters*(89)-9, 1–4.
- Weitz, D.A., Huang,J.S., Lin,M.Y., and Sung,J.,(1985), “Limits of Fractal Dimension for Irreversible Kinetic Aggregation of Gold Colloids”,*Physical Review Letters*(54)-13, 1416–1419.
- Weitz, D.A., and OLiveria, M., (1984), “Fractal Structures Formed by Kinetic Aggregation of Aqueous Gold Colloids”,*Physical Review Letters*(52)-16, 1433–1437.
- Weitz, D.A., and PineD.J.,(1992), "*Dynamic Light Scattering*. Oxford University Press.
-

- Wu, J., Zhou, B., and Hu, Z., (2003), "Phase Behavior of Thermally Responsive Microgel Colloids." *Physical Review Letters*(90), 1–4.
- Wu, X., Pelton, R.H., Hamielec, A.E., Woods, D.R., and McPhee, W., (1994), "The Kinetics of poly(N-isopropylacrylamide) Microgel Latex Formation", *Colloid & Polymer Science*(272), 467–477.
- Wyss, H., Miyazaki, K., Mattsson, J., Hu, Z., Reichman, D., and Weitz, D., (2007), "Strain-Rate Frequency Superposition: A Rheological Probe of Structural Relaxation in Soft Materials", *Physical Review Letters*(98)-23, 1–4.
- Yamamoto, R., and Onuki, A., (1998), "Dynamics of Highly Supercooled Liquids: Heterogeneity, Rheology, and Diffusion", *Physical Review E*(58)-3, 3515–3529.
- Yang, S., Yan, D., Tan, H., and Shi, A.C., (2006), "Depletion Interaction Between Two Colloidal Particles in a Nonadsorbing Polymer Solution", *Physical Review E*(74), 041808.
- Zaccarelli, E., and Poon, W.C.K., (2009), "Colloidal Glasses and Gels: The Interplay of Bonding and Caging", *Proceedings of the National Academy of Sciences of the United States of America*(106)-36, 15203–8.
- Zaccarelli, E., Valeriani, C., Sanz, E., Poon, W.C.K., Cates, M.E., and Pusey, P.N., (2009), "Crystallization of Hard-Sphere Glasses", *Physical Review Letters*(103), 135704.
- Zaccarelli, E., and Poon, W., (2009), "Colloidal Glasses and Gels: The Interplay of Bonding and Caging", *Proceedings of the National Academy of Sciences of the United States of America*(106)-36, 15203–8.
- Zakharov, P., Cardinaux, F., and Scheffold, F., (2006), "Multispeckle Diffusing-wave Spectroscopy with a Single-mode Detection Scheme", *Physical Review E*(73), 011413.
- Zhang, S.Q., Zha, L., Ma, J., Liang, B., (2007), "Synthesis and Characterization of Novel, Temperature Sensitive Microgels Based on N-isopropylacrylamide and Ter-butylacrylate." *Journal of Applied Polymer Science*(103), 2962–2967.

References

Zhou, Z., and Chu, B.,(1991). "Light-scattering Study on the Fractal Aggregates of Polystyrene Spheres: Kinetic and Structural Approaches",*Journal of Colloid and Interface Science*(143)-2, 356–365.

List of Publications

Kamble Samruddhi, Anurag Pandey, Sanjay Rastogi and Ashish Lele. 2013. "Ascertaining Universal Features of Yielding of Soft Materials." *Rheologica Acta* 52, 859-865.

Kamble Samruddhi, Ashish Lele, Cardinaux Frederic, Frank Scheffold, Rajdip Bandopadhyaya and Suresh Bhat. 2013. "Dynamics of Dense Microgel Suspensions." (Manuscript under preparation)

Kalelkar Chirag, Ashish Lele, and Samruddhi Kamble. 2010. "Strain-rate Frequency Superposition in Large-amplitude Oscillatory Shear." *Physical Review E* 81 (3) (March): 1–10.

Jijo, V J, Kamendra P Sharma, R Mathew, Samruddhi Kamble, P R Rajamohanan, T G Ajithkumar, M V Badiger, and Guruswamy Kumaraswamy. 2010. "Volume Transition of PNIPAM in a Nonionic Surfactant Hexagonal Mesophase." *Macromolecules* 43: 4782–4790.

List of presentation in Conferences

- *'Dynamics of Dense microgel suspensions of PNIPAM'* , FAPS-Polymer Congress and Macro, Indian Institute of Science, Bangalore, 2013.
- *'Yielding in concentrated microgel suspensions of Poly N-isopropylacrylamide (PNIPAM) under Large Amplitude Oscillatory Shear'*, *International Congress on Rheology, Lisbon, Portugal 2012.*
- *'Investigation of the role of Frequency in Classification of Complex Fluids by Large Amplitude Oscillatory shear (LAOS)'* Mumbai-Pune soft matter meeting, National Chemical Laboratory Pune, 2011.
- *'Strain Rate Frequency Superposition in large Amplitude Oscillatory Shear'*, Complex fluids Symposium (COMPFLU 2010), at Indian Institute of Technology Madras (IITM) Chennai, 2010.
- *'Smart Material: Thermoresponsive Poly N-isopropylacrylamide(PNIPAM) gels'* Small angle Neutron Scattering SANS Conference, International Centre Goa, 2009.
- *'Synthesis and characterization of thermoresponsive Poly N-isopropylacrylamide (PNIPAM) gels'*, Science Day Poster Competition, National Chemical Laboratory, Pune, 2008.

Acknowledgements

I would like to thank my supervisors, Prof. Rajdip Bandopadhyay, Dr. Suresh Bhat and Dr. Ashish Lele for their encouraging support and invaluable inputs throughout my PhD. Prof. Rajdip helped me during my coursework at IITB and has always been approachable to my queries while I carried out my research at NCL. I express my sincere thanks to Dr. Suresh Bhat who accepted me as his research student. It was truly an enriching experience to set up a light scattering laboratory from scratch under the guidance of Dr. Suresh Bhat.

I am extremely grateful to Dr. Ashish Lele to be my mentor in throughout my stay at NCL. His far-reaching insights in the field of rheology led to a critical review of this work. He has tirelessly taught me to look for the larger picture without losing focus on rigorous scientific methodology. In spite of his extremely busy schedule he has helped me to improve my presentation and communication skills during my several national and international presentations. I am indebted to him for his advice and help during upheavals in my professional as well as personal life.

My sincere thanks to the research progress committee members Dr Vinod Aswal (BAARC), Prof. Mahesh Tirumkudulu, Prof. Rochish Thaokar and Prof. Jayesh Bellare from IITB for evaluating and reviewing my work yearly.

A very special word of thanks goes to Dr. Guruswamy who is not just my first mentor but has guided me at several fronts during my stay at NCL. As a result of his encouragement I qualified CSIR-JRF-NET, without which the journey of this PhD would have not started. Daily meetings with Dr. Guruswamy were really invaluable and led to foundation work in my career in research.

I will miss the thought provoking discussions with Dr. Sarika Bhattacharya who helped me with the analysis of light scattering data on dense microgel suspensions. I admired how she could manage to explain complicated concepts without use of a single equation although being a theoretician! It was her critical analysis which shaped an important chapter of this Thesis.

I really appreciate discussion with Dr. V. Premnath and his introduction course in business and entrepreneur development introducing me to the commercialization aspects of research.

I also thank Dr. Anurag Pandey who is not just my best friend and well-wisher, but also has been the great critic of my work. His critical views of my daily schedule and time management helped me to give my best. He was one of the persons who ensured that I clear the CSIR exam so that I could do a PhD. He convinced me that the best in anyone can be brought not just by smart work alone but hard work as well. Being a computer wizard, he kept me updated with the latest software which was essential during data plotting and writing. A part of his PhD work has been extended to one of my Thesis chapters. His guidance and experience with the experiments helped me finish the work faster.

I am also grateful to Dr. Chirag Kalelkar for my learning from his super-organisational skills and speedy work culture, which helped me get my first publication and consequently a Thesis Chapter.

Special thanks to Dr. Cardinaux Frederic and Prof. Frank Scheffold from the University of Fribourg, Switzerland to give me an opportunity to work in their light scattering lab as an exchange student. Working with Dr Frederic helped me understand the intricacy of sample preparation of soft colloidal glasses. A trip to Switzerland has also given me opportunity to experience and learn different culture.

I acknowledge Council of Scientific and Industrial Research (CSIR) for the research fellowship for my Ph.D. I also extend my thanks to the Indian Institute of Technology, Bombay (IITB) and the National Chemical Laboratory, Pune (NCL) for this collaborative Ph.D programme and allowing me to avail facilities from these premium research institutes in India. I also thank Indo-Swiss Joint Research Program (ISJRP) for funding my research and accommodation as an exchange student.

This journey of 6 years couldn't have been completed without the moral support of many friends from light scattering group. My special thanks to Venu, Girish, Divya and Tina for their help in synthesis of PNIPAm microgels. It was great fun to work with Jijo on the self-assembly of microgels. I thank all the summer trainees Tejas, Shivanjali and Manasi.

I am also grateful to my friends and colleagues at CFPE - Balaji, Shailesh, Vikrant, Manoj, Kiran, Rigwed, Sameer, Dhanalaxmi, Kamendra, Indrawadhan,

Harshwardhan, Shamsunder, Mr. Borkar, Dr. Ashish Orpe and many others who were always there for support.

A special mention to the CFPE *women club* that comprises of Amruta, Kalyani, Anuya, Anushree, Sangeeta, Neelima and Amarja. I will really miss the sizzling brownie, chat sessions, coffee meets, poor jokes, gossips, laughter, mimicry and the photo sessions. I will really miss all these pretty ladies and the fun we had together.

I also thank friends in Switzerland namely, Julian, Irmguard, Marco, Tahrin, Vikas, Kiran, Rehmati, Sumit, Museer and Ujjwala who made my stay comfortable at the University of Fribourg.

My friends at IITB - Priya, Yogita, Aparna, Rutuja, Amol, Anees, Ethaya, Saptarshi, Ribu, Deepti, Shreya, Megha, Niharika, Ragini and many others made my stay delightful and have been stress-bruster during the tough coursework at IITB. I would have never been able to cope with mathematics, without constant help and encouragement from Priya - the mathematician and Venu - the programmer.

My acknowledgment cannot be complete without thanking the help from Jyoti, Asha, Shakuntala and Rani who helped me in daily chores. I also thank Agnes who helped me commuting to NCL in rainy days. These people took care of my parents while I was busy and sometimes away for my research work.

I am fortunate to have a loving and caring family, especially my nieces Tanvi and Shamvi had been great stress relievers during hard times. I thank my two sisters Shraddha and Vrushali; my brothers-in-laws Sameer and Dheeraj.

My special gratitude goes to the most important people in my life; my mother Mrs Anupam Kamble and my father Arch. Bharat Kamble for their untiring patience during the entire stay at NCL. My mother never forgot to keep a bottle of water during my night study and my father used to stand at the college gate for hours until I finished my exam papers. Whatever I am today, and intend to be in future is solely because of their immense support and unconditional love. My success in life will always be dedicated to them. Finally, I acknowledge the Almighty for the strength and determination to face the hardships during my PhD.